Fall 2012

Oxidation of nitrogen monoxide by oxoiron(IV) complexes: mechanistic studies and related investigations with an iron nitrosyl complex

Travis Michael Owen
University of Iowa

OXIDATION OF NITROGEN MONOXIDE BY OXOIRON(IV) COMPLEXES: MECHANISTIC STUDIES AND RELATED INVESTIGATIONS WITH AN IRON NITROSYL COMPLEX

by

Travis Michael Owen

An Abstract

Of a thesis submitted in partial fulfillment
of the requirements for the Doctor of
Philosophy degree in Chemistry
in the Graduate College of
The University of Iowa

December 2012

Thesis Supervisor: Assistant Professor Jan-Uwe Rohde

ABSTRACT

Reactions of the free radical nitrogen monoxide (NO) with metal–oxygen species of metalloproteins are relevant to NO metabolism and detoxification. For example, oxyhemoglobin and oxymyoglobin react with NO to form nitrate. The ferryl state of these globins also reacts with NO to reduce them to the Fe^{III} state, forming nitrite. This has led to the suggestion that the role of NO could be that of an antioxidant of oxoiron(IV) and oxoiron(IV) protein radicals to inhibit oxidative damage. In turn, the ferrylglobin-mediated oxidation of NO to nitrite may play a role in NO scavenging and detoxification. In the case of peroxidase enzymes, NO has been shown to increase the activity of some enzymes by accelerating reduction of compound **II** to the Fe^{III} state.

While synthetic examples do exist for the chemistry of superoxometal complexes and NO, knowledge of the fundamental reactivity between oxometal complexes and NO is limited. To gain insight into the reactivity of synthetic oxoiron(IV) complexes toward NO, the reaction of $[Fe^{IV}O(tmc)(OAc)]^{+}$ with NO, where the Fe center is coordinated by the macrocyclic nitrogen-donor ligand 1,4,8,11-tetramethyl-1,4,8,11-tetraazacyclotetradecane (tmc), has been investigated. This reaction caused reduction of the Fe^{IV} center to Fe^{II} and produced nitrite, which was identified in the form of $[Fe^{II}(tmc)(ONO)]^{+}$. Mechanistic studies have been conducted to distinguish between two possible pathways involving either oxygen atom or oxide(•1–) ion transfer from the $Fe^{IV}O$ group to NO.

As a result of studying the reactivity of a different oxoiron(IV) complex, $[Fe^{IV}O(N4Py)]^{2+}$, toward NO, the formation of Fe^{II} and nitrate was observed. Mechanistic studies have revealed a 2:1 stoichiometry between Fe^{IV} and NO. From these results, a mechanism can be proposed that includes an initial oxide(•1–) ion transfer from $Fe^{IV}O$ group to NO to form nitrite, followed by an oxygen atom transfer from a second equivalent of $[Fe^{IV}O(N4Py)]^{2+}$ to the nitrite intermediate to form nitrate. This second step

chemistry was confirmed by independently studying the reaction of $[Fe^{IV}O(N4Py)]^{2+}$ with nitrite to form nitrate.

There is also a biological inorganic chemistry in which metal nitrosyl species are oxidized to form innocuous nitrite or nitrate. In this context, the oxidation of the synthetic nitrosyl complex $[Fe(tmc)(NO)]^{2+}$ has been studied, which also produced $[Fe^{II}(tmc)(ONO)]^{+}$. The molecular structure of $[Fe^{II}(tmc)(ONO)]^{+}$ determined by X-ray crystallography indicates a bidentate binding mode of the nitrito ligand *via* both oxygen atoms. The oxidation results are consistent with a net oxide(•1–) ion transfer mechanism forming $[Fe^{II}(tmc)(NO_2)]^{+}$, followed by a subsequent linkage isomerization. For comparison purposes, several related, independently synthesized $[Fe^{II}(tmc)X]^{+}$ complexes ($X = NO_2^{-}$, NO_3^{-}, AcO^{-}) have been characterized by spectroscopic techniques, X-ray crystallography and differential pulse and cyclic voltammetry.

A final investigation involved studying the reactivity of a series of $[Fe^{IV}O(tmc)X]^{+}$ ($X = CF_3SO_3^{-}$, $CF_3CO_2^{-}$, AcO^{-}) complexes toward organic substrates by oxygen atom transfer and hydrogen atom abstraction to construct a reactivity trend depending on the strength of the axial ligand X.

Abstract Approved: _____
Thesis Supervisor

_____
Title and Department

_____
Date

OXIDATION OF NITROGEN MONOXIDE BY OXOIRON(IV) COMPLEXES: MECHANISTIC STUDIES AND RELATED INVESTIGATIONS WITH AN IRON NITROSYL COMPLEX

by

Travis Michael Owen

A thesis submitted in partial fulfillment
of the requirements for the Doctor of
Philosophy degree in Chemistry
in the Graduate College of
The University of Iowa

December 2012

Thesis Supervisor: Assistant Professor Jan-Uwe Rohde

Graduate College
The University of Iowa
Iowa City, Iowa

CERTIFICATE OF APPROVAL

_____

PH.D. THESIS

_____

This is to certify that the Ph.D. thesis of

Travis Michael Owen

has been approved by the Examining Committee
for the thesis requirement for the Doctor of Philosophy
degree in Chemistry at the December 2012 graduation.

Thesis Committee: _____
Jan-Uwe Rohde, Thesis Supervisor

_____
Christopher M. Cheatum

_____
Tori Z. Forbes

_____
Ernesto Fuentes

_____
Leonard R. MacGillivray

To my mother, Marva Kay Owen

ACKNOWLEDGMENTS

First of all I would like to thank my advisor, Jan-Uwe Rohde, as he has been a helpful and attentive mentor, aiding me in my growth as a research chemist and teacher, and is responsible for helping me increase my overall knowledge of chemistry.

My wife, Mary-Jane, has been my greatest supporter during our marriage, especially during our time in Iowa as I have pursued my degree. She has been understanding and sacrificed her own time so that I would be able to have time to achieve my goal of obtaining my degree. I can not be able to thank her enough for what she has meant to me in this process.

I would also like to thank my family, and specifically my parents, for encouraging me to pursue this dream and supporting me and my wife in this journey. I want to especially thank my mom, who is no longer living, for her unwavering support even during her last days fighting cancer. Also, a thank you to my grandfather and my wife's parents who have given additional support to me during this process.

Thank you to the current and past members of Dr. Rohde's research group, who have been very helpful from a day-to-day perspective on my efforts to complete my research tasks. Dr. Wei-Tsung Lee, Dr. Matthew Kelley, and Tony Manuel have been fantastic to work with and have made the process of working toward this degree easier due to their chemical knowledge and support.

During my time in the chemistry department, a lot of staff members have been instrumental in aiding me in my research efforts and I would like to thank them. Thanks to Dr. Dale Swenson for this assistance in collection of X-ray data and his help with questions in solving X-ray crystal structures. I would like to thank Dr. Lynn Teesch and Vic Parcell in the mass spectrometry facility for their assistance and patience in aiding me in operation of the instruments and collection of data, especially in unique situations. Thanks go to Dr. Earlene Erbe, Shonda Monette, and Brian Morrison in the instructional

laboratories as it has been a joy to work with them within my teaching assistant responsibilities, and they have been instrumental in helping to shape me as an educator.

Lastly, I would like to thank Sharon, Betty, Janet and Jessica in the administrative offices and chemistry center office. Without these ladies the handling of paperwork and logistics for attaining my degree, meeting deadlines, and teaching in this department would have been an even more mountainous task. All of the above mentioned staff have always been incredibly helpful, and I owe them all a great deal of gratitude in answering all of my questions throughout my time working on my degree. Thank you.

ABSTRACT

Reactions of the free radical nitrogen monoxide (NO) with metal–oxygen species of metalloproteins are relevant to NO metabolism and detoxification. For example, oxyhemoglobin and oxymyoglobin react with NO to form nitrate. The ferryl state of these globins also reacts with NO to reduce them to the Fe^{III} state, forming nitrite. This has led to the suggestion that the role of NO could be that of an antioxidant of oxoiron(IV) and oxoiron(IV) protein radicals to inhibit oxidative damage. In turn, the ferrylglobin-mediated oxidation of NO to nitrite may play a role in NO scavenging and detoxification. In the case of peroxidase enzymes, NO has been shown to increase the activity of some enzymes by accelerating reduction of compound **II** to the Fe^{III} state.

While synthetic examples do exist for the chemistry of superoxometal complexes and NO, knowledge of the fundamental reactivity between oxometal complexes and NO is limited. To gain insight into the reactivity of synthetic oxoiron(IV) complexes toward NO, the reaction of $[Fe^{IV}O(tmc)(OAc)]^{+}$ with NO, where the Fe center is coordinated by the macrocyclic nitrogen-donor ligand 1,4,8,11-tetramethyl-1,4,8,11-tetraazacyclotetradecane (tmc), has been investigated. This reaction caused reduction of the Fe^{IV} center to Fe^{II} and produced nitrite, which was identified in the form of $[Fe^{II}(tmc)(ONO)]^{+}$. Mechanistic studies have been conducted to distinguish between two possible pathways involving either oxygen atom or oxide(•1–) ion transfer from the $Fe^{IV}O$ group to NO.

As a result of studying the reactivity of a different oxoiron(IV) complex, $[Fe^{IV}O(N4Py)]^{2+}$, toward NO, the formation of Fe^{II} and nitrate was observed. Mechanistic studies have revealed a 2:1 stoichiometry between Fe^{IV} and NO. From these results, a mechanism can be proposed that includes an initial oxide(•1–) ion transfer from $Fe^{IV}O$ group to NO to form nitrite, followed by an oxygen atom transfer from a second equivalent of $[Fe^{IV}O(N4Py)]^{2+}$ to the nitrite intermediate to form nitrate. This second step

chemistry was confirmed by independently studying the reaction of $[Fe^{IV}O(N4Py)]^{2+}$ with nitrite to form nitrate.

There is also a biological inorganic chemistry in which metal nitrosyl species are oxidized to form innocuous nitrite or nitrate. In this context, the oxidation of the synthetic nitrosyl complex $[Fe(tmc)(NO)]^{2+}$ has been studied, which also produced $[Fe^{II}(tmc)(ONO)]^{+}$. The molecular structure of $[Fe^{II}(tmc)(ONO)]^{+}$ determined by X-ray crystallography indicates a bidentate binding mode of the nitrito ligand *via* both oxygen atoms. The oxidation results are consistent with a net oxide(•1–) ion transfer mechanism forming $[Fe^{II}(tmc)(NO_2)]^{+}$, followed by a subsequent linkage isomerization. For comparison purposes, several related, independently synthesized $[Fe^{II}(tmc)X]^{+}$ complexes ($X = NO_2^{-}$, NO_3^{-}, AcO^{-}) have been characterized by spectroscopic techniques, X-ray crystallography and differential pulse and cyclic voltammetry.

A final investigation involved studying the reactivity of a series of $[Fe^{IV}O(tmc)X]^{+}$ ($X = CF_3SO_3^{-}$, $CF_3CO_2^{-}$, AcO^{-}) complexes toward organic substrates by oxygen atom transfer and hydrogen atom abstraction to construct a reactivity trend depending on the strength of the axial ligand X.

TABLE OF CONTENTS

LIST OF TABLES

Table

LIST OF FIGURES

Figure

LIST OF SCHEMES

Scheme

CHAPTER 1

INTRODUCTION

This thesis covers the investigation of oxidizing nitrogen monoxide (NO) through the use of nonheme iron complexes. Additionally, it covers some related syntheses and reactivity of the nonheme iron complexes. It has been reported in the literature that NO can be oxidized by metal–oxygen species and metal nitrosyls can be oxidized by oxygen to form nitrite and nitrate. Results reported in this thesis show that the high-valent nonheme oxoiron(IV) complexes react with NO to form a nonheme nitrosyliron(II) complex reacts with trimethylamine *N*-oxide to form nitrite *via* an oxide(•1–) ion transfer mechanism.

Examples of both biological and synthetic metal–oxygen species and their reactivity toward NO will be discussed in Chapter 2. Further reactivity of some of these metal–oxygen species will also be covered. The area of NO oxidation by superoxometal complexes has been investigated with both biological (globins, enzymes) and synthetic complexes, with a proposed mechanism involving a peroxynitrite rearrangement. However, the knowledge of NO oxidation by oxometal complexes is not as nearly complete. Some work with ferryl myoglobin and hemoglobin, along with a range of synthetic oxometal complexes has been completed, resulting in proposed or inferred products, but no insight into the mechanisms by which these reactions occur. An appropriate and thorough study of the oxidation of NO by an oxometal complex is necessary and would provide a view into the fundamental reactivity of these complexes.

The synthesis and characterization of iron(II) complexes of the nonheme tetraamine ligand 1,4,8,11-tetramethyl-1,4,8,11-tetraazacyclotetradecane (tmc) will be covered in Chapter 3. Investigation of the reduction/oxidation potentials of these complexes will be discussed in context of the accessibility of the iron(III) oxidation state. Discussion of the single crystal X-ray structures will include the bidentate binding modes

of the nitritoiron(II) and nitratoiron(II) complexes, making them a unique example of six-coordiante iron(II) complexes of tmc. Spectroscopic characterization of the iron(II) complexes have been shown to be consistent with results of the single crystal X-ray crystallography.

The reactivity of the high valent oxoiron(IV) complex of tmc toward NO will be discussed in Chapter 4. This reaction results in the reduction of Fe^{IV} to Fe^{II} and the production of nitrite, observed as the nitritoiron(II) complex of tmc using electrospray mass spectrometry (ESI MS). Monitoring of the reaction by UV–Vis spectroscopy and ESI MS reveals an Fe^{III} intermediate that is able to be observed for approximately 15 minutes after initiation of the reaction. Quantification of the nitrite product reveals 1 equiv of nitrite formed with respect to iron. This study has revealed that the oxo ligand is transferred to NO to form the nitrite product by an oxide(•1–) ion transfer mechanism. This chapter provides an example of a mechanistic study of the oxidation of NO by a synthetic biological oxometal complex.

The generation of a previously known nitrosyliron(II) complex of tmc is revisited in Chapter 5, within the context of examining its reactivity with the O atom donor, trimethylamine *N*-oxide. The results of this reaction include the formation of 1 equiv of nitrite, quantified in the same manner as in chapter 4, using ESI MS and isotopically labeled ^{15}N nitrite. My studies indicate that the reaction proceeds through an oxide(•1–) ion transfer mechanism, followed by a linkage isomerization to go from the N-bound to the O-bound nitritoiron(II) product. Analysis of single crystal X-ray diffraction data depicts the nitrito ligand to be bidentate, identical to the independently synthesized nitritoiron(II) complex of tmc described in Chapter 3.

The reaction of a different oxoiron(IV) complex, supported by the ligand [bis(2-pyridyl)methyl]bis(2-pyridylmethyl)amine) (N4Py), with NO is discussed in Chapter 6. This reaction results in a 2:1 stoichiometry between Fe^{IV} and NO, in which nitrate and Fe^{II} are formed as products. Mechanistic studies utilizing UV–Vis and IR

spectroscopy and ESI MS revealed a two-step mechanism – an initial oxide(•1–) ion transfer from Fe^{IV} to NO to form nitrite, followed by an oxygen atom transfer from a second equivalent of Fe^{IV} to nitrite to form nitrate. The chemistry of the second step was investigated by reacting $[Fe^{IV}O(N4Py)]^{2+}$ with nitrite to confirm a 1:1 stoichiometry between Fe^{IV} and nitrite, in which mechanistic studies support an oxygen atom transfer to form Fe^{II} and nitrate.

The reactivity of a series of oxoiron(IV) complexes of tmc with organic substrates are described in Chapter 7. The complexes $[Fe^{IV}O(tmc)X]^{+}$, where X = TfO^{-}, AcO^{-}, $CF_3CO_2^{-}$, have been reacted with phosphines, and the relative rates of reactions have been compared. This reaction has been known to for oxoiron(IV) complexes of tmc to proceed through an O atom transfer mechanism. The reaction of each complex with triphenylphosphine forms 1 equiv of triphenylphosphine oxide as monitored by ^{31}P NMR. In another set of reactions, the oxoiron(IV) complexes were reacted with the organic substrate 9,10-dihydroanthracene, proceeding through a known H atom abstraction mechanism. When comparing the two reactivity modes in regard to this series of oxoiron(IV), a trend has emerged in which a electron donating axial ligand, trans to the oxo ligand, results in faster reaction with 9,10-dihydroanthracene, while the reactivity toward triphenylphosphine is enhanced by an electron donating axial ligand.

CHAPTER 2
BACKGROUND

2.1 Introduction

The oxidation of nitrogen monoxide (NO) is a process that merits time and energy into further understanding, as shown by the years of efforts and publications that have gone into revealing information on this chemical process. The biological relevance of NO lies in many roles that NO holds[1-5]. Among other things, NO acts as a regulatory molecule in controlling blood pressure, it assists in alleviating inflammation within the body, participates as a signaling molecule in neurotransmission processes (especially located within the brain), is generated and used by the body as a toxic defense molecule to attack intruding entities within the body, and recently has been considered to be able to act as an antioxidant by the body in removing reactive oxygen species (ROS) that are damaging to biological tissues.

This role as an antioxidant is particularly interesting in the area of ROS that involve transition metal complexes. Transition metal complexes are often at the active site of enzymes, and in some cases ROS can be generated as intermediates of the enzymatic cycles. As NO is a biologically relevant small molecule that may aid in removing these ROS during the course of an enzymatic cycle, specific efforts have gone into studying the reaction between metal–oxygen species over the concern of how these interactions may take place within a biological system. A number of biological systems and synthetic models of biological systems have been used to study reactions with NO to further understand how NO is oxidized within the body. We have utilized multiple synthetic oxometal complexes to fully study the oxidation of NO as well as a related study involving a nitrosyl complex (in which NO is a ligand, bound to a transition metal).

This chapter begins with a background look at different metal–oxygen species, both biological and synthetic, and their studied reactions with NO. In some cases mechanistic studies have been carried out and proposed pathways for the studied reactions have been included. Substantial work has been done with some biological examples and provides insight into how nitrate can be formed from the oxidation of NO. Reactions of analogous synthetic complexes with NO have also been included and in some cases are not as thorough in their mechanistic approach and leave room for giving a more detailed mechanistic study. Also, there are included studies done on the oxidation of biological and synthetic examples of nitrosyl complexes. While a select few have provided very thorough studies, most provide results that could be expanded upon to better understand the chemistry behind this oxidation process. Lastly, background on oxoiron(IV) complexes and their reactivity will be discussed as they are the metal–oxygen species that are used in the studies covered in this thesis.

2.2 Oxidation of NO with Biological Metal–Oxygen Species

2.2.1 Oxidation of NO by Superoxometal Complexes

Reactions of the free radical NO with metal–oxygen species of metalloproteins have been recognized as mechanisms relevant to NO metabolism and detoxification *in vivo*. For example, oxygenated metalloproteins such as oxyhemoglobin and oxymyoglobin react rapidly with NO causing dioxygenation to nitrate (Scheme 1).[6-10]

Scheme 1. Oxidation of NO with Oxyhemoglobin or Oxymyoglobin

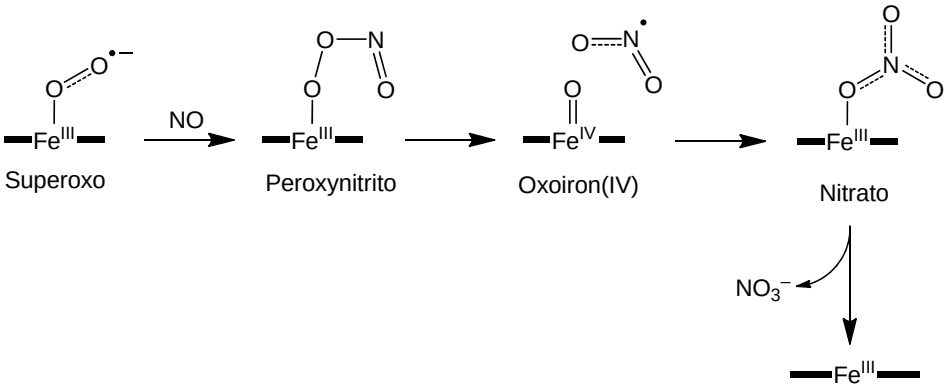

Fe = heme

Thorough studies have been completed in this area investigating the products formed, reaction kinetics, and mechanism determinations of the oxidation of NO with these oxy-globins in solution.

2.2.2 Oxidation of NO by Oxometal Complexes

The reaction of NO with the ferryl state of hemoglobin and myoglobin and related proteins is of interest, as well. Studies with several globins have shown that NO can efficiently and rapidly reduce the high-valent state to the Fe^{III} state with concomitant formation of innocuous nitrite.[1-2,11-13] It has been suggested that the role of NO could be that of an antioxidant of oxoiron(IV) and oxoiron(IV) protein radical species to inhibit oxidative damage (Scheme 2).[1-2,11-17]

Scheme 2. Oxidation of NO by Ferrylglobin or Ferrylglobin Porphyrin Cation Radical

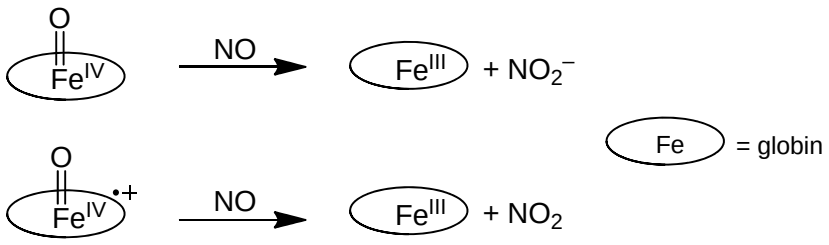

Conversely, the transformation of NO into nitrite mediated by ferryl globins may be important as a mechanism for NO scavenging and detoxification.[1-2,11-13] Nitric oxide may then be viewed as a substrate for globins displaying peroxidase activity.[12-13]

2.2.3 Reaction of NO with Metal–Oxygen species of enzymes

In reactions of NO with the compounds **I** of peroxidase enzymes, reduction occurs in two one-electron steps *via* compound **II** to the Fe^{III} state (Scheme 3).[18-21] At low NO levels, NO increases the activity of some peroxidases, and this effect has been linked to the ability of NO to accelerate the reduction of compound **II** to the Fe^{III} state which is the rate-limiting step in the catalytic cycles of these enzymes.[19-21]

Scheme 3. Oxidation of NO by Compound **I** and **II** of a Peroxidase Enzyme

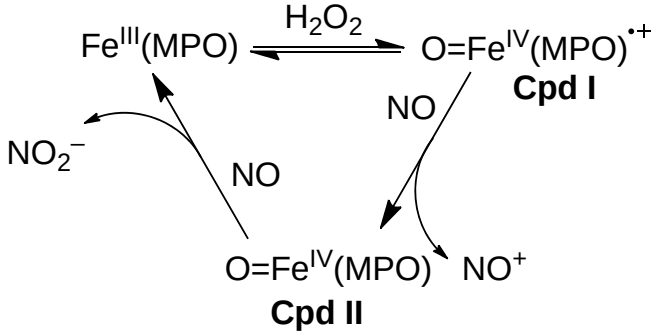

Similar to the interaction between NO and ferryl globins, the idea of a bidirectional relationship between NO and peroxidases has been put forward where NO affects peroxidase catalaysis and compound **I** functions as a sink for NO.[19-21] Also, catalase has been reported to consume NO in the presence of H_2O_2, presumably by reaction of NO with catalase compound **I**.[22] Lastly, the possibility of a direct reaction between the ferryl group of cytochrome *bd* and NO has been discussed in the context of inhibition of this oxidase by NO.[23]

2.2.4 Oxidation of NO by Synthetic Metal–Oxygen Species

While synthetic precedent exists for the chemistry of superoxometal complexes and NO showing conversion of NO into peroxynitrite and subsequently into nitrate, nitrite and/or nitrogen dioxide,[24-31] knowledge of the fundamental reactivity between oxometal complexes and NO is limited. Studies with Cr and Mn complexes suggested that the reactions of oxometal species with NO are very fast.[27,32-34] For example, the first step in the NO reaction of aqueous $Cr^{IV}O^{2+}(aq)$ is too fast to be observed spectrophotometrically, but $Cr^{III}(ONO)^{2+}(aq)$ is believed to be the primary product based on its decay kinetics.[27] In another case, photolysis of the macrocyclic ligand complex *trans*-$[Cr^{III}([14]aneN_4)(ONO)_2]^+$ generated a transient species, proposed to be the corresponding $Cr^{IV}O$ complex, which underwent rapid recombination with NO ([14]aneN$_4$ = 1,4,8,11-tetraazacyclotetradecane or cyclam) (Scheme 4).[32-33]

Scheme 4. Photolytic Formation of Oxochromium(IV) and NO

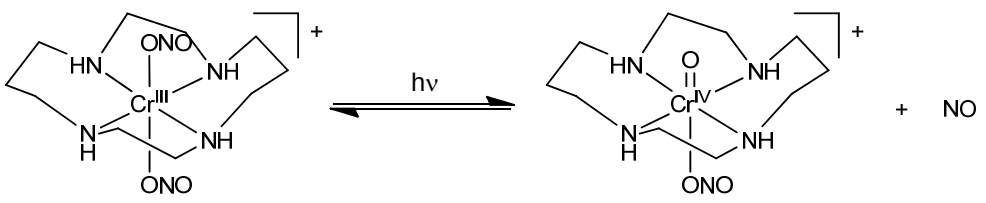

The reactions of oxoiron(IV) porphyrin π-cation radicals, $[Fe^{IV}O(tpfpp)^{+\bullet}]^{+}$ and $[Fe^{IV}O(ppIX)^{+\bullet}]^{+}$, with NO were studied in the gas phase (H_2tpfpp = 5,10,15,20-tetrakis(2,3,4,5,6-pentafluorophenyl)-21*H*,23*H*-porphine; H_2ppIX = 7,12-diethenyl-3,8,13,17-tetramethyl-21*H*,23*H*-porphine-2,18-dipropanoic acid or protoporphyrin IX).[35-37] These reactions were proposed to proceed through oxygen-atom transfer, because the corresponding iron(III) porphyrins, which are two oxidizing equivalents below the oxoiron(IV) porphyrin π-cation radicals, were detected as primary products.[35-37] Consequently, NO_2 was inferred as the product of oxidation of NO. In contrast, the reaction of electrochemically generated oxoiron(IV) and oxomanganese(IV) porphyrins with NO in aqueous solution yielded nitrite.[38-40] These studies serve as examples of oxidations of NO by oxometal complexes, but are not thorough from a mechanistic point of view.

In the reverse direction, some oxo complexes and NO were produced irreversibly by thermal or photo-induced dissociation of nitrito complexes[41-43] of Mn^{III} and Cr^{III} and by oxygen-atom transfer[44] from NO_2 to a Cr^{III} complex. Other examples of reactions related to NO reactivity of oxo complexes are nitrogen-atom-transfer reactions from nitrido complexes to NO, which have been reported to liberate N_2O.[45-46]

2.3 Oxidation of Metal–Nitrosyl Complexes

2.3.1 Oxidation of Biological Nitrosyl Complexes

Looking at the oxidation of NO from the viewpoint of switching the roles of NO and oxidant leaves the reaction of a metal–nitrosyl complex oxidized by an external oxidant. In the case of the nitrosyl state of hemoglobin or myoglobin, the reaction with oxygen has been studied to find that nitrate is formed.[47] Mechanistic studies of the reaction determined that the oxidation proceeds through an initial dissociation of the

nitrosyl ligand, followed by subsequent binding of the oxygen molecule to the iron in the heme unit. The reaction then proceeds through the same mechanism as described for the reaction of oxyhemoglobin or oxymyoglobin with NO (Scheme 5).

Scheme 5. Reaction of Nitrosylhemoglobin or Nitrosylmyoglobin with O_2.

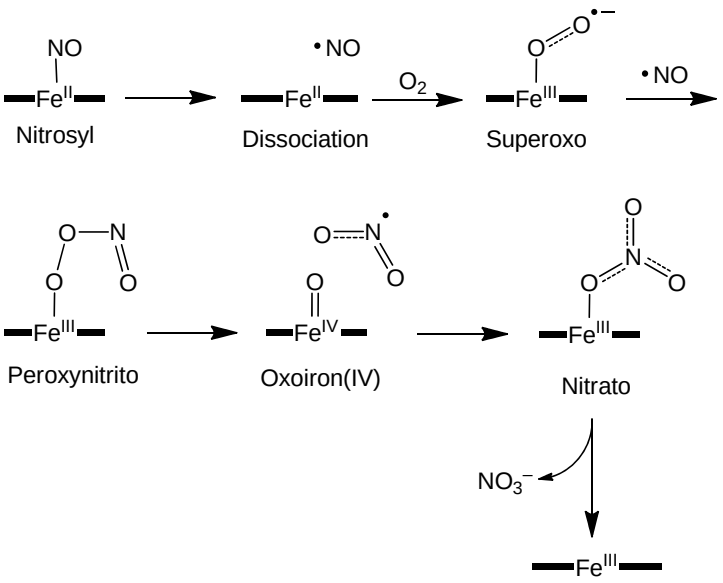

▬Fe▬ = heme

This provides an interesting example in which the activation of NO as the nitrosyl ligand did not increase the reactivity of NO, but instead the activation of oxygen is required to then react with NO.

2.3.2 Oxidation of Synthetic Nitrosyl Complexes

While some synthetic studies on the oxidation of synthetic nitrosyl complexes have been carried out, they lack in thorough mechanistic studies, normally only collecting

some product characterization and suggestions of probable mechanisms based on biological examples.[48-50] Some of the examples include metal complexes with multiple nitrosyl ligands that are oxidized by O_2 to form nitrate[48-49], and there is an example of a copper–nitrosyl complex that, when oxidized with O_2, forms nitrite through a proposed peroxynitrite intermediate followed by subsequent self-decay.[50]

2.4 Reactivity of Oxometal Complexes

Synthetic oxoiron(IV) complexes are relatively unstable, and only a select group of ligands can stabilize these high-valent oxidation states of iron. The equatorial coordination of iron by the macrocyclic ligand 1,4,8,11-tetramethyl-1,4,8,11-tetraazacylcotetradecane (tmc) offers a stabilizing environment for the Fe^{IV}=O group. The established reactivity modes of oxoiron(IV) complexes include oxygen-atom transfer to organic substrates and other iron complexes, hydrogen-atom abstraction, electron transfer, and hydride transfer (Scheme 6).[51-53]

Scheme 6. Reactivity Modes of $Fe^{IV}O$(tmc) Complexes.

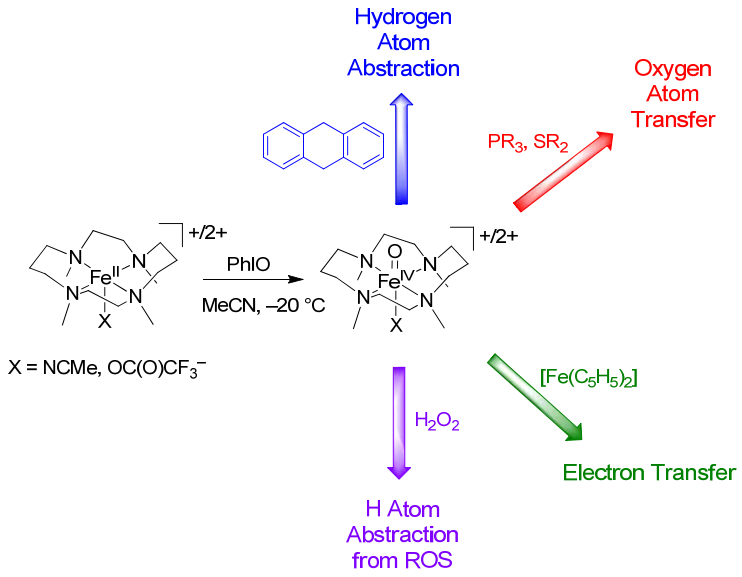

The $Fe^{IV}O$ group can also be stabilized by the pentadentate ligand N,N-bis(2-pyridylmethyl)-N-(bis-2-pyridylmethyl)amine (N4Py). Within the efforts of generating the $Fe^{IV}O$ moiety stabilized by the N4Py ligand, there has been the observation of an Fe^{III}(N4Py) complex,[54] and the Fe^{III} dimer $[Fe^{III}_2O(N4Py)_2]^{4+}$ has been isolated and its structure shown.[55] The complex $[Fe^{IV}O(N4Py)]^{2+}$ has been generated,[56-58] and the structure presented[59] relatively recently. Since then, significant amount of research has been done on this oxoiron(IV) complex in the context of the known reactivity modes of $Fe^{IV}O$ complexes shown in Scheme 6.[60-65]

2.5 Conclusion

Oxidation of nitrogen monoxide by metal–oxygen species is a very important reaction, particularly in the context of biological reactions. Along with many roles in which NO plays within the body, the one as a potential antioxidant to ROS needs further investigation. Providing further insight into this chemistry is an important task as much of the work in the current literature is not fully-detailed. The interesting possibilities that come with the investigation of synthetic, nonheme high-valent oxoiron(IV) complexes and their reactivity with NO is that it provides an accessible metal–oxygen species with which to probe this oxidation of NO to a more thorough level. The ability to investigate the oxidation of NO as a bound, activated nitrosyl ligand is also possible, and will provide more information into how the chemistry between metal complexes and the oxidation of NO takes place. We have studied the reaction of two oxoiron(IV) complexes, $[Fe^{IV}O(tmc)(OAc)]^+$ and $[Fe^{IV}O(N4Py)]^{2+}$ with NO. Additionally, we have studied the oxidation of a nitrosyl complex, $[Fe(tmc)(NO)]^{2+}$, with an external oxidant. While complementing the known reactivity of oxoiron(IV) complexes, the reactions studied, along with independent studies on the products resulting from these reactions, help further the fundamental understanding of the oxidation of nitrogen monoxide.

CHAPTER 3

SYNTHESIS AND CHARACTERIZATION OF IRON(II) COMPLEXES OF 1,4,8,11-TETRAMETHYL-1,4,8,11-TETRAAZACYCLOTETRADECANE (TMC)

3.1 Introduction

In this chapter the synthesis of new Fe^{II} complexes supported by the macrocyclic ligand 1,4,8,11-tetramethyl-1,4,8,11-tetraazacyclotetradecane (tmc) will be covered. The syntheses of these complexes are all carried out by reacting an Fe^{II}(tmc) starting material, $[Fe(tmc)\{OS(O)_2CF_3\}]CF_3SO_3$ with the sodium salt of the X ligand to be exchanged with the bound $CF_3SO_3^-$ (X = NO_2^-, NO_3^-, $CH_3CO_2^-$). This exchange is completed in a nitromethane–methanol solution under an inert atmosphere. These complexes have been characterized by ultraviolet–visible (UV–Vis) and infrared (IR) spectroscopy, electrospray ionization mass spectrometry (ESI MS), and elemental analysis. As determined by spectroscopic methods and single-crystal X-ray diffraction, the nitrito and nitrato ligands bind to the Fe^{II} center in a bidentate fashion and are unique examples of six-coordinate Fe^{II}(tmc) complexes. The bidentate binding mode of the nitrito ligand is *via* two oxygen atoms. In addition, the acetato ligand has been determined to bind in a monodentate fashion to the Fe^{II} center. The nitritoiron(II) complex displays a feature in the visible region of the absorption spectrum distinguishing it from the other Fe^{II}(tmc) complexes which are without absorption bands in the visible region of the spectrum. The binding modes determined from the IR spectra of the nitratoiron(II) and acetatoiron(II) complexes are consistent with literature data[66] for other complexes and the X-ray diffraction data. Attempts at identifying bands in the IR spectrum of the nitritoiron(II) complex attributable to bound nitrite were futile due to bands from the tmc ligand and $CF_3SO_3^-$ counterion blocking the spectral ranges where the nitrito bands were expected to be observed.[66]

These complexes were also subjected to differential pulse voltammetry (DPV) and cyclic voltammetry (CV). The electrochemical measurements show that these complexes have oxidation events at relatively high potentials and that the oxidations are irreversible. This can be interpreted as indication of unstable, difficult to achieve, Fe^{III} complexes of the studied ligands. This is consistent with what is known in the literature about Fe^{III}(tmc) complexes; they are very rare and unstable.[67-68]

3.2 Experimental Section

3.2.1 Materials and Methods

Materials. All reagents and solvents were purchased from commercial sources and were used as received, unless noted otherwise. Acetonitrile, dichloromethane, and diethyl ether were deoxygenated by sparging with N_2 and purified by passage through two packed columns of molecular sieves under an N_2 pressure (MBraun solvent purification system). Anhydrous methanol (99.8%) was used as received. Nitromethane was refluxed over CaH_2 under an Ar atmosphere, distilled, and passed through a column of basic Al_2O_3.[69] Preparation and handling of air- and moisture-sensitive materials were carried out under an inert gas atmosphere by using standard Schlenk and vacuum line techniques or a glovebox. $Fe(OTf)_2{\cdot}2MeCN$ was synthesized by a modified literature method[70] from anhydrous $FeCl_2$ and trimethylsilyl trifluoromethanesulfonate in acetonitrile and recrystallized from acetonitrile–diethyl ether (TfOH = CF_3SO_3H, trifluoromethanesulfonic or triflic acid).[71] The ligand 1,4,8,11-tetramethyl-1,4,8,11-tetraazacyclotetradecane (tmc)[72] and [Fe^{II}(tmc)(OTf)]OTf,[73] **1**–OTf(OTf), were prepared following published procedures. The complex **1**–OTf(OTf) was stored in an N_2 atmosphere. Isotope-enriched $Na^{15}NO_2$ (98% ^{15}N) and $Na^{15}NO_3$ (98% ^{15}N) were purchased from Cambridge Isotope Laboratories, Andover, MA, USA.

Physical Methods. UV–Visible spectra were recorded on an HP 8453A diode array spectrophotometer (Agilent Technologies) with samples maintained at the desired temperature using a cryostat/heater from Unisoku Scientific Instruments, Japan. IR spectra were recorded on a Bruker Vertex 70 Fourier-transform IR spectrometer using samples prepared by grinding the solid compound with KBr and pressing the mixture into a disk. The complexes **1**–OTf, **1**–OTf, **1**–OTf and **1**–OTf were prepared using gentle grinding of the sample with KBr, and pellets were formed at 5000 psi and for 30 s. Mass spectral data were acquired on a quadrupole ion trap ThermoFinnigan LCQ Deca mass spectrometer using an electrospray ionization source. Electrochemical measurements were carried out with a CH Instruments potentiostat (Model 620C Electrochemical Analyzer) and a standard three-electrode configuration consisting of a Pt working electrode, a Pt wire counter electrode and a $Ag/AgNO_3$ reference electrode (0.01 M $AgNO_3$ in nitromethane; supporting electrolyte, 0.1 M NBu_4ClO_4). Voltammograms were recorded on solutions of the analyte (0.001 M) and the supporting electrolyte (0.1 M NBu_4ClO_4) in nitromethane under an Ar atmosphere at 295 K with scan rates ranging from 0.05–0.5 $V \cdot s^{-1}$ for CV and a potential increment of 4 mV, an amplitude of 50 mV, and a pulse period of 0.2 s for DPV. Potentials are reported referenced to an external $[FeCp_2]/[FeCp_2]^+$ redox system, which can be converted to the SCE scale by adding 0.34 V (SCE, aqueous saturated calomel electrode).[74-75] Potentials relative to SCE can be converted to the NHE scale by adding 0.24 V (NHE, normal hydrogen electrode).[76] (*Caution:* Mixtures of perchlorate salts and metal complexes are potentially explosive and should be handled with care.)

3.2.2 Preparation of Iron(II) Complexes

Synthesis of [Fe(tmc)(O_2N)]OTf [1–ONO(OTf)]. Upon addition of a solution of 22.8 mg (0.33 mmol) of $NaNO_2$ in 1.5 mL of methanol to a solution of 0.20 g (0.33

mmol) of [Fe(tmc)(OTf)]OTf [**1**–OTf(OTf)] in 3.5 mL of nitromethane under stirring at 20 °C in an inert atmosphere, the color of the solution changed immediately from colorless to yellow. Isotopically-labeled 1–$O^{15}NO$ was synthesized in an analogous manner. After 1 h, the solvents were removed under reduced pressure. The residue was redissolved in dichloromethane and the complex recrystallized from vapor diffusion of diethyl ether into the complex solution at –35 °C. Crystals were collected *via* fractional crystallization with the termination of collection determined by the loss of color in the mother liquor. Single crystals of X-ray diffraction quality which were orange plates were grown in 2–5 days. Yield: 130 mg (78%). Anal. Calcd for $C_{15}H_{32}F_3FeN_5O_5S$: C, 35.51; H, 6.36; N, 13.80; S, 6.32. Found, C, 35.69; H, 6.41; N, 13.94; S, 6.47. ESI(+)MS ($MeNO_2$) *m/z* calcd for $C_{14}H_{32}FeN_5O_2$ ({**1**–ONO}$^+$), 358.19; found, 358.1 ({**1**–ONO}$^+$), 328.1 ({**1**–ONO – NO}$^+$), 257.3 ({tmc + H}$^+$). UV–Vis ($MeNO_2$) λ_{max}, nm (ε): 440 (180).

Synthesis of [Fe(tmc)(O_2NO)]OTf [1–ONO_2(OTf)]. Upon addition of a solution of 28.1 mg (0.33 mmol) of $NaNO_3$ in 1.5 mL of methanol to a solution of 0.20 g (0.33 mmol) of **1**–OTf(OTf) in 3.5 mL of nitromethane under stirring at 20 °C in an inert atmosphere, the color of the solution changed immediately from colorless to pale yellow. Isotopically-labeled 1–$O^{15}NO_2$ was synthesized in an analogous manner. After 1 h, the solvents were removed under reduced pressure. The residue was redissolved in dichloromethane and the complex recrystallized from vapor diffusion of diethyl ether into the complex solution at –35 °C. Crystals were collected *via* multiple recrystallizations. Crystals of **1**–ONO_2 and NaOTf formed simultaneously, thus physical separation of the yellow crystals of **1**–ONO_2 from the white crystals of NaOTf was required with each recrystallization attempt. The recrystallization process was complete when only yellow crystals representative of the **1**–ONO_2 product were present. Single crystals of X-ray diffraction quality which were yellow plates were grown from the final recrystallization in 2–5 days. Yield: 35 mg (20%). Anal. Calcd for $C_{15}H_{32}F_3FeN_5O_6S$: C, 34.42; H, 6.16; N, 13.38; S, 6.13. Found, C, 34.77; H, 6.16; N, 12.90; S, 6.30. ESI(+)MS ($MeNO_2$) *m/z*

calcd for $C_{14}H_{32}FeN_5O_3$ ({**1**–ONO_2}$^+$), 374.19; found, 374.1 ({**1**–ONO_2}$^+$), 328.2 ({**1**–ONO_2 – NO_2}$^+$), 461.3 ({**1**–OTf}$^+$), 257.3 ({tmc + H}$^+$). IR (KBr, cm^{-1}): 1492 (ν_{NO}), 740 (δ_{NO3}). IR for **1**–$O^{15}NO_2$(OTf) (KBr, cm^{-1}); 1472 (ν_{NO}), 739 (δ_{NO3}).

Synthesis of [Fe(tmc)(OC(O)CH$_3$)]OTf [1–OAc(OTf)]. Upon addition of a solution of 27.1 mg (0.33 mmol) of NaAcO in 1.5 mL of methanol to a solution of 0.20 g (0.33 mmol) of **1**–OTf(OTf) in 3.5 mL of nitromethane under stirring at 20 °C in an inert atmosphere, the color of the solution changed immediately from colorless to pale pink. After 1 h, the solvents were removed under reduced pressure. The residue was redissolved in dichloromethane and the complex recrystallized from vapor diffusion of diethyl ether into the complex solution at –35 °C. Crystals were collected *via* fractional crystallization with the termination of collection determined by the loss of color in the mother liquor. Single crystals of X-ray diffraction quality which were lavender cubes were grown in 2–5 days. Yield: 115 mg (67%). Anal. Calcd for $C_{17}H_{35}F_3FeN_4O_5S$: C, 39.24; H, 6.78; N, 10.77; S, 6.16. Found, C, 39.21; H, 6.59; N, 10.92; S, 6.10. ESI(+)MS ($MeNO_2$) *m/z* calcd for $C_{17}H_{35}FeN_4O_2$ ({**1**–OAc}$^+$), 371.21; found, 371.3 ({**1**–OAc}$^+$), 328.2 ({**1**–OAc – CH_3CO}$^+$). IR (KBr, cm^{-1}): 1623 [$\nu_{as}(CO_2)$], 1327 [$\nu_s(CO_2)$].

3.2.3 X-ray Crystallographic Analyses

A single crystal of each compound was coated with Paratone N oil and mounted on a glass capillary for data collection at 190(2) or 210(2) K on a Nonius KappaCCD diffractometer using Mo *Kα* radiation (graphite monochromator). The temperature was controlled by an Oxford Cryostream Cooler (700 series, N_2 gas). Data collection, data reduction, and absorption correction were carried out following standard CCD techniques using the software packages Collect and HKL-2000. Final cell constants were calculated from 9737, **1**–ONO(OTf), 10200, **1**–ONO_2(OTf), or 10791 **1**–OAc(OTf), reflections from the complete data set. The space groups $P2_1/c$, **1**–ONO(OTf), $P2_1/c$, **1**–ONO_2(OTf), and

$P2_1/n$, **1**–OAc(OTf), were determined based on systematic absences and intensity statistics. The structures were solved by direct methods and refined by full-matrix least-squares minimization and difference Fourier methods (SHELXTL v.6.12). All non-hydrogen atoms were refined with anisotropic displacement parameters. All hydrogen atoms were placed in ideal positions and refined as riding atoms with relative isotropic displacement parameters. For **1**–ONO(OTf), the final full-matrix least-squared refinement converged to $R1 = 0.0494$ and $wR2 = 0.1177$ (F^2, all data). For **1**–ONO_2(OTf), the final full-matrix least-squared refinement converged to $R1 = 0.0846$ and $wR2 = 0.1558$ (F^2, all data). For **1**–OAc(OTf), the final full-matrix least-squared refinement converged to $R1 = 0.0445$ and $wR2 = 0.0833$ (F^2, all data). Tables 1–3 contain additional crystal refinement information. Selected distances and angles are summarized in Tables 4–6.

3.3 Results and Discussion

3.3.1 Synthesis and Characterization of $[Fe^{II}(tmc)X]^+$ Complexes

The complexes [Fe(tmc)(O_2N)]OTf, **1**–ONO(OTf), [Fe(tmc)(O_2NO)]OTf, **1**–ONO_2(OTf), and [Fe(tmc)(OAc)]OTf, **1**–OAc(OTf), were synthesized from a methanol solution of $NaNO_2$, $NaNO_3$, or NaAcO and a nitromethane solution of [Fe(tmc)(OTf)]OTf, **1**–OTf(OTf) (Scheme 7). Mixing of the two solutions under an inert atmosphere resulted in the ligand substitution of TfO^-, forming the respective new iron(II) complexes, indicated by immediate color changes. The complex solution of **1**–ONO became yellow, **1**–ONO_2 became pale yellow, and **1**–OAc became pale pink in color. After 1 h, the product solutuion was evaporated to dryness and the residues were dissolved in dichlormethane and recrystallized by vapor diffusion of diethyl ether into the

complex solution at –35 °C. Yields of 78%, 20% and 67% were obtained for **1**–ONO, **1**–ONO_2 and **1**–OAc, respectively. The yield for **1**–ONO_2 is appreciably lower due to the difficulty in separation resulting from the **1**–ONO_2(OTf) product and NaOTf crystallizing at the same rate.

Scheme 7. Synthesis of Fe^{II}(tmc) Complexes **1**–ONO, **1**–ONO_2 and **1**–OAc.

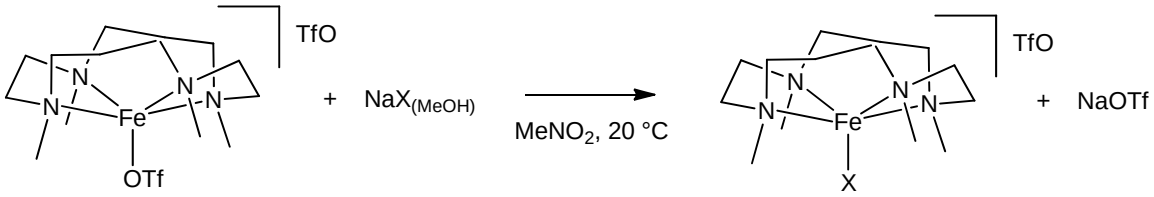

The product was separated from the byproduct over five recrystallizaiton attempts. ESI(+) mass spectrometry indicated the formation of the new complexes by observation of *m/z* = 358, 374, and 371 for complexes **1**–ONO, **1**–ONO_2 and **1**–OAc respectively. The relative binding strength of the X ligands were assessed by viewing mass spectra which contained equal mixtures of X ligands. The NO_2^- and AcO^- ligands have very similar binding strengths due to the peaks with *m*/*z* values due to both **1**–ONO and **1**–OAc being present in a spectrum of a solution containing a mixture of each.

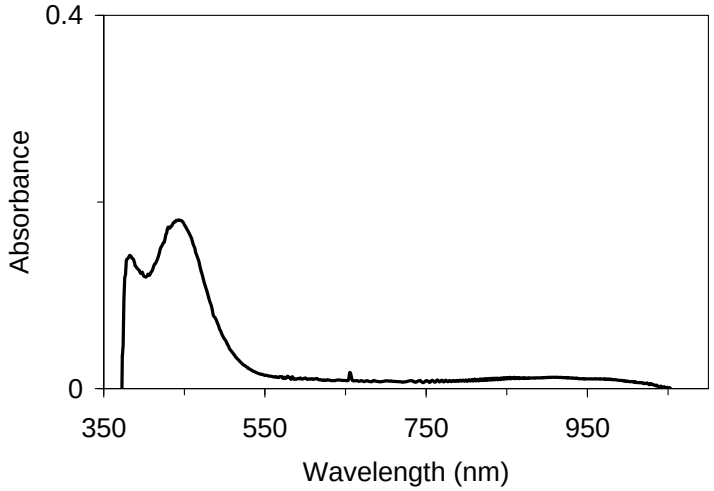

Figure 1. UV–Vis spectrum of 1 mM **1**–ONO in nitromethane (path length, 1 cm).

The NO_3^- ligand is weaker than NO_2^- or AcO^- since when it is mixed with either **1**–ONO or **1**–OAc, the *m*/*z* signal for **1**–ONO_2 is not observed. UV–Vis spectroscopy was not useful for **1**–ONO_2 and **1**–OAc because bands that may exist are not able to be observed in the employed wavelength range due to the solvent cutoff at *ca*. 380 nm. However, **1**–ONO does show a band (λ_{max} = 440 nm, ε = 180 $M^{-1}\cdot cm^{-1}$) that is easily discernible (Figure 1).

3.3.2 Crystal Structures

Single crystals of **1**–ONO(OTf) (orange plates), **1**–ONO_2(OTf) (yellow plates), and **1**–OAc(OTf) (lavender cubes), were each grown by vapor diffusion of diethyl ether into a solution of dichloromethane (**1**–ONO_2 and **1**–OAc) or nitromethane (**1**–ONO) upon standing at –35 °C. The solid-state molecular structures of all three compounds were determined from crystallographic analyses and confirm the bidentate binding mode of the nitrato and nitrito ligands in **1**–ONO_2 and **1**–ONO, and the monodentate binding mode of the acetato ligand in **1**–OAc suggested by IR spectroscopy.

It should be noted that the single crystal used for the crystallographic analysis of **1**–ONO shown here was grown from a product solution from the reaction of $[Fe(tmc)(NO)]^{2+}$ with trimethylamine *N*-oxide that will be discussed in Chapter 5. Crystallographic analysis was also carried out on a single crystal from the independently synthesized **1**–ONO(OTf). Due to disorder in a $CF_3SO_3^-$ counterion, the overall refinement was of lower quality. However, the refined structure from the independently synthesized **1**–ONO(OTf) set did depict the same molecular structure and atom connectivity, and yielded similar metrical parameters for the complex cation.

Crystallographic analyses on single crystals of **1**–ONO, **1**–ONO_2 and **1**–OAc confirmed the formation of the new complexes, along with revealing the bidentate binding modes of the nitrito and nitrato ligands (Figures 2–4), indicative of a unique six-

coordinate Fe center. Crystal and structure refinement data for these complexes are summarized in Tables 1–3. Selected bond lengths and angles are given in Tables 4–6.

For the nitrito complex **1**–ONO, the Fe–N bond lengths range from 2.2153(18) to 2.2460(18) Å while the lengths of the bonds from Fe to O are 2.243(2) Å for Fe–O1 and 2.218(2) Å for Fe–O2, demonstrating that the nitrito ligand is binding to Fe in a bindentate mode through both oxygen atoms. The angles including the nitrogen atoms trans to each other and Fe are 164.82(7)° and 132.48(6)° for N1–Fe–N3 and N2–Fe–N4 respectively. The incident angles between the tmc ligand, Fe and the nitrito ligand are 140.52(8)° for N4–Fe–O1 and 141.84(8)° for N2–Fe–O2. The angle involving the two oxygen atoms bound to the Fe is 54.88(8)° for O1–Fe–O2. There are two dihedral angles of interest with regards of how the nitrito ligand sits with respect to the tmc ligand. The angle between the plane defined as N1–Fe–N3 and the plane defined as Fe–O1–N5–O2 is 84.5(2)° while the angle between the plane defined as N2–Fe–N4 and Fe–O1–N5–O2 is 2.2(2)°. The structure of **1**–ONO depicts a type of distorted octahedral geometry with N1 and N3 sitting on the z-axis and N2, N4, O1 and O2 creating the distorted x-y plane. The bond lengths within the nitrito ligand are 1.218(3) and 1.231(3) Å for O1–N5 and N5–O2 respectively, and the O2–N5–O1 bond angle is 114.2(2)°. A correlation exists between the Fe–O bonds and N5–O bonds in the nitrito ligand. The longer Fe–O bond and the shorter N5–O bond both involve the same oxygen atom (O1), with the opposite being true for O2. The bond angles of Fe–O1–N5 and Fe–O2–N5 are 95.04(15)° and 95.86(15)°, respectively.

Table 1. Crystallographic data and structure refinement for [Fe(tmc)(O_2N)]OTf, **1**– ONO(OTf).

	1–ONO
Empirical formula	$C_{15}H_{32}F_3FeN_5O_5S$
Formula weight	507.37
Crystal habit, color	prism, orange
Crystal size	0.37 x 0.24 x 0.16 mm^3
Temperature, T	210(2) K
Wavelength, λ	0.71073 Å
Crystal system	monoclinic
Space group	$P2_1/c$
Unit cell dimensions	a = 10.9547(12) Å
	b = 12.4732(13) Å
	c = 16.4339(17) Å
	β = 97.034(5)°
Volume, V	2228.6(4) $Å^3$
Z	4
Calculated density	1.512 $Mg \cdot m^{-3}$
Absorption coefficient, μ	0.831 mm^{-1}
F(000)	1064
θ range for data collection	2.88 to 27.71°
Limiting indices	$-14 \le h \le 14$, $-16 \le k \le 16$, $-21 \le l \le 21$
Reflections collected / unique	18538 / 5170 [R(int) = 0.0252]
Completeness to θ	99.0 % (θ = 27.71°)
Max. and min. transmission	0.8785 and 0.7485
Refinement method	Full-matrix least-squares on F^2
Data / restraints / parameters	5170 / 0 / 275
Goodness-of-fit on F^2	1.093
Final R indices [I>2sigma(I)]	$R1$ = 0.0400, $wR2$ = 0.1111
R indices (all data)	$R1$ = 0.0494, $wR2$ = 0.1177
Largest diff. peak and hole	1.110 and –0.477 $e \cdot Å^{-3}$

Table 2. Crystallographic data and structure refinement for [Fe(tmc)(O_2NO)]OTf, **1**–ONO_2(OTf).

	1–ONO_2
Empirical formula	$C_{15}H_{32}F_3FeN_5O_6S$
Formula weight	523.37
Crystal habit, color	prism, yellow
Crystal size	0.38 x 0.18 x 0.16 mm^3
Temperature, T	190(2) K
Wavelength, λ	0.71073 Å
Crystal system	monoclinic
Space group	$P2_1/c$
Unit cell dimensions	a = 11.1181(12) Å
	b = 12.5633(14) Å
	c = 16.5093(17) Å
	β = 97.510(5)°
Volume, V	2286.2(4) $Å^3$
Z	4
Calculated density	1.521 $Mg \cdot m^{-3}$
Absorption coefficient, μ	0.816 mm^{-1}
F(000)	1096
θ range for data collection	2.90 to 27.90°
Limiting indices	$-14 \le h \le 14$, $-16 \le k \le 16$, $-21 \le l \le 21$
Reflections collected / unique	19798 / 5451 [R(int) = 0.0403]
Completeness to θ	99.7 % (θ = 27.90°)
Max. and min. transmission	0.8806 and 0.7469
Refinement method	Full-matrix least-squares on F^2
Data / restraints / parameters	5451 / 0 / 284
Goodness-of-fit on F^2	1.072
Final R indices [I>2sigma(I)]	$R1$ = 0.0581, $wR2$ = 0.1412
R indices (all data)	$R1$ = 0.0846, $wR2$ = 0.1558
Largest diff. peak and hole	1.124 and –0.770 $e \cdot Å^{-3}$

Table 3. Crystallographic data and structure refinement for [Fe(tmc)(OAc)]OTf, **1**–OAc(OTf).

	1–OAc
Empirical formula	$C_{17}H_{35}F_3FeN_4O_5S$
Formula weight	520.40
Crystal habit, color	prism, colorless
Crystal size	0.26 x 0.20 x 0.16 mm^3
Temperature, T	210(2) K
Wavelength, λ	0.71073 Å
Crystal system	monoclinic
Space group	$P2_1/n$
Unit cell dimensions	a = 11.3393(12) Å
	b = 13.4126(14) Å
	c = 15.8374(17) Å
	β = 100.437(5)°
Volume, V	2368.8(4) $Å^3$
Z	4
Calculated density	1.459 $Mg \cdot m^{-3}$
Absorption coefficient, μ	0.783 mm^{-1}
F(000)	1096
θ range for data collection	2.87 to 27.88°
Limiting indices	$-14 \le h \le 14$, $-17 \le k \le 17$, $-20 \le l \le 20$
Reflections collected / unique	19956 / 5631 [R(int) = 0.0290]
Completeness to θ	99.8 % (θ = 27.88°)
Max. and min. transmission	0.8850 and 0.8224
Refinement method	Full-matrix least-squares on F^2
Data / restraints / parameters	5631 / 0 / 285
Goodness-of-fit on F^2	1.038
Final R indices [I>2sigma(I)]	$R1$ = 0.0314, $wR2$ = 0.0776
R indices (all data)	$R1$ = 0.0445, $wR2$ = 0.0833
Largest diff. peak and hole	0.465 and –0.599 $e \cdot Å^{-3}$

Table *4*. Selected interatomic distances (Å) for [Fe(tmc)(O_2N)]OTf, **1**–ONO, [Fe(tmc)(O_2NO)]OTf, **1**–ONO_2, and [Fe(tmc)(OAc)]OTf, **1**–OAc.[a]

	1–ONO	**1**–ONO_2		**1**–OAc
Fe–N1	2.2247(17)	2.211(3)	Fe–N1	2.2398(14)
Fe–N2	2.2153(18)	2.220(3)	Fe–N2	2.2016(14)
Fe–N3	2.2460(18)	2.211(3)	Fe–N3	2.2318(13)
Fe–N4	2.2265(18)	2.243(3)	Fe–N4	2.1874(13)
Fe–O1	2.243(2)	2.275(3)	Fe–O1	1.9423(12)
Fe–O2	2.218(2)	2.281(3)	Fe···O2	3.3826(14)
O1–N5	1.218(3)	1.260(3)	O1–C15	1.283(2)
N5–O2	1.231(3)	1.229(4)	C15–O2	1.226(2)
N5–O3		1.248(3)	C15–C16	1.508(2)

[a] Numbers in parentheses are standard uncertainties in the last significant figures. Atoms are labeled as indicated in Figures 2–4.

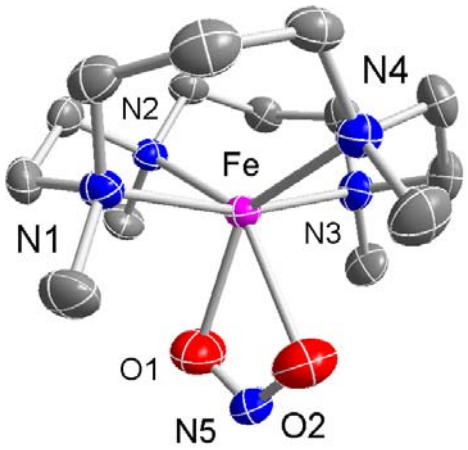

Figure 2. Molecular structure of [Fe(tmc)(O_2N)]$^+$, **1**–ONO. Displacement ellipsoids are drawn at 50% probability level; hydrogen atoms have been omitted for clarity. Color key: pink = Fe, blue = N, red = O, gray = C.

Table 5. Selected angles (°) for [Fe(tmc)(O_2N)]OTf, **1**–ONO, [Fe(tmc)(O_2NO)]OTf, **1**–ONO_2, and [Fe(tmc)(OAc)]OTf, **1**–OAc.[a]

	1–ONO	**1**–ONO_2		**1**–OAc
N1–Fe–N2	82.47(7)	83.15(11)	N1–Fe–N2	82.50(5)
N3–Fe–N2	91.36(7)	92.08(11)	N3–Fe–N2	91.57(5)
N3–Fe–N4	82.18(7)	82.38(11)	N3–Fe–N4	81.68(5)
N1–Fe–N4	91.75(7)	92.04(11)	N1–Fe–N4	91.09(5)
N3–Fe–N1	164.82(7)	134.02(11)	N3–Fe–N1	162.89(5)
N2–Fe–N4	132.48(6)	166.76(11)	N2–Fe–N4	134.74(5)
N1–Fe–O1	95.56(8)	85.32(10)	N1–Fe–O1	94.11(5)
N2–Fe–O1	86.98(7)	94.78(11)	N2–Fe–O1	99.92(5)
N3–Fe–O1	97.96(8)	140.63(10)	N3–Fe–O1	102.74(5)
N4–Fe–O1	140.52(8)	97.12(12)	N4–Fe–O1	125.27(5)
N1–Fe–O2	100.53(8)	140.99(10)		
N2–Fe–O2	141.84(8)	99.77(11)		
N3–Fe–O2	92.90(8)	84.95(10)		
N4–Fe–O2	85.65(8)	91.74(11)		
O1–Fe–O2	54.88(8)	55.68(10)		
N5–O1–Fe	95.04(15)	93.10(19)	C15–O1–Fe	135.71(12)
N5–O2–Fe	95.86(15)	93.68(18)		
O2–N5–O1	114.2(2)	117.5(3)	O2–C15–O1	124.29(17)
O3–N5–O1		120.3(3)	O1–C15–C16	114.65(16)
O2–N5–O3		122.2(3)	O2–C15–C16	121.06(17)

[a] Numbers in parentheses are standard uncertainties in the last significant figures. Atoms are labeled as indicated in Figures 2–4.

Table 6. Selected dihedral angles (°) for [Fe(tmc)(ONO_2)]OTf, **1**–ONO_2, [Fe(tmc)(ONO)]OTf, **1**–ONO, and [Fe(tmc)(OAc)]OTf, **1**–OAc.[a]

	1–ONO	**1**–ONO_2	**1**–OAc
N1–Fe–N3 / Fe–O1–N5–O2[b]	84.5(2)	2.6(2)	
N2–Fe–N4 / Fe–O1–N5–O2[b]	2.2(2)	84.3(2)	
N1–Fe–N3 / Fe–O1–C15–O2[b]			59.4(1)
N2–Fe–N4 / Fe–O1–C15–O2[b]			25.6(1)

[a] Numbers in parentheses are standard uncertainties in the last significant figures. Atoms are labeled as indicated in Figures 2–4. [b] Angle between the N–Fe–N plane and the least-squares plane of the atoms of the Fe–OXO group (X = N, C).

For the nitrato complex **1**–ONO_2, the Fe–N bond lengths range from 2.211(3) to 2.243(3) Å while the lengths of the bonds from Fe to O are 2.275(3) Å for Fe–O1 and 2.281(3) Å for Fe–O2, demonstrating that the nitrato ligand is binding to Fe in a bindentate mode through two oxygen atoms. The angles including the nitrogen atoms trans to each other and Fe are 134.02(11)° and 166.76(11)° for N1–Fe–N3 and N2–Fe–N4, respectively. The incident angles between the tmc ligand, Fe and the nitrato ligand are 140.63(10)° for N3–Fe–O1 and 140.99(10)° for N1–Fe–O2. The angle involving the two oxygen atoms bound to the Fe is 55.68(10)° for O1–Fe–O2. There are two dihedral angles of interest with regards of how the nitrato ligand sits with respect to the tmc ligand. The angle between the plane defined as N1–Fe–N3 and the plane defined as Fe–O1–N5–O2 is 2.6(2)° while the angle between the plane defined as N2–Fe–N4 and Fe–O1–N5–O2 is 84.3(2)°. The structure of **1**–ONO_2 depicts a type of distorted octahedral geometry with N2 and N4 sitting on the z-axis and N1, N3, O1 and O2 creating the distorted x-y plane. The bond lengths within the nitrato ligand are 1.260(3), 1.229(4) and 1.248(3) Å for O1–N5, N5–O2 and N5–O3 respectively, and the O2–N5–O1, O3–N5–O1 and O2–N5–O3 bond angles are 117.5(3)°, 120.3(3)° and 122.2(3)°,

respectively. While all three N5–O bond lengths are similar, there appears to be the most double bond character in N5–O2. The same correlation exists between the Fe–O bonds and N5–O bonds in the nitrato ligand as did in **1**–ONO. The longer Fe–O bond and the shorter N5–O bond both involve the same oxygen atom (O2), with the opposite being true for O1. The bond angles of Fe–O1–N5 and Fe–O2–N5 are 93.10(19)° and 93.68(18)° respectively.

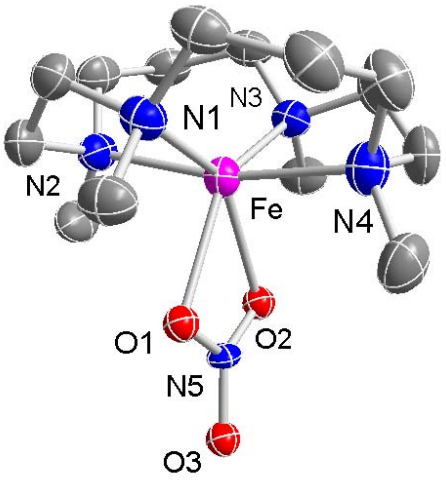

Figure 3. Molecular structure of $[Fe(tmc)(O_2NO)]^+$, **1**–ONO_2. Displacement ellipsoids are drawn at 50% probability level; hydrogen atoms have been omitted for clarity. Color key: pink = Fe, blue = N, red = O, gray = C.

For the acetato complex **1**–OAc, the Fe–N bond lengths range from 2.1874(13) to 2.2398(14) Å while the length of the bond from Fe to O1 is 1.9423(12) Å and the interatomic distance form Fe to O2 is 3.3826(14) Å, demonstrating that the acetato ligand is binding to Fe in a monodentate mode through one oxygen atom. The angles including the nitrogen atoms trans to each other and Fe are 162.89(5)° and 134.74(5)° for N1–Fe–N3 and N2–Fe–N4 respectively. The incident angle between the tmc ligand, Fe and the acetato ligand is 125.27(5)° for N4–Fe–O1. There are two dihedral angles of interest with regards of how the acetato ligand sits with respect to the tmc ligand. The

angle between the plane defined as N1–Fe–N3 and the plane defined as Fe–O1–C15–O2 is 59.4(1)° while the angle between the plane defined as N2–Fe–N4 and Fe–O1–N5–O2 is 25.6(1)°.

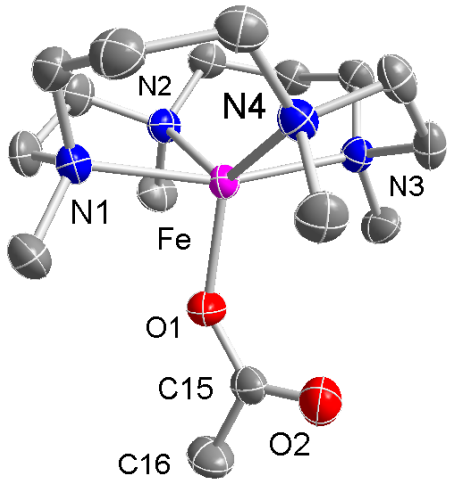

Figure 4. Molecular structure of $[Fe(tmc)(OC(O)CH_3)]^+$, **1**–OAc. Displacement ellipsoids are drawn at 50% probability level; hydrogen atoms have been omitted for clarity. Color key: pink = Fe, blue = N, red = O, gray = C.

Since **1**–OAc is a five-coordinate complex, the τ parameter can be calculated, which is a measurement of trigonality within the compositional range between square pyramidal (τ = 0) and trigonal bipyramidal (τ = 1) geometries.[77] The value of τ is calculated by the equation τ = (β – α)/60 (where β = larger angle and α = smaller angle of the set of trans donor atoms). For **1**–OAc, τ = 0.47, calculated using the N2–Fe–N4 angle (134.74(5)°) and the N3–Fe–N1 angle (162.89(5)°). This τ value of 0.47 suggests that the geometry of **1**–OAc can be definied as approximately halfway between the ideal geometries of square pyramidal and trigonal bipyramidal. The bond lengths within the acetato ligand are 1.283(2), 1.226(2) and 1.508(2) Å for O1–C15, C15–O2 and C15–C16 respectively, and the O2–C15–O1, O1–N5–C16 and O2–C15–C16 bond angles are 124.29(17)°, 114.65(16)° and 121.06(17)°, respectively. There is a clear difference in the

C15–O1 and C15–O2 bond lengths, demonstrating the double bond character of the C15–O2, the carbonyl unit of the acetato ligand. The bond angle of Fe–O1–C15 is 135.71(12)°.

The tmc ligand binds to iron in a similar fashion in **1**–ONO, **1**–ONO_2 and **1**–OAc; in the case the *N*-methyl groups are all pointed down in the same direction. Using the description put forth by Bosnich and co-workers.[78] for octahedral complexes involving tetradentate macrocylcic ligands, the tmc ligand adapts the (I) configuration. Overall, the **1**–ONO and **1**–ONO_2 complexes exhibit the *cis*(I) configuration. Also, in each complex the tmc ligand is coordinated with one large N–Fe–N and one relatively smaller one. This shows the non-planarity of the tmc ligand when bound to each Fe^{II} center. While the τ parameter for **1**–OAc, where τ = 0.47, is defined for five-coordinate systems, the corresponding parameter can be calculated using the β and α values of **1**–ONO and **1**–ONO_2 in which they equal 0.54 and 0.55 respectively. This comparison suggests that the tmc nitrogen atoms in **1**–ONO and **1**–ONO_2 are further from planarity than the tmc nitrogen atoms in **1**–OAc. The coordination number for iron is six in the case of **1**–ONO and **1**–ONO_2, while it is five for **1**–OAc. The bidentate binding mode of nitrite and nitrate are confirmed when investigating the bond lengths from Fe–O in each case. They fall in the range of 2.218(2) to 2.281(3) Å. When investigating the corresponding distances in **1**–OAc, the distance of 1.9423(12) from Fe to O1 indicates a coordination bond, while the distance of 3.3826(14) from Fe to O2 is too long for a coordination bond and indicates a monodentate binding mode of acetate.

The structures of these new complexes agree well with the known Fe(tmc) structures $[Fe(tmc)(SC_6H_4OCH_3)]^+$,[79] $[Fe(tmc)(OSOC_6H_5)]^+$,[80] $[Fe(tmc)(NCS)]^+$,[81] and $[Fe(tmc)(NO)]^{2+}$.[67] These examples of Fe^{II}(tmc) complexes have Fe–N_{tmc} bond lengths ranging from 2.147 to 2.279 Å and the Fe–N_{tmc} bond lengths of **1**–ONO, **1**–ONO_2 and **1**–OAc all lie within this range. These previously published structures of Fe^{II}(tmc) complexes each have a unique ligand that is monodenate (analgous to the acetato ligand

in **1**–OAc, and this illustrates the novelty of the nitrito and nitrato ligands binding in the bidentate mode), and the bond length from Fe to the unique ligand ranges from 1.737 to 2.3220 Å depending on the nature of the coordinating atom. The Fe–O1 bond length for **1**–OAc falls within this range. The τ values for the known complexes range from 0.33 to 0.50. The τ = 0.33 belongs to a $\{FeNO\}^7$ complex supported by tmc and may not be able to be classified as a formal Fe^{II}, which may explain its large deviation from the τ values of the other Fe^{II} complexes (the others range from 0.46 to 0.50). The examples of Fe^{IV}(tmc) complexes, $[FeO(tmc)(NCCH_3)]OTf$[73] and [Fe(tmc)(OSc(OTf)4OH)],[82] along with two examples of Fe^{III}(tmc) complexes, $[Fe(tmc)(NO)(OH)]BF_4$[67] and $[Fe(tmc)(O_2)]^+$,[68] vary slightly in the tmc parameters with overall shorter $Fe–N_{tmc}$ distances.

The bidentate binding mode of the nitrito and nitrato ligands give rise to six-coordinate complexes which have not been observed before for Fe^{II} supported by the tmc ligand. Structures of nitritoiron complexes are limited, with there only being four examples in which nitrite binds in a bidentate fashion through the oxygen atoms.[83-85] In the majority of iron complexes in which nitrite is a ligand, nitrite binds through the nitrogen atom. Structures of nitritoiron complexes supported by polydentate ligands include a tetraazaannulene complex,[86] triazacyclononane complex,[87] and tris(pyrazolyl)borate complex,[83] in which nitrite binds in a monodentate fashion, and a tris(pyrazolyl)borate complex,[83] where nitrite takes on the bidentate binding mode. The rarity of nitritoiron structures in general makes the **1**–ONO(OTf) very interesting, as well as the fact the nitrito ligand exists in a bidentate binding mode.

Structures of nitratoiron complexes are not as rare as nitritoiron complexes, as several structures exist for these complexes in which nitrate acts as a monodentate or bidentate ligand. Examples of polydentate ligands that support monodentate nitratoiron complexes are porphyrins,[88-91] salen ligands,[92] tris(pyrazolyl)borate ligands,[93] and polydentate amine ligands.[94-96] Structures of bidentate nitratoiron complexes are also

supported by polydentate ligands which include porphyrins,[97-99] salen ligands,[100-102] triazine ligands,[103-104] and an oxydiacetato ligand.[105] The structure of **1**–ONO_2(OTf) is an addition to approximately ten known structures of nitratoiron complexes in which iron is supported by a polydentate ligand and nitrate is a bidentate ligand.

3.3.3 Infrared Spectroscopy

As a follow-up to determining the structures of the new Fe^{II} complexes with XRD, we have decided to investigate each complex using IR spectroscopy. IR spectroscopy is a useful tool to probe the binding modes of the nitrito, nitrato and acetato ligands in the complexes. The expected ranges of vibrational modes of these ligands depending upon their binding mode[66] have been shown in Tables 7–9.

Table 7. Infrared spectra data of nitrito complexes (cm^{-1})[a]

	ν(N=O)	ν(NO)	$\nu_s(NO_2)$	$\nu_{as}(NO_2)$	δ(ONO)
M–ONO	1393–1485	1048–1114			824–839
M–O_2N			1241–1390	1160–1230	841–887
NO_2^-			1335	1250	not reported

[a] Data shown from reference 66

Table 8. Infrared spectra data of nitrato complexes (cm^{-1})[a]

	$\nu_{as}(NO_2)$	$\nu_s(NO_2)$	ν(NO)	ν(N=O)	$\nu_{as}(NO_3)$
M–ONO_2	1497–1510	1271–1275	992–997		
M–O_2NO	1162–1300	963–1041		1485–1630	
NO_3^-					1385

[a] Data shown from reference 66

Special precautions were taken with each of the Fe^{II} complexes to help avoid any exchange between the anionic ligands of the complex and Br^-. Each of the Fe^{II} complexes was prepared with KBr using gentle grinding and pellets were formed at lower pressure (5000 psi) and for a shorter time (30 s) than standard procedures.

Table 9. Infrared spectra data of acetato complexes (cm^{-1})[a]

	$\nu_{as}(CO_2)$	$\nu_s(CO_2)$
M–O(O)CCH_3	1604–1745	1240–1376
M–O_2CCH_3	1507–1610	1377–1465
$CH_3CO_2^-$	1578	1414

[a] Data shown from reference 66

The complex **1**–OTf was subjected to IR spectroscopy and that resulting spectrum is shown for reference in Figure 5. IR spectra of **1**–ONO along with its isotopologue **1**–$O^{15}NO$ were collected, however when compared to the spectrum of **1**–OTf, there are no new bands observed. There is however, a loss of bands at 1166 cm^{-1} and 1046 cm^{-1} (Figure 6). These bands may have been due to bound TfO^- in **1**–OTf that is no longer

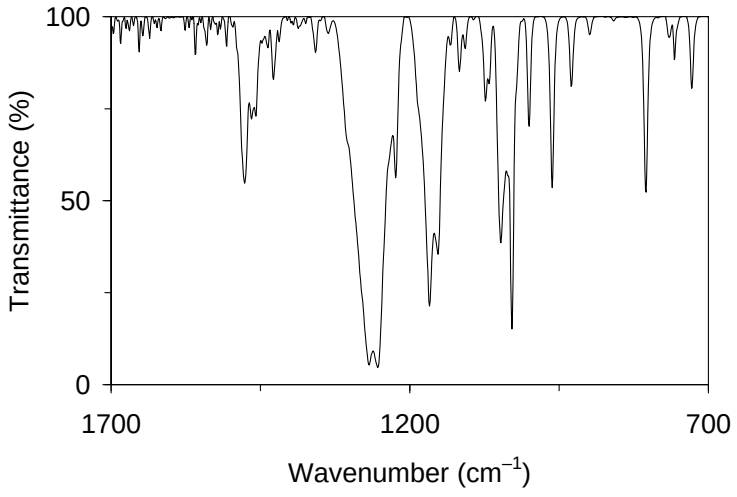

Figure 5. IR spectra of **1**–OTf **i**n the range of 700–1700 cm^{-1}.

present in **1**–ONO. When assessing where the new peaks due to bound bidentate nitrite should be observed, it can be seen that it is likely that $\nu_s(NO_2)$, $\nu_{as}(NO_2)$ and $\delta(ONO)$ are covered by bands due to tmc or free TfO^-. Additionally, the same result can be observed for the isotopically labeled complex as there is no observed shifting of bands. There were also no new bands observed in the region expected for a monodentate nitrito ligand. No evidence of the nitrito ligand is able to be observed.

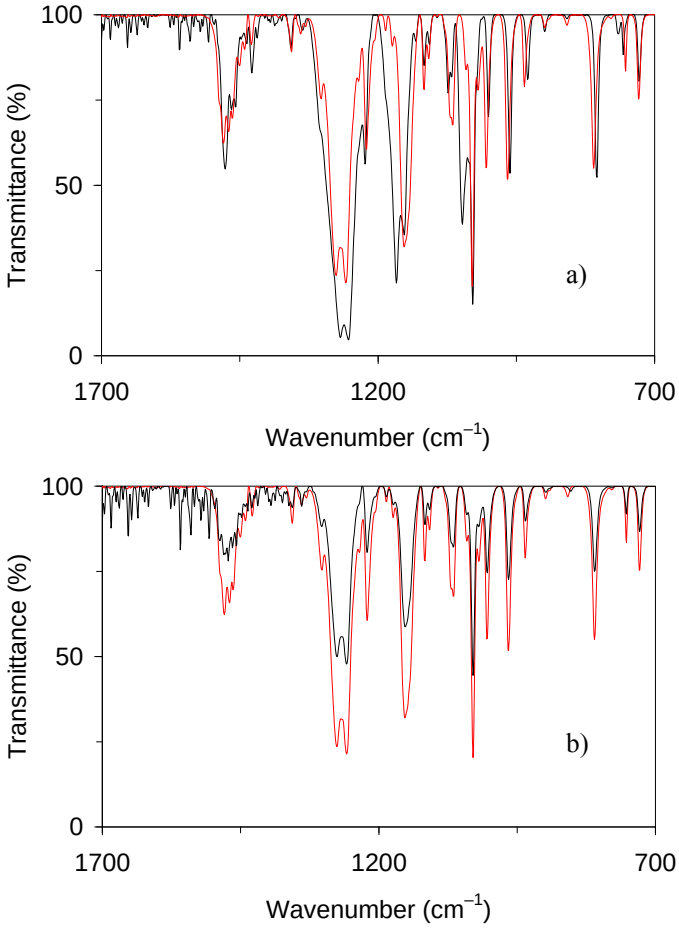

Figure 6. IR spectra of a) **1**–OTf (—, black) overlaid with **1**–ONO (—, red) and b) **1**–ONO (—, red) overlaid with **1**–$O^{15}NO$ (—, red) in the range of 700–1700 cm^{-1}.

The IR spectra of **1**–ONO_2 and the isotopically-labeled **1**–$O^{15}NO_2$ are shown in Figure 7. Immediately a difference is observed between **1**–ONO_2 and **1**–OTf, as a set of new bands at 1493 cm^{-1} and 739 cm^{-1} in **1**–ONO_2 have appeared and there is again a loss of bands at 1166 cm^{-1} and 1046 cm^{-1} (most likely due to bound TfO^- being replaced by NO_3^-). Looking at Table 8, the band at 1493 cm^{-1} would fit in the range of ν(N=O) for bidentate binding nitrato ligands. The other bands $\nu_{as}(NO_2)$ and $\nu_s(NO_2)$ are most likely covered by bands due to tmc or free TfO^-. The band at 739 cm^{-1} is most likely a δ band of the NO_3 group.

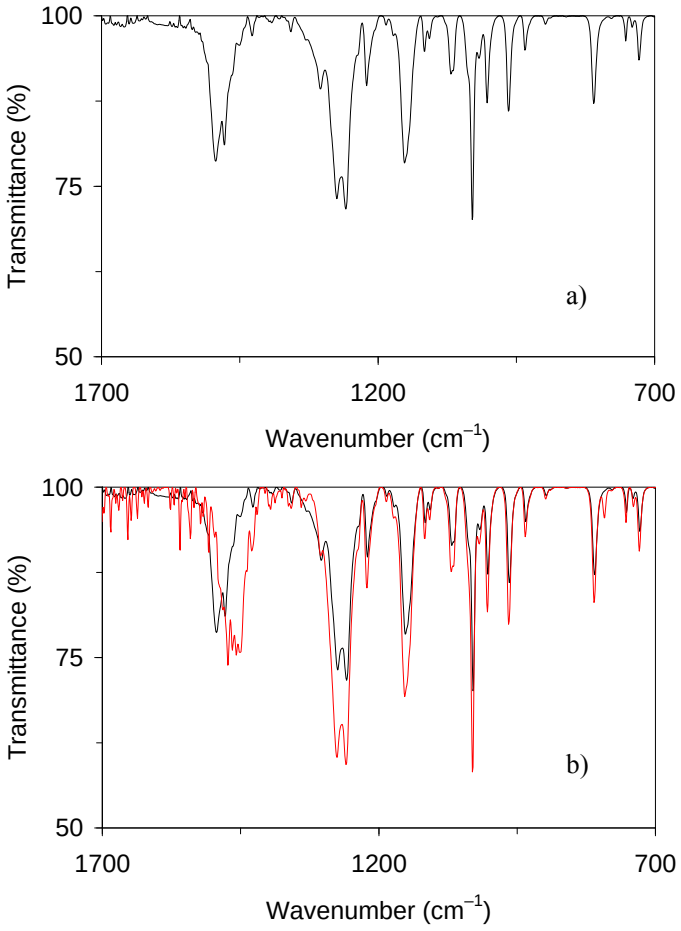

Figure 7. IR spectra of a) **1**–ONO_2 b) **1**–ONO_2 (—, black) overlaid with **1**–$O^{15}NO_2$ (—, red) in the range of 700–1700 cm^{-1}.

These bands were confirmed to be due to the nitrato ligand of **1**–ONO_2 by comparing the spectra of **1**–ONO_2 with **1**–$O^{15}NO_2$ to observe the shift of the band at 1493 cm^{-1} to 1472 cm^{-1} and shift of the band at 739 cm^{-1} to 738 cm^{-1}. This conclusion that the IR bands observed for **1**–ONO_2 depict a bidentate binding mode of the nitrato ligand is in agreement with the X-ray diffraction data.

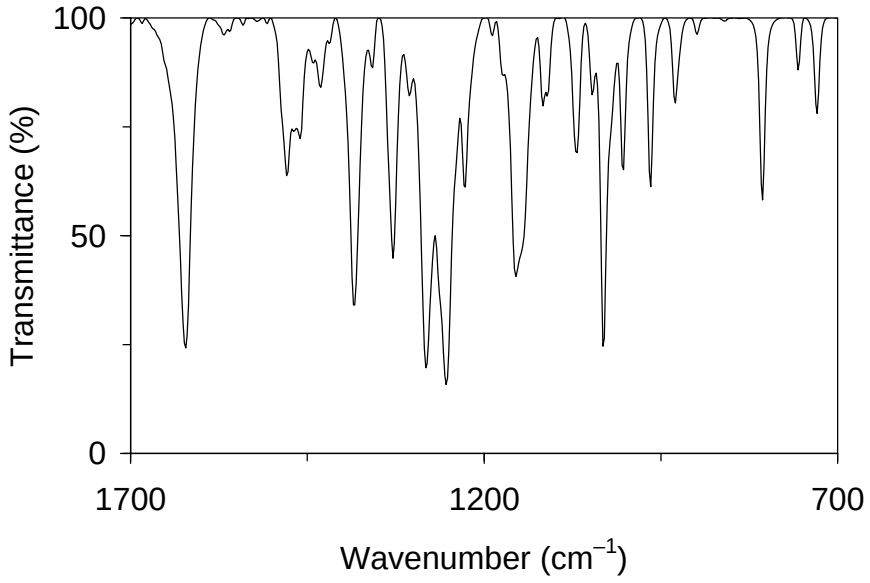

Figure 8. IR spectra of **1**–OAc **i**n the range of 700–1700 cm^{-1}.

The IR spectrum of **1**–OAc is shown in Figure 8. A clear difference is observed between **1**–OAc and **1**–OTf, as a set of new bands at 1623 cm^{-1} and 1327 cm^{-1} in **1**–OAc have appeared and there is once again a loss of the bands at 1166 cm^{-1} and 1046 cm^{-1} (most likely due to bound TfO^- being replaced by AcO^-). Looking at Table 9, the band at 1623 cm^{-1} would fit in the range of $\nu_{as}(CO_2)$ and the band at 1327 cm^{-1} would fit in the range of $\nu_s(CO_2)$ for monodentate binding acetato ligands. The distinction in the case of the acetato ligand is very clear, since the values of the stretching bands to not match a

bidentate binding mode. The monodentate binding acetato ligand evidenced by IR spectroscopy is in agreement with the structure solved from the X-ray diffraction data.

3.3.4 Electrochemical Measurements

For these Fe^{II}(tmc) complexes, differential pulse voltammograms (DPVs) revealed that each of these complexes exhibit an oxidation at a relatively high potential. The lowest oxidation potential of the three complexes is demonstrated by **1**–OAc at 0.364 V with respect to $[FeCp_2]/[FeCp_2]^+$ redox couple, with **1**–ONO and **1**–ONO_2 exhibiting oxidation potentials at 0.644 V and 0.744 V respectively (Figures 9–11). The cyclic voltammograms (CVs) have been investigated using a scan rate of 0.1 $V \cdot s^{-1}$ and demonstrate that the oxidation events are irreversible (Figures 9–11). Different scan rates over a range from 0.05–0.5 $V \cdot s^{-1}$ were also investigated with no improvement in the data observed.

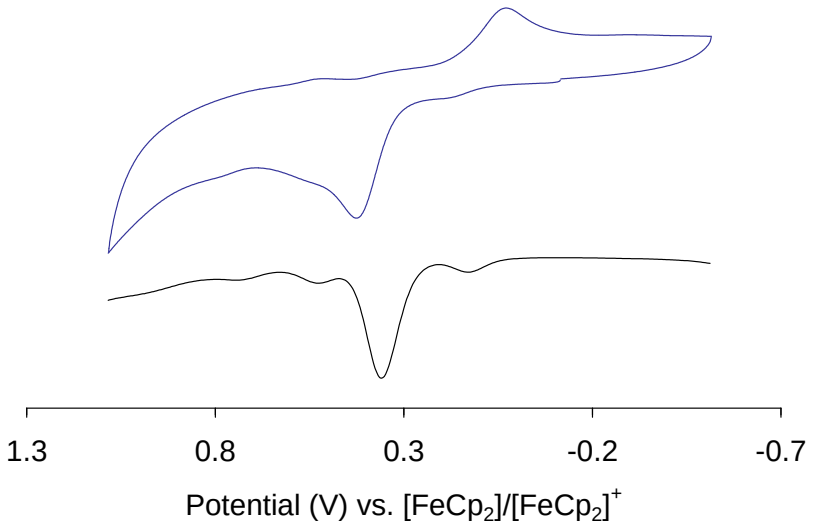

Figure 9. Cyclic and differential pulse voltammogram of 1 mM **1**–OAc in nitromethane (0.1 M NBu_4ClO_4) at a scan rate of 0.1 $V \cdot s^{-1}$.

Upon consideration of these values, an oxidative trend emerges amongst the Fe^{II}(tmc) complexes such that ease of oxidation results as **1**–OAc < **1**–ONO < **1**–ONO_2. This could be indicative of the more strongly-binding acetate ligand forming a complex that is easier to oxidize from Fe^{II} to Fe^{III}. Another interesting correlation of the oxidation potentials is with the binding mode of the unique ligand. If the binding mode observed in the solid state holds true in solution, then the **1**–OAc, which has a monodentate AcO^- ligand, is easier to oxidize than **1**–ONO and **1**–ONO_2 complexes which have bidentate NO_2^- and NO_3^- ligands. Finally, the irreversible character of the oxidation events of these Fe^{II} complexes suggests that the oxidized complexes are unstable.

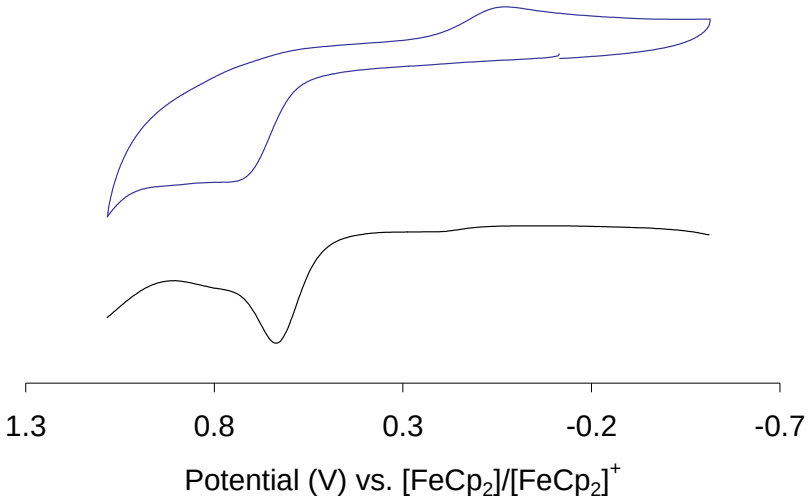

Figure 10. Cyclic and differential pulse voltammogram of 1 mM **1**–ONO in nitromethane (0.1 M NBu_4ClO_4) at a scan rate of 0.1 $V \cdot s^{-1}$.

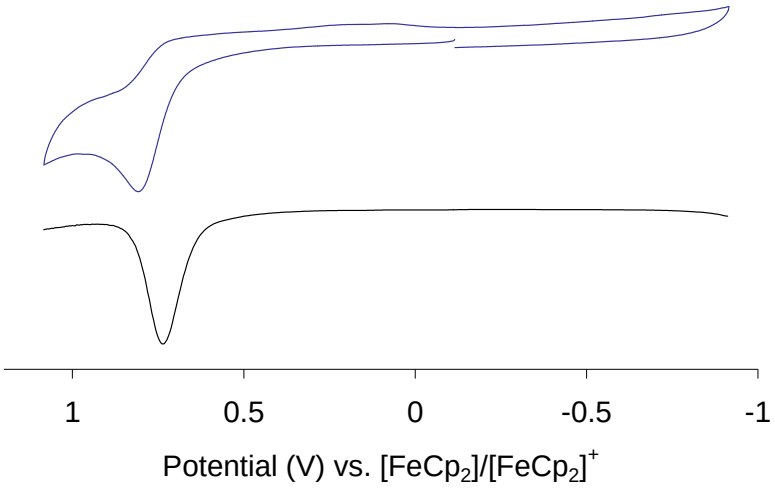

Figure 11. Cyclic and differential pulse voltammogram of 1 mM **1**–ONO_2 in nitromethane (0.1 M NBu_4ClO_4) at a scan rate of 0.1 $V \cdot s^{-1}$.

3.4 Conclusion

The synthesis and characterization of Fe^{II} complexes supported by the tmc ligand has been described in this chapter. These complexes have been characterized by IR spectroscopy, ESI mass spectrometry, elemental analysis and single-crystal X-ray diffraction. The analysis shows that the nitrito and nitrato ligands bind to iron in a bidentate fashion giving rise to two examples of the unique six-coordinate Fe^{II}(tmc) complex. The acetato ligand has been shown to bind in a monodentate fashion. The complex **1**–OAc has a τ value of 0.47, indicating that its geometry is about halfway between the ideal geometry of a square pyramidal complex and a trigonal bipyramidal complex. The IR analyses of **1**–ONO_2 and **1**–OAc confirm the binding modes determined from X-ray diffraction data, but IR analyses of **1**–ONO was not able to be used to confirm the binding of the nitrito ligand as bands due to the nitrito ligand were obstructed

by bands from the tmc ligand or $CF_3SO_3^-$ counterion. The UV–Vis spectrum of **1**–ONO was measured and showed a band at 440 nm. Finally, it was shown with electrochemical measurements (CV and DPV) that these complexes have relatively high oxidation potentials and that they are irreversible events. The irreversibility of these oxidations is consistent with literature reports of Fe^{III}(tmc) complexes being unstable and difficult to isolate.

CHAPTER 4

REACTION OF AN OXOIRON(IV) COMPLEX OF 1,4,8,11-TETRAMETHYL-1,4,8,11-TETRAAZACYCLOTETRADECANE WITH NITROGEN MONOXIDE: FORMATION OF A NITRITOIRON(II) COMPLEX VIA AN IRON(III) INTERMEDIATE

4.1 Introduction

In this chapter the reaction of $[Fe^{IV}O(tmc)(OAc)]^+$ with the free radical nitrogen monoxide will be covered. The study presented in this chapter has been previously published.[106] While the equatorial coordination of the Fe center by the macrocyclic ligand offers a stabilizing environment for the Fe^{IV}=O group, the acetate anion was chosen as the sixth ligand to discourage direct interaction between NO and the Fe center. The reaction afforded a mixture of two Fe^{II} complexes, $[Fe(tmc)(OAc)]^+$ and $[Fe(tmc)(ONO)]^+$. The amount of nitrite produced in this reaction (*ca*. 1 equiv with respect to Fe) was determined by ESI mass spectrometry after addition of ^{15}N-enriched $NaNO_2$. In contrast to oxygen-atom transfer to PPh_3, the NO reaction of $[FeO(tmc)(OAc)]^+$ proceeds through an Fe^{III} intermediate which was identified by UV–Vis–NIR spectroscopy and ESI mass spectrometry and whose decay is dependent on the concentration of methanol. The observations are consistent with a mechanism involving oxide(•1–) ion transfer from $[Fe^{IV}O(tmc)(OAc)]^+$ to NO to form an Fe^{III} complex and NO_2^-, followed by reduction of the Fe^{III} complex. Competitive binding of AcO^- and NO_2^- to Fe^{II} then leads to an equilibrium mixture of two Fe^{II}(tmc) complexes. Evidence for the incorporation of oxygen from the oxoiron(IV) complex into NO_2^- was obtained from an ^{18}O-labeling experiment. The reported reaction serves as a synthetic example of the NO reactivity of biological oxoiron(IV) species, which has been proposed to have physiological functions such as inhibition of oxidative damage, enhancement of

peroxidase activity and NO scavenging. The reaction also complements the established reactivity modes of oxoiron(IV) complexes, which include oxygen-atom transfer to organic substrates and other iron complexes, hydrogen-atom abstraction, electron transfer, and hydride transfer.[51-53]

4.2 Experimental Section

4.2.1 Materials and Methods

Materials. All reagents and solvents were purchased from commercial sources and were used as received, unless noted otherwise. Acetonitrile, dichloromethane, and diethyl ether were deoxygenated by sparging with N_2 and purified by passage through two packed columns of molecular sieves under an N_2 pressure (MBraun solvent purification system). Anhydrous methanol (99.8%) and CD_3OD, 99.8% D, were used as received. Nitromethane was refluxed over CaH_2 under an Ar atmosphere, distilled, and passed through a column of basic Al_2O_3.[69] Preparation and handling of air- and moisture-sensitive materials were carried out under an inert gas atmosphere by using standard Schlenk and vacuum line techniques or a glovebox. Nitrogen monoxide was prepared by reaction of concentrated hydrochloric acid with sodium nitrite.[107] The gas mixture produced was passed through a 50-cm column of KOH pellets, a 2-m stainless steel coil cooled to –94 °C (acetone–liquid N_2), and a bubbler charged with a concentrated aqueous NaOH solution for removal of unwanted nitrogen oxides; the gas was dried by passing it through a short column (*ca*. 20 cm) of KOH pellets.[69] (*Caution*: Nitrogen monoxide is a toxic gas.) $Fe(OTf)_2{\cdot}2MeCN$ was synthesized by a modified literature method[70] from anhydrous $FeCl_2$ and trimethylsilyl trifluoromethanesulfonate in acetonitrile and recrystallized from acetonitrile–diethyl ether (TfOH = CF_3SO_3H, trifluoromethanesulfonic or triflic acid).[71] The ligand 1,4,8,11-tetramethyl-1,4,8,11-

tetraazacyclotetradecane (tmc),[72] $[Fe^{II}(tmc)(OTf)]OTf$,[73] **1**–OTf(OTf), and iodosylbenzene[108] were prepared following published procedures. The complex **1**–OTf(OTf) was stored in an N_2 atmosphere. (*Caution*: Iodosylbenzene is potentially explosive, if dried extensively, and should be handled with care.[109]) Isotope-enriched $H_2{}^{18}O$ (98% ^{18}O) and $Na^{15}NO_2$ (98% ^{15}N) were purchased from Cambridge Isotope Laboratories, Andover, MA, USA.

Physical Methods. UV–Visible spectra were recorded on an HP 8453A diode array spectrophotometer (Agilent Technologies) with samples maintained at the desired temperature using a cryostat/heater from Unisoku Scientific Instruments, Japan. For solutions containing both nitromethane and methanol, the same solvent mixture was used for the background sample. NMR spectra were recorded on a Bruker Avance DPX 300 spectrometer at ambient temperature. ^{19}F and ^{31}P chemical shifts are reported in parts per million (ppm) and were referenced to an external standard [$CFCl_3$ (δ = 0 ppm) for ^{19}F NMR and H_3PO_4 (85%, 0 ppm) for ^{31}P NMR spectra]. Relative peak areas for ^{19}F signals were calculated using NUTS 2.1. Mass spectral data were acquired on a quadrupole ion trap ThermoFinnigan LCQ Deca mass spectrometer using an electrospray ionization source. Analysis by GC–MS was performed on a TRACE GC 2000 gas chromatograph (column, TRACE TR-1) coupled with a single quadrupole ThermoFinnigan Voyager mass spectrometer.

4.2.2 Generation of Oxoiron(IV) Complexes

Generation of $[Fe^{IV}O(tmc)(OTf)]OTf$, 2–OTf(OTf), and $[Fe^{IV}O(tmc)(OAc)]OTf$, 2–OAc(OTf). Method A. For the purpose of investigating the reaction of **2**–OAc with NO, the preparation of **2**–OTf and **2**–OAc was carried out in an N_2 atmosphere. A 1 mM solution of **1**–OTf(OTf) (0.002 mmol) in 2.0 mL of nitromethane was placed in a 1-cm UV–Vis cuvette and precooled to –20 °C. Upon

addition of 0.050 mL of a solution of iodosylbenzene (0.002 mmol) in methanol (anhydrous, 99%), **2**–OTf formed within 5 min. ESI(+)MS ($MeNO_2$) *m/z*: M^+ calcd for $C_{15}H_{32}F_3FeN_4O_4S$ ({**2**–OTf}$^+$), 477.14; found, 477.1 (M^+), 461.2 ({M – O}$^+$), 257.3 ({tmc + H}$^+$). UV–Vis ($MeNO_2$) λ_{max}, nm (ε): 825 (230).

Subsequently, a solution of 0.002 mmol of tetraethylammonium acetate in 0.050 mL of nitromethane was added to the solution of **2**–OTf in nitromethane at –20 °C. The formation of **2**–OAc from **2**–OTf was indicated by a decrease of intensity at λ = 825 nm and the appearance of a new peak at λ = 995 nm over a period of *ca*. 1 h. ESI(+)MS ($MeNO_2$) *m/z*: M^+ calcd for $C_{16}H_{35}FeN_4O_3$ ({**2**–OAc}$^+$), 387.21; found, 387.0 (M^+), 371.3 ({M – O}$^+$), 257.3 ({tmc + H}$^+$). UV–Vis ($MeNO_2$) λ_{max}, nm (ε): 825 (120), 995 (100).

For the conversion of **2**–OTf into **2**–OAc by incremental addition of NEt_4AcO, a 1 mM solution of **2**–OTf (0.002 mmol) in 2.0 mL of nitromethane was prepared in a 1-cm UV–Vis cuvette at –20 °C as described above. Volume increments of 0.015 mL of a 33 mM solution of NEt_4AcO ($5 \cdot 10^{-4}$ mmol) in nitromethane were added in 2-min intervals to the solution of the Fe complex up to a total of 1.5 molar equiv of NEt_4AcO (with respect to Fe).

Method B. Upon addition of 0.150 mL of a solution of (diacetoxyiodo)benzene (0.006 mmol) in nitromethane to a 1 mM solution of **1**–OTf(OTf) (0.002 mmol) in 2.0 mL of nitromethane at 20 °C, **2**–OTf formed within 30 s. UV–Vis ($MeNO_2$) λ_{max}, nm (ε): 825 (230). Samples for ^{19}F NMR spectroscopy were prepared at a concentration of 10 mM in CD_3NO_2. ^{19}F NMR (282.4 MHz, CD_3NO_2, δ): –77.5 ([FeO(tmc){$OS(O)_2CF_3$}]$^+$), –79.2 ($CF_3SO_3^-$). For comparison, ^{19}F NMR of **1**–OTf(OTf) (282.4 MHz, CD_3NO_2, δ): –0.6 ([Fe(tmc){$OS(O)_2CF_3$}]$^+$), –79.3 ($CF_3SO_3^-$).

Addition of a solution of 0.002 mmol of NEt_4AcO in 0.050 mL of nitromethane to this solution caused conversion of **2**–OTf into **2**–OAc (*ca*. 30 s). UV–Vis ($MeNO_2$) λ_{max}, nm (ε): 832 (120), 1005 (110). ^{19}F NMR (282.4 MHz, CD_3NO_2, δ): –79.4 ($CF_3SO_3^-$).

4.2.3 Reactivity of the Oxoiron(IV) Complex $[Fe^{IV}O(tmc)(OAc)]^+$

Reaction of 2–OAc with Triphenylphosphine. A 1 mM solution of **2**–OAc (0.002 mmol) in 2.0 mL of nitromethane was prepared in a UV–Vis cuvette at –20 °C as described above (Method A), cooled to –25 °C, and treated with a solution of 0.020 mmol of triphenylphosphine in 0.35 mL of nitromethane. The half-life of the reaction was *ca*. 10 min. The product solution was subjected to ESI mass spectrometry. ESI(+)MS ($MeNO_2$) *m/z* calcd for $C_{16}H_{35}FeN_4O_2$ ($[Fe^{II}(tmc)(OAc)]^+$, $\{\mathbf{1}–OAc\}^+$), 371.21; found, 371.4 ($\{\mathbf{1}–OAc\}^+$). The product solution was evaporated to dryness, and the residue was dissolved in $CDCl_3$ for ^{31}P NMR spectroscopy. ^{31}P NMR (121.5 MHz, $CDCl_3$, δ): 29.0 ($OPPh_3$), –5.4 (PPh_3).

Reaction of 2–OAc with NO. A 1 mM solution of **2**–OAc (0.002 mmol) in 2.0 mL of nitromethane was prepared as described above (Method A) in a UV–Vis cuvette at –20 °C and then cooled to –25 °C. A total of 5 mL of NO(*g*) was purged *via* gas-tight syringe through this solution (<5 s), and the reaction was monitored by UV–Visible spectroscopy. (The solubility of NO in nitromethane is not known but may be similar to that in other organic solvents, which is in the range of *ca*. 10–20 mM at –25 °C.[110] Here, the actual concentration of dissolved NO will likely be below the solubility limit.) After complete disappearance of the characteristic bands of **2**–OAc, the solution was purged for 10 min with Ar to remove excess NO. ESI(+)MS ($MeNO_2$) *m/z* calcd for $C_{16}H_{35}FeN_4O_2$ ($\{\mathbf{1}–OAc\}^+$), 371.21; $C_{14}H_{32}FeN_5O_2$ ($[Fe^{II}(tmc)(ONO)]^+$, $\{\mathbf{1}–ONO\}^+$), 358.19. Found, 371.3 ($\{\mathbf{1}–OAc\}^+$), 358.1 ($\{\mathbf{1}–ONO\}^+$), 328.1 ($\{\mathbf{1}–ONO – NO\}^+$), 257.3 ($\{tmc + H\}^+$).

Mass spectra of samples withdrawn from the reaction solution within 1.5 min of the initiation of the reaction showed additional peaks (Table 13) : ESI(+)MS ($MeNO_2$) *m/z*: 492.1 ($[Fe^{III}(tmc)(OMe)(OTf)]^+$), 402.2 ($[Fe^{III}(tmc)(OMe)(OAc)]^+$), 343.3 ($[Fe^{II}(tmc)(OMe)]^+$), 171.7 ($[Fe^{III}(tmc)(OMe)]^{2+}$). Relative abundance of Fe^{III} ions,

10–25% (t = 1.5 min), <5 % (1 h), not observed (4 h). Samples prepared using deuterated methanol (CD_3OD, 99.8% D): ESI(+)MS ($MeNO_2$) *m/z*: 495.2, 405.2, 346.4, 173.2.

Comparison of Self-Decay and NO Reaction of 2–OAc. A 1 mM solution of **2**–OAc in nitromethane was prepared at –20 °C, as described above (Method A), and then warmed to 20 °C. The half-live of the decay, as determined by UV–Visible spectroscopy, was *ca*. 25 min. ESI(+)MS ($MeNO_2$) *m/z* calcd for $C_{16}H_{35}FeN_4O_2$ ({**1**–OAc}$^+$), 371.21; found, 371.3 ({**1**–OAc}$^+$), 257.3 ({tmc + H}$^+$).

In a separate experiment, a solution of **2**–OAc was prepared at –20 °C, warmed to 20 °C, and immediately purged with 5 mL of NO(*g*) (<5 s). After complete disappearance of the characteristic bands of **2**–OAc (<10 s), the solution was purged for 10 min with Ar to remove excess NO and subjected to ESI mass spectrometry. The mass spectrum displayed peaks identical to those observed for the reaction of **2**–OAc with NO at –25 °C.

4.2.4 Product Quantification and Isotope Labeling Study

Quantification of NO_2^- Formed in the Reaction of 2–OAc with NO. The reaction of **2**–OAc with NO at –25 °C was carried out as described above. After removal of excess NO, a solution of $Na^{15}NO_2$ (0.002 mmol, 98% ^{15}N) in 0.015 mL of methanol was added as a standard to the product solution at 20 °C (1 equiv of $Na^{15}NO_2$ with respect to Fe). Following an equilibration time of 1 h, the solution was subjected to ESI mass spectrometry. The isotope distribution pattern of {**1**–ONO}$^+$ was simulated using the patterns calculated for {**1**–O$^{n.a.}$NO}$^+$ and a mixture of {**1**–O^{14}NO}$^+$ (2%) and {**1**–O^{15}NO}$^+$ (98%). In six trials, the ratio of $^{n.a.}NO_2^-$ produced to ^{15}N-enriched NO_2^- added (and thus to Fe) ranged from 1.03:1 to 1.49:1 (Table 11) [average, 1.32(18)]. [Because 0.27(6) equiv of NO_2^- (with respect to Fe) was found in solutions of **1**–OAc treated with an excess of NO (*vide infra*), the average amount of NO_2^- produced from the NO reaction of **2**–OAc was estimated as 1.05(19) equiv of NO_2^- (with respect to Fe).]

The validity of this method was tested on two series of authentic samples consisting of a) equimolar amounts of **1**–OTf(OTf) and $Na^{15}NO_2$ and varying amounts of $Na^{n.a.}NO_2$ (0.25–1.5 equiv) and b) equimolar amounts of **1**–OTf(OTf), NEt_4AcO and $Na^{15}NO_2$ and varying amounts of $Na^{n.a.}NO_2$ (0.25–1.5 equiv). The ratio of $^{n.a.}NO_2^-$ to ^{15}N-enriched NO_2^- [*i.e.*, ratio of $\{\mathbf{1}–O^{n.a.}NO\}^+$ to a mixture of $\{\mathbf{1}–O^{14}NO\}^+$ (2%) and $\{\mathbf{1}–O^{15}NO\}^+$ (98%)] determined from the observed intensity ratio was typically slightly overestimated (<20%).

The amount of NO_2^- present in solutions of NO in $MeNO_2$–MeOH was estimated as follows. A mixture of 2.0 mL of nitromethane and 0.050 mL of methanol was purged with 5 mL of NO(*g*) and, after standing for 30 min, purged for 10 min with Ar to remove excess NO. To this solution were added a solution of 0.002 mmol of **1**–OTf(OTf) in 2.0 mL of nitromethane and a solution of $Na^{15}NO_2$ (0.002 mmol, 98% ^{15}N) in 0.015 mL of methanol. Analysis of the isotope distribution pattern of $\{\mathbf{1}–ONO\}^+$ by ESI mass spectrometry indicated that typically less than 0.1 mM $^{n.a.}NO_2^-$ was present (<0.2 equiv of $^{n.a.}NO_2^-$ with respect to ^{15}N-enriched NO_2^- and Fe added).

Similarly, the possible formation of NO_2^- from the reaction of **1**–OAc with NO was tested. A solution of 0.002 mmol of **1**–OTf(OTf) and 0.002 mmol of NEt_4AcO in 2.0 mL of nitromethane and 0.050 mL of methanol was purged with 5 mL of NO(*g*) and, after standing for 30 min, purged for 10 min with Ar to remove excess NO. To this solution was added a solution of $Na^{15}NO_2$ (0.002 mmol, 98% ^{15}N) in 0.015 mL of methanol. Analysis of the isotope distribution pattern of $\{\mathbf{1}–ONO\}^+$ by ESI mass spectrometry (Table12) showed that 0.27(6) equiv of $^{n.a.}NO_2^-$ was present (with respect to ^{15}N-enriched NO_2^- and Fe).

Investigation of Methyl Nitrite Presence in Reaction of 2–OAc with NO. A solution of 2.0 mL of nitromethane and 0.050 mL of CD_3OD was prepared in a UV–Vis cuvette in a freezer at *ca*. –25 °C. A total of 5 mL of NO(*g*) was purged *via* gas-tight syringe through this solution (<5 s), and the cuvette was kept for 30 min at –25 °C. A

0.050 mL sample of the gas headspace in the cuvette was removed *via* gas-tight syringe and was subjected to GC–MS. Analysis of the GC–MS data established a peak area attributable to the background concentration due to CD_3ONO present in the headspace.

A 1 mM solution of **2**–OAc (0.002 mmol) in 2.0 mL of nitromethane was prepared as described in Section 4.2.2 (Method A), but using CD_3OD, in a UV–Vis cuvette in a freezer at *ca*. –20 °C. The cuvette was then cooled to –25 °C, then a total of 5 mL of NO(*g*) was purged *via* gas-tight syringe through this solution (<5 s), and the reaction was kept at –25 °C for 30 min. A 0.050 mL sample of the gas headspace in the cuvette was removed *via* gas-tight syringe and was subjected to GC–MS. Analysis of the GC–MS data indicated no change in the concentration of CD_3ONO relative to the background concentration established in the above description.

Subsequently, a solution of 2.0 mL of nitromethane and 0.050 mL of CD_3OD was prepared in a UV–Vis cuvette in a freezer at *ca*. –25 °C. A total of 5 mL of NO(*g*) was purged *via* gas-tight syringe through this solution (<5 s), and the cuvette was kept for 30 min at –25 °C. To the headspace of this reaction, 0.025 mL of O_2 was added. After 5 min a 0.050 mL sample of the gas headspace in the cuvette was removed *via* gas-tight syringe and was subjected to GC–MS. Analysis of GC–MS data indicated a significant increase in the peak area of the signal due to CD_3ONO (peak area doubled on average versus background concentration). Subsequent quantification of NO_2^- (0.25–0.40 mM) present in solution (*vide supra*) correlated with the amount of CD_3ONO indicated from the GC–MS data.

Isotope Labeling Experiments. For the generation of ^{18}O-enriched $[Fe^{IV}(^{18}O)(tmc)(OAc)]^+$, [^{18}O]-**2**–OAc, a solution of iodosylbenzene in methanol was treated with 10 equiv of $H_2{}^{18}O$ (98% ^{18}O) for 30 min at 20 °C. The generation of [^{18}O]-**2**–OAc at –20 °C and subsequent reaction with NO at –25 °C were carried out as described above for **2**–OAc. To determine the extent of ^{18}O incorporation, the isotope distribution patterns observed by ESI mass spectrometry for $\{$**2**–OAc$\}^+$ and $\{$**1**–ONO$\}^+$, respectively,

were simulated using the patterns calculated for the ^{16}O and ^{18}O isotopologues. For **2**–OAc, ^{18}O incorporation was in the range of 52–72% (based on the peaks at *m/z* = 387.0 and 389.0 for $\{[^{16}O]$-**2**–OAc$\}^+$ and $\{[^{18}O]$-**2**–OAc$\}^+$, respectively). For **1**–ONO, ^{18}O incorporation was in the range of 6–18% (based on the peaks at *m/z* = 358.1 and 360.1 for $\{$**1**–$^{16}ON^{16}O\}^+$ and $\{$**1**–$^{18}ON^{16}O\}^+$, respectively). The retention of ^{18}O in **1**–ONO from **2**–OAc was 12–25% (average of six trials, 18%). When the reaction of unlabeled **2**–OAc with NO was carried out in the presence of 10 equiv of $H_2{}^{18}O$, no incorporation of ^{18}O into **2**–OAc or **1**–ONO was observed.

Scheme 8. Structures of **1**–X and **2**–X[a]

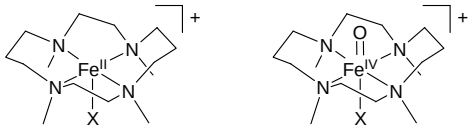

1–X **2**–X

[a] X = TfO^-, AcO^-, NO_2^-.

4.3 Results and Discussion

4.3.1 Generation and Characterization of Oxoiron(IV) Complexes

The complex $[Fe^{IV}O(tmc)(OAc)]^+$, **2**–OAc (Scheme 8), was generated by oxidation of $[Fe^{II}(tmc)(OTf)]^+$, **1**–OTf, and subsequent ligand substitution in a manner similar to that reported for the corresponding trifluoroacetato complex, $[Fe^{IV}O(tmc)\{OC(O)CF_3\}]^+$.[111] Reaction of **1**–OTf with iodosylbenzene in the weakly coordinating solvent nitromethane at –20 °C produced $[Fe^{IV}O(tmc)(OTf)]^+$, **2**–OTf, which was converted into **2**–OAc by exchange of the triflato ligand with acetate. Both

2–OTf and **2**–OAc exhibit absorption bands in the near-IR region characteristic of $[Fe^{IV}O(tmc)(L/X)]^{2+/+}$ complexes[111] [**2**–OTf, λ_{max} = 825 nm (ε = 230 $M^{-1}\cdot cm^{-1}$); **2**–OAc, λ_{max} = 825 (ε = 120 $M^{-1}\cdot cm^{-1}$) and 995 nm (100)]. As shown by incremental addition of NEt_4AcO, 1 equiv of acetate is required for the conversion of **2**–OTf into **2**–OAc in nitromethane (Figure 12). The complexes also were identified by peaks at *m*/*z* = 477 (**2**–OTf) and 387 (**2**–OAc) in their ESI mass spectra.

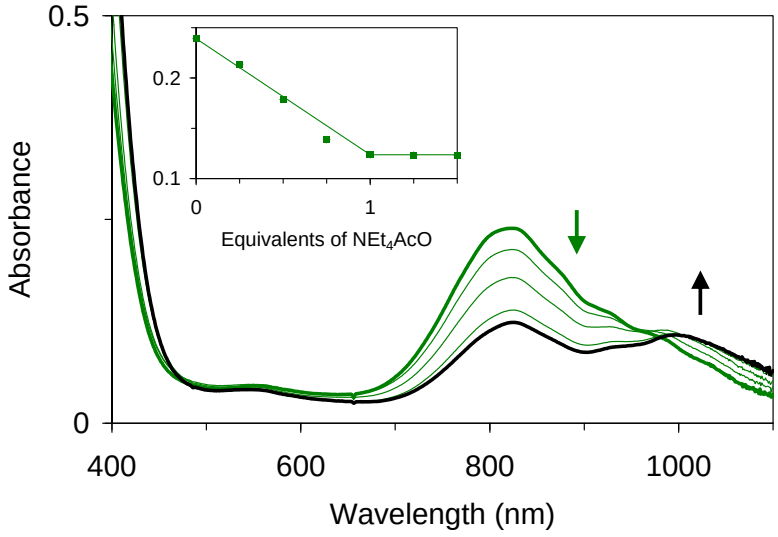

Figure 12. Conversion of 1 mM **2**–OTf (▬, green) into **2**–OAc (▬, black) in nitromethane by addition of NEt_4AcO in increments of 0.25 equiv at –20 °C as monitored by electronic absorption spectroscopy (path length, 1 cm). Inset: Corresponding changes of absorbance at 825 nm (■, green).

The coordination of the triflate anion to the Fe centers in **1**–OTf and **2**–OTf in solution and its dissociation upon addition of NEt_4AcO were investigated by ^{19}F NMR spectroscopy. For this purpose, **2**–OTf was generated by oxidation of **1**–OTf with $PhI(OAc)_2$, because **2**–OTf exhibits greater stability under these conditions. The ^{19}F NMR spectrum of **1**–OTf(OTf) in CD_3NO_2 displays two resonance signals at δ = –0.6 and –79.3 ppm, (Table 10) where the latter is attributed to the free $CF_3SO_3^-$ anion and the former to $CF_3SO_3^-$ bound to the high-spin Fe^{II} center (Figure 13). Based on the relative

intensities of these two peaks, the resonance signal at $\delta = -0.6$ ppm accounts for *ca*. 40% of the $CF_3SO_3^-$ present (*i.e.*, *ca*. 0.8 equiv with respect to Fe). This indicates that *ca*. 80% of the Fe^{II}(tmc) is present in the form of **1**–OTf, whereas the remainder corresponds to a complex without coordinated $CF_3SO_3^-$, presumably the solvento complex $[Fe^{II}(tmc)\{ON(O)CD_3\}]^{2+}$. Similarly, two ^{19}F resonance signals were observed for **2**–OTf(OTf), $\delta = -77.5$ and -79.2 ppm. Here, the peak at $\delta = -77.5$ ppm is attributed to $CF_3SO_3^-$ bound to the Fe^{IV} center and accounts for *ca*. 30% of the $CF_3SO_3^-$ present (Table 10). Thus, *ca*. 60% of the Fe in CD_3NO_2 solution corresponds to **2**–OTf and 40% to $[Fe^{IV}O(tmc)\{ON(O)CD_3\}]^{2+}$ or perhaps $[Fe^{IV}O(tmc)]^{2+}$. Upon addition of NEt_4AcO to the solution of **2**–OTf(OTf), the resonance signal of coordinated $CF_3SO_3^-$ disappeared, while that of free $CF_3SO_3^-$ became more intense and sharper ($\delta = -79.4$ ppm). These observations confirm the displacement of the $CF_3SO_3^-$ ligand in **2**–OTf by AcO^- to afford **2**–OAc.

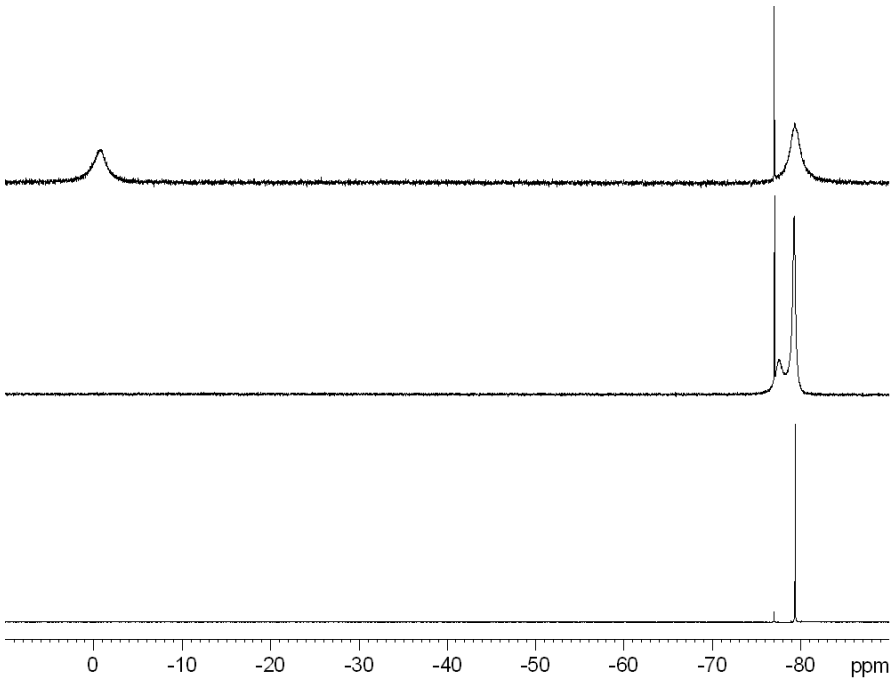

Figure 13. ^{19}F NMR spectra of **1**–OTf (top), **2**–OTf (middle), and **2**–OAc (bottom) in nitromethane-d_3 (10 mM, 282 MHz, 20 °C).

Table 10. ^{19}F NMR data for **1**–OTf, **2**–OTf and **2**–OAc in nitromethane. [a,b]

Compound	$\delta(^{19}F)$ (ppm)		Relative Peak Area		Percentage of Fe with TfO^- Bound
	Unbound TfO^-	Bound TfO^-	Unbound TfO^-	Bound TfO^-	
1–OTf(OTf)	–79.3	–0.6	1.00	0.70	82
2–OTf(OTf)	–79.2	–77.5	1.00	0.43	60
2–OAc(OTf)	–79.4		1.00		0
Free TfO^-	–79.3				

[a] Oxidation completed with $PhI(OAc)_2$.
[b] 10 mM, 282 MHz, 20 °C

To explain the different ^{19}F chemical shifts for the triflato ligands in **1**–OTf and **2**–OTf, several factors must be considered. First, coordination of the triflate ion to a Lewis-acidic metal center can be expected to cause a downfield shift of the ^{19}F resonance relative to that of free triflate. Second, the ^{19}F resonances in **1**–OTf and **2**–OTf may be subject to a hyperfine shift due to the presence of a paramagnetic metal center. By comparison with related $S = 2$ $[Fe(tmc)X]^+$ complexes,[112] the Fe d_{z2} orbital in **1**–OTf is singly-occupied (orientation of z axis defined by Fe–O bond), so a direct σ contact likely is the predominant mechanism for delocalization of unpaired spin density into triflato ligand molecular orbitals. (A π-contact contribution arising from the singly-occupied d_{xz} and d_{yz} orbitals should be negligible due to insignificant, if any, Fe–OTf π bonding.) Complex **2**–OTf, on the other hand, should lack a σ-contact contribution to the ^{19}F chemical shift, because its Fe d_{z2} orbital is vacant ($S = 1$). Furthermore, the oxo ligand being a strong ($\sigma + \pi$) donor ligand may be expected to attenuate the Lewis acidity of the Fe^{IV} center and weaken the Fe–OTf interaction. This is indeed observed as the equilibrium of triflate-bound and dissociated forms is further shifted toward the dissociated form for **2**–OTf than for **1**–OTf. The differences in hyperfine shift contributions and Fe–OTf binding between **1**–OTf and **2**–OTf may account for the large shift difference of *ca*. 77 ppm.

*4.3.2 Reactivity of $[Fe^{IV}O(tmc)(OAc)]^+$, **2**–OAc.*

The principal oxygen-atom-transfer reactivity of **2**–OAc was established by reaction with PPh_3 affording $[Fe^{II}(tmc)(OAc)]^+$ (**1**–OAc) and $OPPh_3$ (eq 1). When a solution of 1 mM **2**–OAc was reacted with 10 equiv of PPh_3 at –25 °C, the half life was *ca*. 10 min as indicated by the disappearance of the near-IR features associated with **2**–OAc (Figure 14). No intermediate was detected in this reaction.

$$[Fe^{IV}O(tmc)(OAc)]^+ + PPh_3 \rightarrow [Fe^{II}(tmc)(OAc)]^+ + OPPh_3 \qquad (1)$$

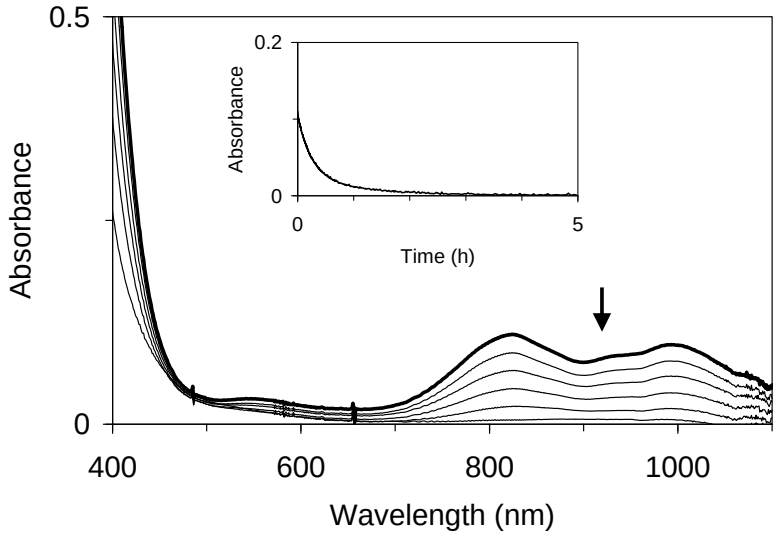

Figure 14. Reaction of 1 mM **2**–OAc (▬) with 10 equiv of PPh_3 in nitromethane at –25 °C as monitored by electronic absorption spectroscopy (path length, 1 cm). Inset: Time course of the reaction (λ = 825 nm).

Under the same conditions, **2**–OAc reacted rapidly with an excess of NO. Experiments with different amounts of NO revealed that a large excess is required for complete decomposition of **2**–OAc. As shown in Figure 15, spectral changes were also observed between 400 and 600 nm. These changes suggest the formation of an

intermediate, which reached maximum accumulation within 1 min. An isosbestic point close to 600 nm persisted for about the same time frame (Figures 15 and 16). When a smaller excess of NO was used, **2**–OAc decayed only partially, followed by tailing of the time trace at 825 nm (Figure 17). The dependence of the total absorbance change at 825 nm on the concentration of NO is consistent with an equilibrium process in the first reaction step, while the continuing slow decay in experiments with a smaller excess of NO can be explained by removal of the unstable intermediate from the equilibrium mixture.

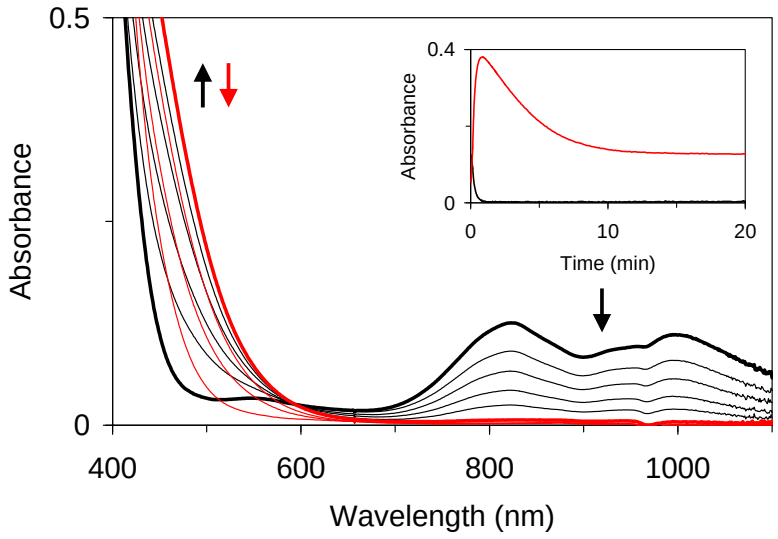

Figure 15. Reaction of 1 mM **2**–OAc (▬, black) in nitromethane with NO at –25 °C (reaction solution after *ca*. 1 min, ▬, red), as monitored by electronic absorption spectroscopy (path length, 1 cm). Inset: Time course of the reaction [λ = 825 (—, black) and 470 nm (—, red)].

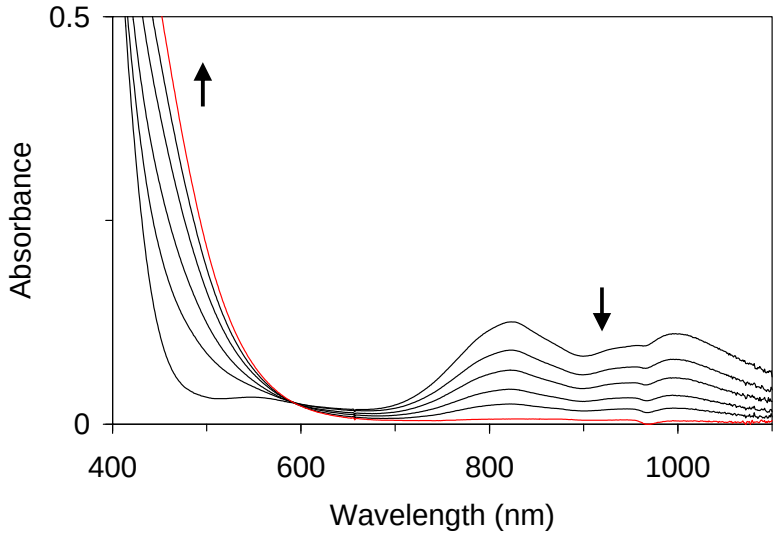

Figure 16. Reaction of 1 mM **2**–OAc (—, black) in nitromethane with NO at –25 °C (reaction solution after *ca*. 1 min, —, red), as monitored by electronic absorption spectroscopy (path length, 1 cm). The first minute of the reaction is shown (*cf.* Figure 16).

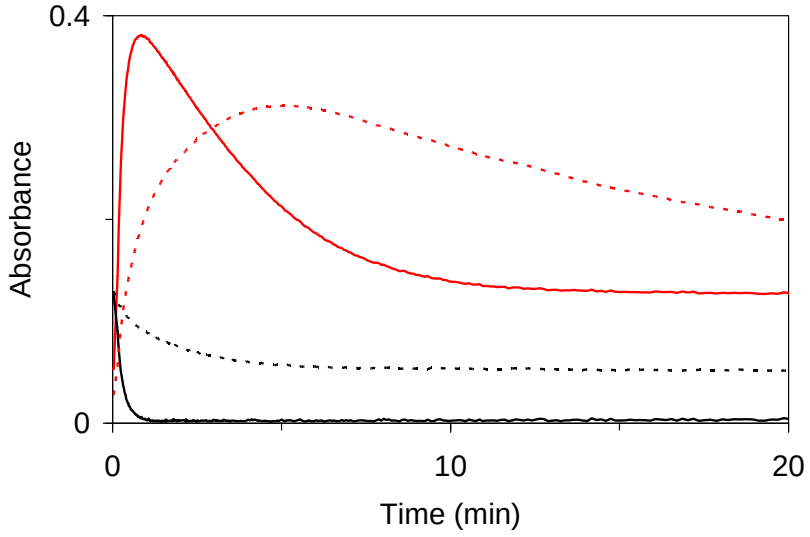

Figure 17. Time course of the decay of 1 mM **2**–OAc in nitromethane after the addition of 0.75 [λ = 825 (– – –, black) and 470 nm (– – –, red)] and 5 mL of NO [λ = 825 (—, black) and 470 nm (—, red)], as monitored by electronic absorption spectroscopy (path length, 1 cm; T = –25 °C). The volumes correspond to approximately 15 and 100 equiv of NO, respectively, with respect to **2**–OAc.

Analysis of the product solution by ESI mass spectrometry revealed peaks at *m*/*z* = 358 and 371, whose masses and isotope distribution patterns are consistent with $[Fe^{II}(tmc)(ONO)]^+$ (**1**–ONO) and **1**–OAc, respectively. Both features also were observed in the mass spectrum of an authentic sample prepared from equimolar amounts of **1**–OTf(OTf), NEt_4AcO and $NaNO_2$, demonstrating competitive binding of AcO^- and NO_2^- to the Fe^{II} center. Consistent with the ^{19}F NMR spectroscopic data for **1**–OTf (*vide supra*) and $[Fe^{II}(tmc)\{OC(O)CF_3\}]^+$,[111] the Fe^{II} center is expected to be coordinated by only one apical ligand.

To quantify the yield of NO_2^-, we added $Na^{15}NO_2$ to the product solution prior to mass-spectrometric analysis and utilized the peak arising from **1**–$O^{15}NO$ as reference. Because the ratio of $Fe^{II}(tmc)$: $^{15}NO_2^-$ was known, the yield of NO_2^- from the reaction of **2**–OAc with NO could be calculated from the intensity ratio of the peaks associated with **1**–$O^{14}NO$ (*m*/*z* = 358) and **1**–$O^{15}NO$ (*m*/*z* = 359). The isotope distribution pattern of $\{$**1**–ONO$\}^+$ was simulated using the patterns calculated for $\{$**1**–$O^{n.a.}NO\}^+$ and a mixture of $\{$**1**–$O^{14}NO\}^+$ (2%) and $\{$**1**–$O^{15}NO\}^+$ (98%). The raw data for the results are shown in Table 11. Six trials show that an average of 1.32 equiv of NO_2^- is produced with respect to Fe. We have also probed other sources of NO_2^-. First, NO_2^- has been reported to be commonly present in aqueous NO solutions[27-28,113-115] due to oxidation of NO by trace amounts of O_2.[116-117] Here, solutions of NO in $MeNO_2$–MeOH were found to contain less than 0.1 mM NO_2^-. Second, a number of transition metal complexes are known to produce NO_2^- by disproportionation of NO.[118-120] When solutions of **1**–OAc, which was identified as a product of the reaction of **2**–OAc with NO, were treated with an excess of NO, we found *ca*. 0.3 equiv of NO_2^- (with respect to Fe). These results are summarized in Table 12. Thus, these two sources of NO_2^- play a minor role in the formation of NO_2^-, here, but likely are responsible for the observation of NO_2^- in excess of 1 equiv (*cf.* Section 4.2.4 for details). The results from six trials indicate that approximately 1 equiv of NO_2^- (with respect to Fe) was produced (Figure 18). Taken together, the observations

reveal that the reaction of **2**–OAc with NO caused reduction of the Fe^{IV} center to Fe^{II} and produced NO_2^-.

Table 11. ESI(+)MS data for quantification of NO_2^- produced in the reaction of **2**–OAc with NO in nitromethane at –25 °C. [a]

Trial	Intensity ratio for peaks of m/z = 358 and 359[b]		Ratio of $^{n.a.}NO_2^-$: $^{15}NO_2^-$ [c]	Equiv of NO_2^- produced (with respect to Fe)
	Observed	Normalized		
1	97 : 100	97 : 100	1.17 : 1	1.19
2	100 : 88	112 : 100	1.41 : 1	1.44
3	100 : 87	115 : 100	1.46 : 1	1.49
4	83 : 96	86 : 1 00	1.01 : 1	1.03
5	95 : 85	112 : 100	1.41 : 1	1.44
6	86 : 82	105 : 100	1.30 : 1	1.32
Avg.		104 : 100	1.29 : 1	1.32

[a] Described in Section 4.2.4
[b] m/z = 358 and m/z = 359 corresponds to **1**–$O^{14}NO$ and **1**–$O^{15}NO$ respectively. The other possibility for the 100% relative abundance signal is m/z = 371 (**1**–OAc).
[c] $^{15}NO_2^-$ corresponds to the labeled nitrite added (98% ^{15}N)

Table 12. ESI(+)MS data for quantification of NO_2^- formed in reaction of **1**–OAc with NO in nitromethane at –25 °C.[a]

Trial	Observed intensity ratio for peaks at m/z = 358 and 359[b]	Ratio of $^{n.a.}NO_2^-$: $^{15}NO_2^-$
1	10:41	0.24:1
2	23:89	0.25:1
3	11:29	0.35:1
4	10:42	0.23:1
Avg.		0.27:1

[a] Described in Section 4.2.4
[b] m/z = 358 and m/z = 359 corresponds to **1**–$O^{14}NO$ and **1**–$O^{15}NO$ respectively. The 100% relative abundance signal is m/z = 371 (**1**–OAc) or m/z = 257 (tmc + H).

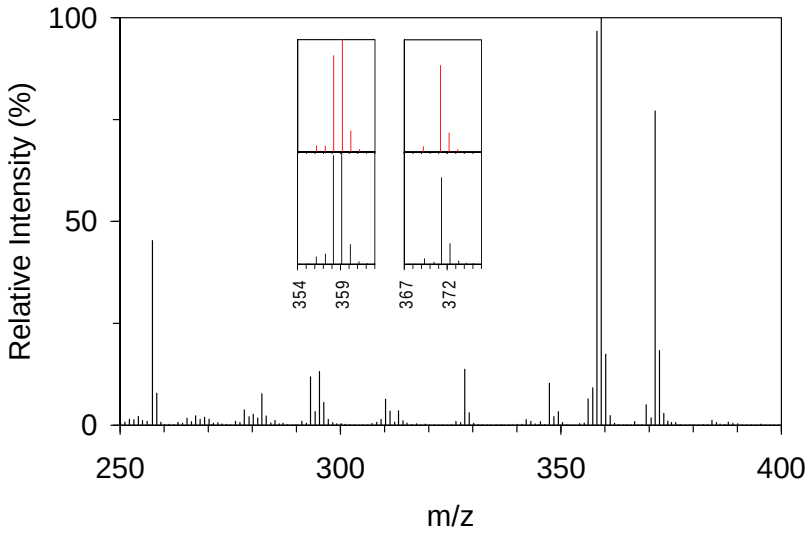

Figure 18. Electrospray ionization mass spectrum of the products of the reaction of **2**–OAc with NO in nitromethane followed by addition of 1 equiv of $Na^{15}NO_2$ (98% ^{15}N). Inset: Expanded views of the features attributed to $\{\mathbf{1}–ONO\}^+$ and $\{\mathbf{1}–OAc\}^+$ (bottom, —, black) and their calculated isotope distribution patterns (top, —, red). For $\{\mathbf{1}–ONO\}^+$, the simulated data represent the isotope distribution pattern calculated for a mixture of $\{\mathbf{1}–O^{n.a.}NO\}^+$ (50%), $\{\mathbf{1}–O^{14}NO\}^+$ (1%) and $\{\mathbf{1}–O^{15}NO\}^+$ (49%).

A plausible mechanism entails attack of NO on the oxo ligand of **2**–OAc to give $[Fe^{III}(tmc)(OAc)(ONO)]^+$ or its dissociated form, $[Fe^{III}(tmc)(OAc)]^{2+} + NO_2^-$ (net $O^{\bullet-}$ ion transfer), followed by reduction of the Fe^{III} center to Fe^{II} (Scheme 9). The absorbance increase and decrease in the 400–600 nm region may then be related to the accumulation and decay of the Fe^{III} intermediate. Indeed, analysis of the reaction mixture by ESI mass spectrometry at earlier reaction times indicated the presence of $Fe^{III}(tmc)$ complexes that are derived from $[Fe^{III}(tmc)(OAc)(ONO)]^+$ by solvent exchange, *i.e.*, $[Fe^{III}(tmc)(OAc)(OMe)]^+$ and $[Fe^{III}(tmc)(OTf)(OMe)]^+$. These species dissipated over time (Table 13).

Scheme 9. Reaction of **2**–OAc with NO[a]

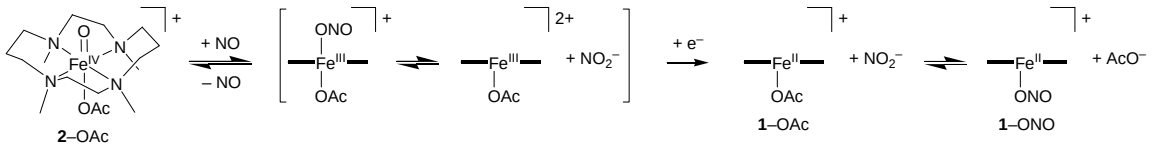

[a] —Fe— = Fe(tmc).

When deuterated methanol was used, the peaks associated with these ions shifted accordingly (*cf.* Section 4.2.3). The fact that the putative $[Fe^{III}(tmc)(OAc)(ONO)]^+$ complex was not directly detected is not surprising as it likely is a consequence of steric constraints imposed by the tetradentate tmc ligand. Fe(tmc) complexes with two axial ligands are only known where at least one of the two axial ligands is either a monoatomic (*e.g.*, O^{2-}) or a linearly coordinated diatomic ligand (*e.g.*, NO, OH^-).[67,73,111-112] Since the nitrite ion is bent and expected to form at the sterically more hindered coordination site, dissociation may be favored. Whether the $[Fe^{III}(tmc)X(OMe)]^+$ ions are the predominant intermediate species in solution or are only formed from $[Fe^{III}(tmc)(OAc)(ONO)]^+$ and methanol during the mass spectrometry experiment cannot be answered at this time.

The apparent instability of the Fe^{III} state is peculiar but must be viewed in light of the almost complete absence of $Fe^{III}(tmc)$ complexes from the literature. There are only two reports of an isolated Fe(tmc) complex with a formal Fe^{III} center.[67-68] We also note that the self-decay of **2**–OAc yields the Fe^{II} complex **1**–OAc rather than an Fe^{III} complex (*cf.* Section 4.2.3). In the reaction of **2**–OAc with NO, methanol must be involved in the decay of the Fe^{III} intermediate, because its decay was decelerated with decreasing concentration of methanol. The decay of **2**–OAc was not affected (Figure 19).

Table 13. ESI(+)MS data of Fe^{III} intermediates detected in the reaction of **2**–OAc with NO in nitromethane at –25 °C.[a]

Trial	Time[b]	Relative abundance (%)[c]		
		$[Fe^{III}(tmc)(OTf)(OMe)]^+$	$[Fe^{III}(tmc)(OAc)(OMe)]^+$	$[Fe^{III}(tmc)(OMe)]^{2+}$
		m/*z* = 492.1	*m*/*z* = 402.2	*m*/*z* = 171.1
1	90 s	12	19	21
	10 min	9.5	7.0	18
	1 h	4.5	0.5	1.5
	4 h	0	0	0.2
2	90 s	12	23	19
	10 min	9.5	6.0	13
	1 h	2.5	0.2	1.0
	4 h	0	0.1	0.2
3	90 s	8.0	1.5	9.0
	1 h	1.0	3.0	1.0
	4 h	0	0	0.2
	16 h	0	0	0

[a] Described in Section 4.2.3
[b] Time at which the sample was collected from the reaction solution after addition of NO to **2**–OAc (t = 0)
[c] Signal at 100% relative abundance is *m*/*z* = 358 or 371 (**1**–ONO or **1**–OAc)

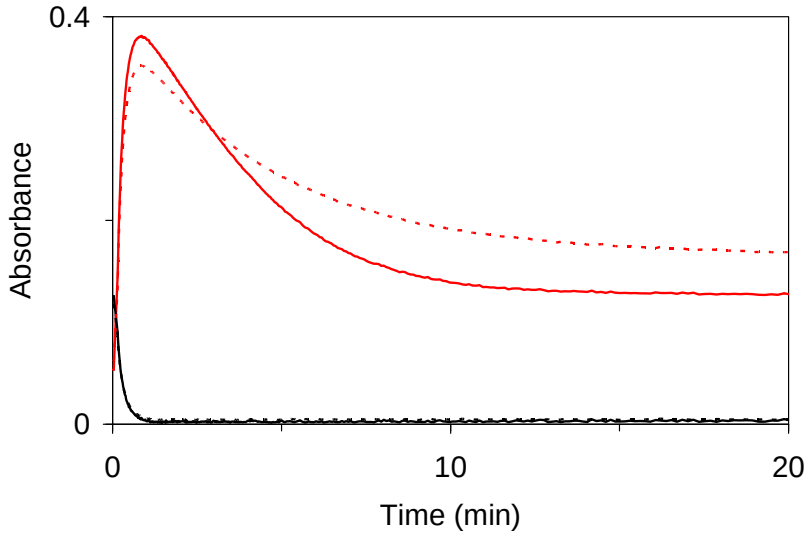

Figure 19. Time course of the reaction of 1 mM **2**–OAc in nitromethane with NO in the presence of 1 [λ = 825 (– – –, black) and 470 nm (– – –, red)] and 2.5 vol % of methanol [λ = 825 (—, black) and 470 nm (—, red)], as monitored by electronic absorption spectroscopy (path length, 1 cm; *T* = –25 °C).

Because of the presence of NO and methanol, we have considered the possibility that reductive nitrosylation (and solvolysis) of the Fe^{III} intermediate takes place, which would result in the formation of an Fe^{II} complex and methyl nitrite (eq 2).[121-126] In addition, NO_2^- is known to catalyze the reductive nitrosylation of some Fe complexes (eqs 3 and 4).[114-115,126] To assess the relevance of reductive nitrosylation, here, we have attempted to determine whether MeONO was produced. GC–MS analysis of the product mixture for MeONO is complicated by solvent interference, so we have opted to analyze the headspace of samples prepared with deuterated methanol. No significant increase in CD_3ONO concentration was observed compared to samples of NO in the same solvent system but without **2**–OAc. In contrast, the CD_3ONO concentration increased upon addition of O_2 to samples of NO in $MeNO_2$–CD_3OD. This increase correlated with the increase in nitrite yield, as measured by ESI mass spectrometry, consistent with chemistry ensuing from oxidation of NO to NO_2.[116-117]

$$[Fe^{III}(tmc)(OAc)]^{2+} + NO + MeOH \rightarrow [Fe^{II}(tmc)(OAc)]^{+} + MeONO + H^{+} \quad (2)$$

$$[Fe^{III}(tmc)(OAc)]^{2+} + NO + NO_2^- \rightarrow [Fe^{II}(tmc)(OAc)]^{+} + N_2O_3 \quad (3)$$

$$N_2O_3 + MeOH \rightarrow NO_2^- + MeONO + H^{+} \quad (4)$$

Alternatively, a two-electron pathway with oxygen-atom transfer from **2**–OAc to NO would produce **1**–OAc and NO_2 (eq 5). Nitrite along with MeONO could be formed from equilibration of NO_2 and NO with N_2O_3 and methanolysis (eqs 6 and 4). This mechanism cannot be ruled out on the basis of the Fe products, **1**–OAc and **1**–ONO. It is incompatible, however, with the lack of MeONO formation and the dependence of the decay rate of the Fe^{III} intermediate on the concentration of methanol.

$$[Fe^{IV}O(tmc)(OAc)]^{+} + NO \rightarrow [Fe^{II}(tmc)(OAc)]^{+} + NO_2 \quad (5)$$

$$NO_2 + NO \rightleftharpoons N_2O_3 \quad (6)$$

As a third alternative, a mechanism initiated by outer-sphere electron transfer from NO to **2**–OAc would likely be unfavorable due to the slow electron-transfer properties of related oxoiron(IV) complexes[52] and the high NO/NO^+ redox potential.[125-126] This mechanism would yield MeONO upon trapping of NO^+ by MeOH and no NO_2^- (in the absence of H_2O).

4.3.3 Isotope Labeling Study

Further insights into the mechanism by which NO_2^- is formed were sought from an ^{18}O-labeling study. When the reaction was carried out with ^{18}O-enriched **2**–OAc, *ca*. 20% of the ^{18}O was incorporated into **1**–ONO, demonstrating that the oxoiron(IV) unit is capable of transferring its oxygen to NO to afford NO_2^-. In contrast, the reaction of unlabeled **2**–OAc with NO in the presence of $H_2{}^{18}O$ did not lead to incorporation of ^{18}O into **2**–OAc or the nitrite product. The low ^{18}O incorporation into **1**–ONO from ^{18}O-enriched **2**–OAc indicates that isotope scrambling had occurred. A possible mechanism accounting for loss of labeled O atoms involves linkage isomerization of the nitrito ligand in $[Fe^{III}(tmc)(OAc)(^{18}ONO)]^+$ and reversible N–O bond cleavage. This process generates unlabeled **2**–OAc (and $N^{18}O$), which in turn reacts with unlabeled NO to produce unlabeled NO_2^- (eqs 7 and 8).

$$L_nFe^{III}\text{–}{}^{18}ONO \rightleftharpoons L_nFe^{III}\text{–}ON^{18}O \rightleftharpoons L_nFe^{IV}{=}O + N^{18}O \quad (7)$$

$$L_nFe^{IV}{=}O + NO \rightleftharpoons L_nFe^{III}\text{–}ONO \rightleftharpoons L_nFe^{III} + NO_2^- \quad (8)$$

A similar mechanism has previously been described for a nitratooxoruthenium(IV) complex that was formed by oxygen-atom transfer from a dioxoruthenium(VI) complex to NO_2^-. On the basis of isotope scrambling, the $L_nRu^{IV}(^{18}O)(^{18}ONO_2)^+$ complex was proposed to undergo linkage isomerization of the

nitrato ligand followed by reversible N–O bond cleavage.[127] Another scrambling mechanism would be possible in the event that NO_2 (or N_2O_3) is formed (eqs 3 and 5). Oxygen exchange would then take place between NO_2 and NO *via* N_2O_3 (eq 6). In the presence of methanol, however, the chemistry in eqs 3 and 5 inadvertently leads to formation of MeONO (eq 4), but this was not observed.

4.4 Conclusion

The reaction of an oxoiron(IV) complex, **2**–OAc, with the free radical NO is rapid and produces NO_2^-, which has been identified in the form of a nitritoiron(II) complex, **1**–ONO. This reaction is considerably faster than oxygen-atom transfer from **2**–OAc to PPh_3 and differs from the latter reaction in the formation of an intermediate, presumably an Fe^{III} complex. Two possible mechanistic scenarios for the reaction between the $Fe^{IV}O$ complex and NO involve *i)* $O^{\bullet-}$ ion transfer to afford an Fe^{III} complex and NO_2^-, followed by reduction of the Fe^{III} complex (Scheme 9), or *ii)* oxygen-atom transfer to afford an Fe^{II} complex and NO_2, which is converted into NO_2^- and MeONO *via* formation of N_2O_3 and methanolysis (eqs 5, 6 and 4). While an ^{18}O-labeling study provides evidence for the incorporation of oxygen from the $Fe^{IV}O$ group into the NO_2^- product, the observation of an intermediate Fe^{III} complex, the dependence of its decay on the concentration of methanol, and the lack of MeONO formation support an $O^{\bullet-}$ ion transfer mechanism. An outer-sphere electron transfer from NO to **2**–OAc may also be considered, but this seems unlikely due to unfavorable electron-transfer properties and redox potentials and must be ruled out because it would produce MeONO and no NO_2^-. In addition to expanding the fundamental chemistry of oxoiron(IV) complexes, the reaction described here serves as a synthetic example of the NO reactivity of biological ferryl species, such as those in myoglobin, hemoglobin, and peroxidase enzymes.

CHAPTER 5

REACTION OF AN IRON-NITROSYL COMPLEX OF 1,4,8,11-TETRAMETHYL-1,4,8,11-TETRAAZACYCLOTETRADECANE WITH TRIMETHYLAMINE *N*-OXIDE: FORMATION OF A NITRITOIRON(II) COMPLEX

5.1 Introduction

In this chapter the reaction of $[Fe(tmc)(NO)]^{2+}$ with trimethylamine N-oxide will be covered. An improved generation of $[Fe(tmc)(NO)]^{2+}$ in nitromethane will be described, along with characterization of the nitrosyl complex by UV–Vis and IR spectroscopy. The reaction with trimethylamine N-oxide afforded the Fe^{II} complex $[Fe(tmc)(ONO)]^{+}$. The reaction was monitored by UV–Vis spectroscopy and the products characterized with ESI mass spectrometry and X-ray crystallography. The amount of nitrite produced in this reaction (*ca*. 1 equiv with respect to Fe) was determined using ESI mass spectrometry after addition of ^{15}N-enriched $NaNO_2$ and supported by UV–Vis spectroscopy. Single crystals were grown from the product solution and the structure was determined to be that of the nitritoiron(II) complex [Fe(tmc)(ONO)]OTf.

The reaction of $[Fe(tmc)(NO)]^{2+}$ with trimethylamine *N*-oxide proceeds through an intermediate which was identified by UV–Vis spectroscopy at low temperatures. The observations from the collected study are consistent with a mechanism involving oxide(•1–) ion transfer from trimethylamine *N*-oxide to the nitrosyl ligand of $[Fe(tmc)(NO)]^{2+}$ to form $[Fe^{II}(tmc)(NO_2)]^{+}$. A linkage isomerization must occur to rearrange the nitrito ligand from N-bound to O-bound to the Fe. Support for the oxide(•1–) ion transfer was obtained from a study involving the presence of a sacrificial reductant during the reaction.

5.2 Experimental Section

5.2.1 Materials and Methods

Materials. All reagents and solvents were purchased from commercial sources and were used as received, unless noted otherwise. Acetonitrile, dichloromethane, and diethyl ether were deoxygenated by sparging with N_2 and purified by passage through two packed columns of molecular sieves under an N_2 pressure (MBraun solvent purification system). Nitromethane was refluxed over CaH_2 under an Ar atmosphere, distilled, and passed through a column of basic Al_2O_3.[69] Preparation and handling of air- and moisture-sensitive materials were carried out under an inert gas atmosphere by using standard Schlenk and vacuum line techniques or a glovebox. Nitrogen monoxide was prepared by reaction of concentrated hydrochloric acid with sodium nitrite.[107] The gas mixture produced was passed through a 50-cm column of KOH pellets, a 2-m stainless steel coil cooled to –94 °C (acetone–liquid N_2), and a bubbler charged with a concentrated aqueous NaOH solution for removal of unwanted nitrogen oxides; the gas was dried by passing it through a short column (*ca*. 20 cm) of KOH pellets.[69] (*Caution*: Nitrogen monoxide is a toxic gas.) $Fe(OTf)_2 \cdot 2MeCN$ was synthesized by a modified literature method[70] from anhydrous $FeCl_2$ and trimethylsilyl trifluoromethanesulfonate in acetonitrile and recrystallized from acetonitrile–diethyl ether (TfOH = CF_3SO_3H, trifluoromethanesulfonic or triflic acid).[71]. The ligand 1,4,8,11-tetramethyl-1,4,8,11-tetraazacyclotetradecane (tmc),[72] and $[Fe^{II}(tmc)(OTf)]OTf$,[73] **1**–OTf(OTf), were prepared following published procedures. The complex **1**–OTf(OTf) was stored in an N_2 atmosphere. Isotope-enriched $Na^{15}NO_2$ (98% ^{15}N) was purchased from Cambridge Isotope Laboratories, Andover, MA, USA.

Physical Methods. UV–Visible spectra were recorded on an HP 8453A diode array spectrophotometer (Agilent Technologies) with samples maintained at the desired

temperature using a cryostat/heater from Unisoku Scientific Instruments, Japan. IR spectra were recorded on a Bruker Vertex 70 Fourier-transform IR spectrometer using solutions of the compounds in nitromethane (10 mM) or solid samples. Solid samples were prepared by grinding the solid compound with KBr and pressing the mixture into a disk. Mass spectral data were acquired on a quadrupole ion trap ThermoFinnigan LCQ Deca mass spectrometer using an electrospray ionization source.

5.2.2 Generation and Reactivity of [Fe(tmc)(NO)]$^{2+}$

Generation of [Fe(tmc)(NO)]$^{2+}$, 1–NO. The preparation of **1**–NO was carried out under an N_2 atmosphere slightly adapted from a published procedure,[67] to avoid negative effects of the presence of excess NO, and it was then subsequently used *in situ* to avoid concern with stability of **1**–NO. A 1 mM solution of **1**–OTf(OTf) (0.002 mmol) in 2.0 mL of nitromethane was placed in a 1-cm UV–Vis cuvette at 20 °C. Upon addition of 0.25 mL of NO(*g*) *via* gas-tight syringe into the solution, **1**–NO formed within 35 min, with the solution turning a bold green color. UV–Vis ($MeNO_2$) λ_{max}, nm (ε): 650 (230). IR spectra of **1**–NO were in agreement with previously published data.[67] IR ($MeNO_2$, cm^{-1}): 1830 [ν(NO)]. IR (KBr, cm^{-1}): 1829 [ν(NO)].

Reaction of 1–NO with Trimethylamine *N*-oxide. A 1 mM solution of **1**–NO (0.002 mmol) in 2.0 mL of nitromethane was prepared in a UV–Vis cuvette as described above and was then treated with 0.15 mg (0.002 mmol) of trimethylamine *N*-oxide in 0.050 mL of nitromethane while being monitored by UV–Vis spectroscopy. The reaction solution changed immediately from green to orange. After complete disappearance of the characteristic bands of **1**–NO, the solution was purged for 10 min with Ar to remove excess NO. The product solution was then subjected to ESI mass spectrometry. Single crystals of X-ray diffraction quality were obtained by transferring the product solution to a vial and allowing slow diffusion of diethyl ether into the product solution over the

course of 8-10 months at –35 °C. This reaction was also carried out at –25 °C with similar products formed. ESI(+)MS ($MeNO_2$) *m/z* calcd for $C_{14}H_{32}FeN_5O_2$ ($[Fe^{II}(tmc)(ONO)]^+$, $\{\mathbf{1}–ONO\}^+$), 358.19; found, 358.1 ($\{\mathbf{1}–ONO\}^+$), 328.2 ($\{\mathbf{1}–ONO – NO\}^+$), 257.3 ($\{tmc + H\}^+$). UV–Vis ($MeNO_2$) λ_{max}, nm (ε): 440 (180).

5.2.3 Product Characterization

The reaction of **1**–NO with trimethylamine *N*-oxide at 20 °C was carried out as described above. After completed formation of **1**–O_2N, a solution of $Na^{15}NO_2$ (0.002 mmol, 98% ^{15}N) in 0.015 mL of methanol was added as a standard to the product solution (1 equiv of $Na^{15}NO_2$ with respect to Fe). Following an equilibration time of 1 h, the solution was subjected to ESI mass spectrometry. The isotope distribution pattern of $\{\mathbf{1}–ONO\}^+$ was simulated using the patterns calculated for $\{\mathbf{1}–O^{n.a.}NO\}^+$ and a mixture of $\{\mathbf{1}–O^{14}NO\}^+$ (2%) and $\{\mathbf{1}–O^{15}NO\}^+$ (98%). In six trials, the ratio of $^{n.a.}NO_2^-$ produced to ^{15}N-enriched NO_2^- added (and thus to Fe) ranged from 1.10:1 to 1.56:1 [average, 1.28(17)]. [Because 0.15(3) equiv of NO_2^- (with respect to Fe) was found in solutions of **1**–OTf treated with an excess of NO (*vide infra*), the average amount of NO_2^- produced from the trimethylamine *N*-oxide reaction of **1**–NO was estimated as 1.13 equiv of NO_2^- (with respect to Fe).] The validity of this method was tested on a series of authentic samples consisting of equimolar amounts of **1**–OTf(OTf) and $Na^{15}NO_2$ and varying amounts of $Na^{n.a.}NO_2$ and has been described previously (see Chapter 4).[106] The ratio of $^{n.a.}NO_2^-$ to ^{15}N-enriched NO_2^- [*i.e.*, ratio of $\{\mathbf{1}–O_2{}^{n.a.}N\}^+$ to a mixture of $\{\mathbf{1}–O_2{}^{14}N\}^+$ (2%) and $\{\mathbf{1}–O_2{}^{15}N\}^+$ (98%)] determined from the observed intensity ratio was typically slightly overestimated (<20%).

The reaction of **1**–OTf with NO might lead to formation of some NO_2^- due to disproportionation. The amount of NO_2^- present in solution due to the reaction of **1**–OTf with NO was estimated as follows. A solution of 0.002 mmol of **1**–OTf(OTf) in 2.0 mL

of nitromethane was purged with 5 mL of NO(*g*) at 20 °C and, after standing for 30 min, purged for 30 min with Ar to remove excess NO and NO bound to Fe. To this solution was added a solution of $Na^{15}NO_2$ (0.002 mmol, 98% ^{15}N) in 0.015 mL of methanol. Analysis of the isotope distribution pattern of $\{$**1**–ONO$\}^+$ by ESI mass spectrometry indicated that 0.15(3) equiv of $^{n.a.}NO_2^-$ was present (with respect to ^{15}N-enriched NO_2^- and Fe).

5.3 Results and Discussion

*5.3.1 Generation of [Fe(tmc)(NO)]$^{2+}$, **1**–NO*

To generate the nitrosyl complex **1**–NO an adaptation of a previous procedure was implemented.[67] Previously, **1**–NO has been prepared by purging NO gas through a solution of $[Fe(tmc)(NCCH_3)](BF_4)_2$ for 10 min, followed by addition of counter solvent to induce precipitation. The previous procedure involved difficulties for using the nitrosyl complex for further reactivity studies. The large excess of NO used to generate **1**–NO in turn leaves a large excess of NO both in solution and in the headspace of the reaction solution. This excess NO interferes in the reactions involving **1**–NO. Additionally, it is also not suitable to isolate **1**–NO as a solid as described previously, because of the instability of **1**–NO when redissolved in solution. This particular nitrosyl complex exhibits a relatively weakly binding nitrosyl ligand, and to be kept stable in solution, an excess of NO must be present.

To investigate the reactivity of **1**–NO, the same technique was used but only 0.25 mL (5 equiv with respect to **1**–OTf) of NO gas was purged through a solution of **1**–OTf to generate **1**–NO, indicated by an observed green color (Figure 20). Formation of **1**–NO was confirmed by IR spectroscopy and observation of a band at 1830 cm^{-1} which is indicative of the ν(NO) band of the bound nitrosyl ligand.[67] The generated **1**–NO was

further reacted *in situ* to avoid stability issues involved with isolating and redissolving the compound. The 5 equiv of NO were sufficient to completely generate **1**–NO ($t_{1/2} \approx 3$ min). The necessity of 5 equiv to fully form **1**–NO was determined by reacting **1**–OTf with 1, 3, 5 and 10 equiv of NO at 20 °C and then comparing the ε values of the 650 nm band with the ε value (230 $M^{-1} \cdot cm^{-1}$) of the 650 band when **1**–NO is formed with extended purging of NO gas as described previously.[67] The least amount of NO required to generate **1**–NO with a ε value of 230 $M^{-1} \cdot cm^{-1}$ was 5 equiv. The **1**–NO complex is stable for *ca*. 1 h when generated with 5 equiv of NO. When **1**–NO is generated with an extended purging of NO gas, it is stable for *ca*. 2 weeks.

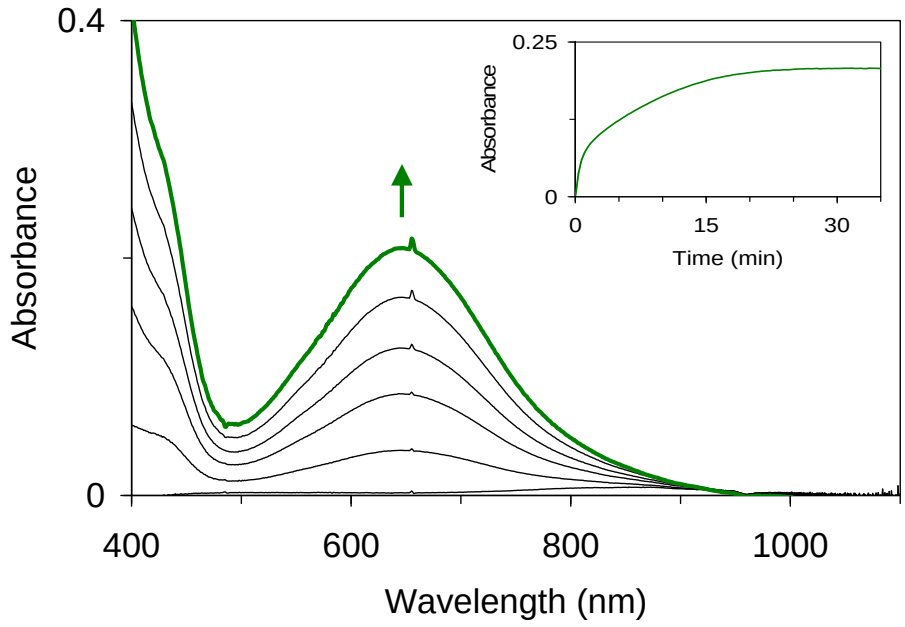

Figure 20. Generation of **1**–NO (▬, green) from1 mM **1**–OTf in nitromethane by addition of 0.25 mL (*ca*. 5 equiv) of NO at 20 °C as monitored by electronic absorption spectroscopy (path length, 1 cm). Inset: Time course of the reaction at 650 nm (—, green).

*5.3.2 Reaction of **1**–NO with Trimethylamine N-oxide*

The oxidation of **1**–NO was examined by use of trimethylamine *N*-oxide at 20 °C, and the reaction proceeded with a color change as the green color of **1**–ONO changed immediately to orange. The reaction was monitored by UV–Visible spectroscopy to observe the decay of the indicative band of **1**–NO, and the formation of a new band at 440 nm with a molar absorptivity of 180 $M^{-1} \cdot cm^{-1}$ (Figure 21).

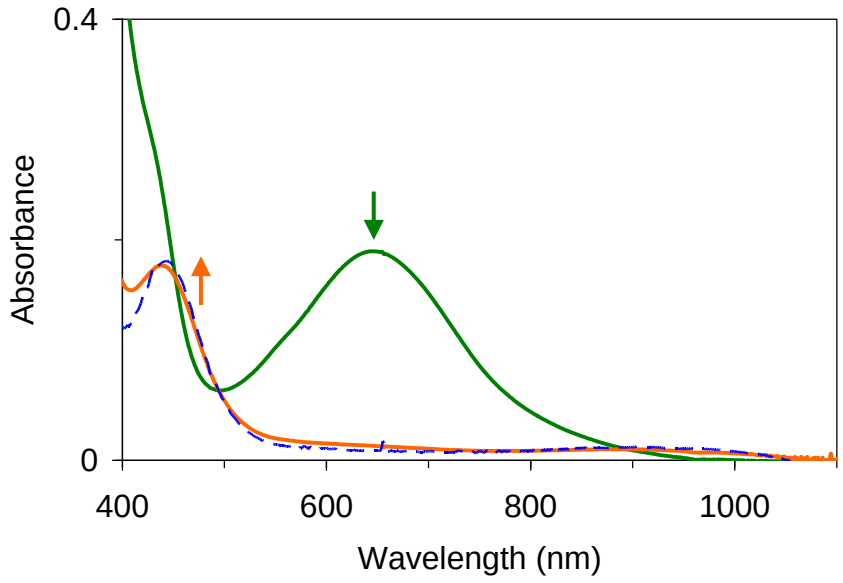

Figure 21. Reaction of 1 mM **1**–NO (—, green) with 1 equiv of trimethylamine *N*-oxide in nitromethane at 20 °C (reaction solution after 1 s, —, orange) as monitored by electronic absorption spectroscopy and electronic absorption spectrum of 1 mM **1**–ONO in nitromethane from Chapter 3, Figure 1 (--- blue) (path length, 1 cm).

This resultant spectrum, including λ_{max} and ε, is identical to that of the independently synthesized compound **1**–ONO described in Chapter 3. This reaction proceeded too quickly at 20 °C to be able to observe any intermediary spectra, so it was performed at a cooler temperature. When the reaction was carried out at –25 °C, the

decay of **1**–NO was slowed, but interestingly, the formation of the band at 440 nm appeared at *ca.* four times the intensity as it formed at 20 °C. This more intense band then decayed to a resultant spectrum identical to the one formed from the reaction at 20 °C over the course of *ca*. 3 min, indicating that some kind of intermediate was formed and then decayed to the final product (Figure 22).

Single crystals of the product from the reaction of **1**–NO and trimethylamine *N*-oxide were grown by vapor diffusion of diethyl ether into a nitromethane solution at –25 °C. A crystallographic analysis confirmed the formation of [Fe(tmc)(ONO)]OTf. Descriptions of the molecular structure of the nitrito product **1**–ONO and comparison to other Fe^{II}(tmc) complexes can be found in Chapter 3.

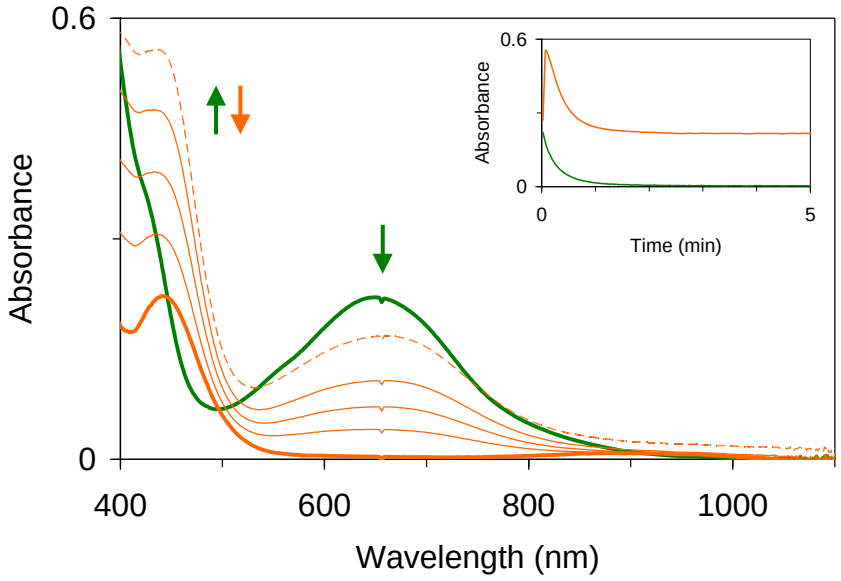

Figure 22. Reaction of 1 mM **1**–NO (▬, green) with 1 equiv of trimethylamine *N*-oxide in nitromethane at –25 °C (reaction solution after 4 s, ---, orange; reaction solution after 250 s, ▬, orange) as monitored by electronic absorption spectroscopy (path length, 1 cm). Inset: Time course of the reaction [λ = 650 (—, green) and 440 nm (—, orange)].

Analysis of the product solution by ESI mass spectrometry revealed an *m/z* value of 358, whose isotope distribution pattern is consistent with $[Fe^{II}(tmc)(ONO)]^+$ (**1**–ONO). To quantify the yield of NO_2^-, $Na^{15}NO_2$ was added to the product solution prior to mass-

spectrometric analysis and the peak arising from **1**–O^{15}NO was utilized as reference (as described in Chapter 4). Given that the ratio of Fe^{II}(tmc) : $^{15}NO_2^-$ was known, the yield of NO_2^- from the reaction of **1**–NO with trimethylamine *N*-oxide could be calculated from the intensity ratio of the peaks associated with **1**–O^{14}NO (*m/z* = 358) and **1**–O^{15}NO (*m/z* = 359). The isotope distribution pattern of {**1**–ONO}$^+$ was simulated using the patterns calculated for {**1**–O$^{n.a.}$NO}$^+$ and a mixture of {**1**–O^{14}NO}$^+$ (2%) and {**1**–O^{15}NO}$^+$ (98%). The raw data for the results are shown in Table 14.

Table 14. ESI(+)MS data for quantification of NO_2^- from the reaction of **1**–NO with Me_3N–O in nitromethane at 20 °C [a]

Trial	Intensity ratio for peaks at *m/z* = 358 and 359[b]		Equiv of NO_2^- produced (with respect to Fe)
	Observed	Normalized	
1	90 : 81	111 : 100	1.38
2	45 : 38	120 : 100	1.56
3	39 : 40	98 : 100	1.17
4	93 : 88	106 : 100	1.30
5	94 : 97	97 : 100	1.17
6	92 : 100	92 : 100	1.10
Avg.		104 : 100	1.28

[a] Described in Section 5.2.3
[b] *m/z* = 358 and *m/z* = 359 corresponds to **1**–O^{14}NO and **1**–O^{15}NO respectively. The other possibility for the 100% relative abundance signal is *m/z* = 257 (tmc + H).

Six trials show that an average of 1.28 equiv of NO_2^- is produced with respect to Fe. We have also probed another source of NO_2^-. As discussed in Chapter 4, a number of transition metal complexes are known to produce NO_2^- by disproportionation of NO.[118-120] When solutions of **1**–OTf were treated with an excess of NO, we found *ca.* 0.15 equiv of NO_2^- with respect to Fe. These results are summarized in Table 15. Thus, this source of NO_2^- plays a minor role in the formation of NO_2^-, here, but likely is

responsible for the observation of NO_2^- in excess of 1 equiv (*cf.* Section 5.2.3 for details). The results from six trials reveal that approximately 1 equiv of NO_2^- (with respect to Fe^{II}(tmc) was produced (Figure 23). Taken together, the observations reveal that the reaction of **1**–NO with trimethylamine *N*-oxide causes oxidation of the nitrosyl ligand to produce Fe^{II} and NO_2^-.

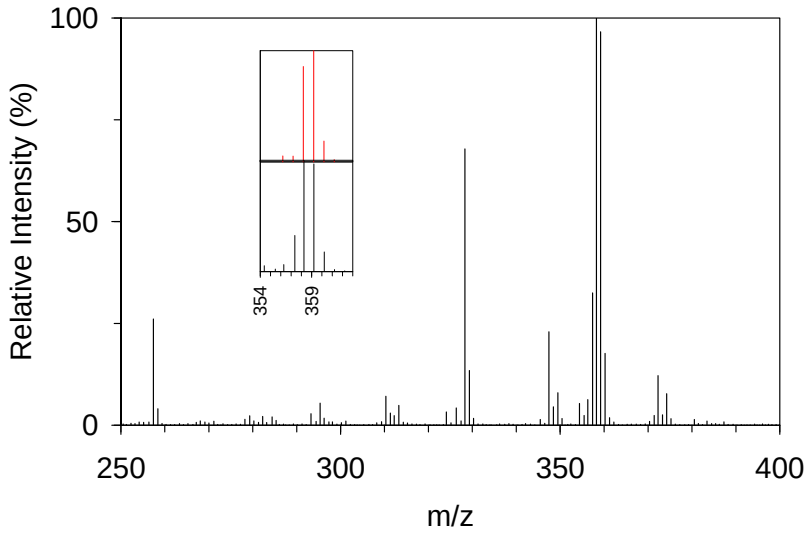

Figure 23. Electrospray ionization mass spectrum of the products of the reaction of **1**–NO with trimethylamine *N*-oxide in nitromethane followed by addition of 1 equiv of $Na^{15}NO_2$ (98% ^{15}N). Inset: Expanded views of the feature attributed to $\{$**1**–ONO$\}^+$ (bottom, —, black) and its calculated isotope distribution pattern (top, —, red). For $\{$**1**–ONO$\}^+$, the simulated data represent the isotope distribution pattern calculated for a mixture of $\{$**1**–$O^{n.a.}NO\}^+$ (50%), $\{$**1**–$O^{14}NO\}^+$ (1%) and $\{$**1**–$O^{15}NO\}^+$ (49%).

Table 15. ESI(+)MS data for quantification of NO_2^- from the reaction of **1**–OTf + NO in nitromethane at 20 °C[a]

Trial	Intensity ratio for peaks at *m*/*z* = 358 and 359[b]		Equiv of NO_2^- produced (with respect to Fe)
	Observed	Normalized	
1	17 : 79	20 : 100	0.18
2	13 : 72	15 : 100	0.13
3	12 : 67	16 : 100	0.14

[a] Described in Section 5.2.3
[b] *m*/*z* = 358 and *m*/*z* = 359 corresponds to **1**–$O^{14}NO$ and **1**–$O^{15}NO$ respectively. The other possibility for the 100% relative abundance signal is *m*/*z* = 257 (tmc + H) or 461 (**1**–OTf).

5.3.3 Mechanistic Studies

Since nitrite has been identified in the reaction of **1**–NO with trimethylamine *N*-oxide, there are two possible outcomes that should be considered. First, net O atom transfer may occur which would result in the formation of Fe^{II} and NO_2 in the $[Fe^{II}(tmc)(NO_2)]^{2+}$ complex (which may also be described as the nitritoiron(III) complex $[Fe^{III}(tmc)(NO_2)]^{2+}$). The second outcome would be that of net $O^{\bullet-}$ ion transfer resulting in the formation of Fe^{II} and NO_2^-. This net $O^{\bullet-}$ ion transfer could occur as a concerted $O^{\bullet-}$ ion transfer step, or as a coupled "O"/e^- transfer (in which the O atom and electron may or may not come from the same source).

These two outcomes would most likely proceed through two different possible mechanisms. There is either direct oxidation of the nitrosyl ligand by trimethylamine *N*-oxide, or initial dissociation of the nitrosyl ligand, oxidation of the Fe^{II} center to Fe^{IV} by trimethylamine *N*-oxide, then reaction of Fe^{IV} with NO (Scheme 10). We have shown previously that an $Fe^{IV}O(tmc)$ complex can react with nitric oxide to form nitrite.[106] To examine the possibility of this mechanism taking place, we have reacted $[Fe^{II}(tmc)(OTf)]^+$ (**1**–OTf) with trimethylamine *N*-oxide in nitromethane to look for formation of the oxoiron(IV) complex $[Fe^{IV}O(tmc)(OTf)]^+$ (**2**–OTf). Addition of both one and multiple equivalents of trimethylamine *N*-oxide to the solution of **1**–OTf resulted in no observed formation of **2**–OTf by either UV–Vis spectroscopy or ESI mass spectrometry. This indicates that trimethylamine *N*-oxide can not oxidize **1**–OTf to form **2**–OTf in nitromethane. Thus the nitrite formed in the reaction between **1**–NO and trimethylamine *N*-oxide can not be formed by an intermediate reaction between **2**–OTf and NO and the mechanism involving initial dissociation of the nitrosyl ligand is not taking place here. This is interesting to note as previous examples of nitrosyl complex oxidation proposes intial nitrosyl dissociation mechanisms.

Scheme 10. Considered Mechanism for **1**–ONO Formation *via* Oxoiron(IV) Intermediate.

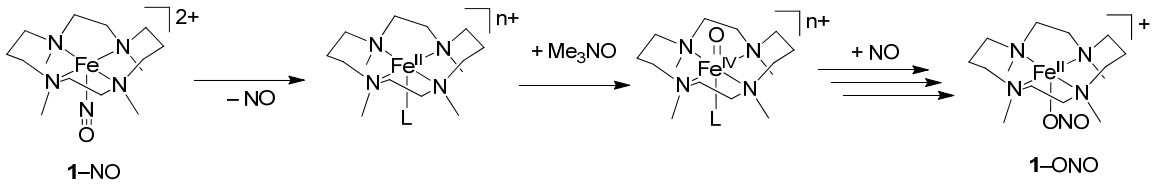

L = $MeNO_2$ or TfO^-

The probable mechanism for this reaction would involve direct oxidation of the nitrosyl ligand by trimethylamine *N*-oxide to ultimately form NO_2^- (either by O atom or $O^{\bullet-}$ ion transfer). An intermediate was observed at –25 °C by monitoring the reaction with UV–Vis spectroscopy, which could be an Fe^{III} complex, so we have subjected the reaction solution in the time-frame of the intermediate being present to ESI mass spectrometry. However, no peaks indicative of an Fe^{III} complex were observed. In our previous work, we have shown that an Fe^{III}(tmc) intermediate could be observed by ESI mass spectrometry in the presence of methanol.[106] For this reason, we carried out the reaction at –25 °C with methanol present. The resulting reaction progression as monitored by UV–Vis spectroscopy showed that the intermediate band in the region of 380–500 nm was stabilized (we have also probed this reaction using deuterated methanol with no difference in reaction progression observed). The intermediate remained present approximately three times as long as when no methanol was present and the decay rate of **1**–NO decreased by the same scale (Figure 24). This stabilization of the intermediate and decrease of the decay of **1**–NO does not rule out the possibility of the intermediate being due to an Fe^{III} complex, but it may be attributable to a linkage isomer (the nitrogen-bound NO_2^- ligand) which is stabilized by a solvent effect. It is also possible that the intermediate is stabilized because the overall reaction of the oxidation of **1**–NO by trimethylamine *N*-oxide is slower due to solvent effect. This can be observed in the decrease in the rate of decay of **1**–NO when methanol is present. Subjection of the

product solution with methanol present during the time the intermediate was present to ESI mass spectrometry showed no peaks indicative of Fe^{III} complexes. The lack of observation of any Fe^{III} complex (but instead only Fe^{II}) indicates that the reaction is not a net O atom transfer, but instead it is a net $O^{\bullet-}$ ion transfer.

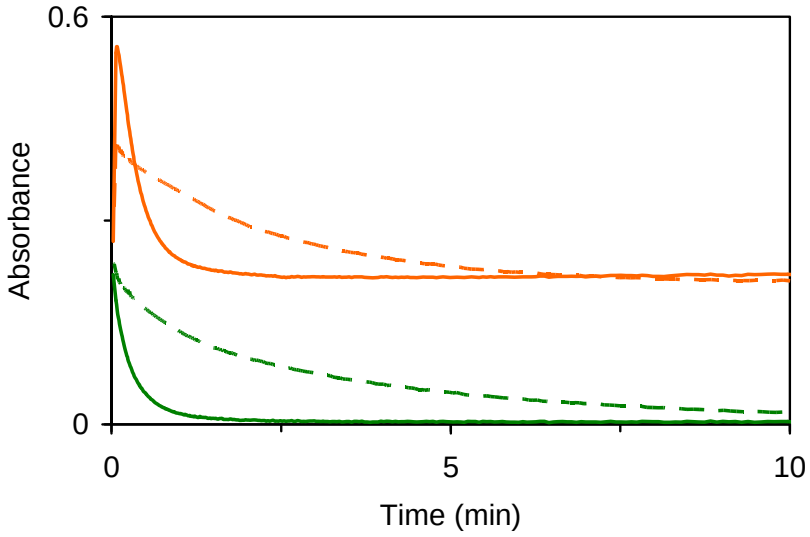

Figure 24. Time course of the reaction of 1 mM **1**–NO in nitromethane with trimethylamine *N*-oxide in the presence of 0 [λ = 650 ▬, green) and 440 nm ▬, orange)] and 1 vol % of methanol [λ = 825 (---, green) and 470 nm (---, orange)], as monitored by electronic absorption spectroscopy (path length, 1 cm; T = –25 °C).

A net $O^{\bullet-}$ ion transfer must involve either a concerted step, or a coupled O atom/electron transfer. It is a possibility that the trimethylamine *N*-oxide could transfer the oxygen atom and electron in a concerted $O^{\bullet-}$ ion transfer. However, to investigate the possibility of a coupled transfer, we have searched to determine the source of the electron in the mechanism. All other species present in solution must be considered to determine what is most likely to participate as the electron transfer agent (Table 16). Other species present in solution include the solvent nitromethane, nitric oxide (excess from the generation of **1**–NO), and trimethylamine (the resulting by-product of trimethylamine *N*-oxide reaction). Considering that after the first step, once the oxygen atom has transferred

to the nitrosyl ligand, the trimethylamine molecule would be immediately adjacent to the Fe complex, this would provide for easy electron transfer to reduce the Fe complex based on proximity. Additionally, the redox potential of trialkylamines is generally lower than that of nitric oxide and nitromethane, making it the most easily oxidized component in solution.

Table 16. List of Relevant Reducing Agents and their Oxidation Potentials.

Possible Reducing Agent	Potential vs. Fc/Fc^+ (V)	ref
$N(CH_2CH_3)_3$	0.41[a]	This work
$N(CH_2CH_3)_3$	0.47[b]	74
NO	0.92[a]	128
CH_3NO_2	>0.6	129
1–ONO	0.644[a]	This work (Section 3.2.1)

[a] Measurement taken in nitromethane
[b] Measurement taken in acetonitrile

In further efforts to deduce the mechanism by which this reaction takes place, and working under the hypothesis that trimethylamine *N*-oxide is both the source of the oxygen atom and the electron, we have investigated the reaction by adding *N,N*-dimethylaniline (DMA), as a sacrificial reducant. The redox potential of DMA (0.26 V)[130] is lower than trimethylamine, and DMA is known to go through a three-step oxidation process, resulting in the formation of the *N,N,N',N'*-tetramethylbenzidine cation radical ($TMB^{\bullet+}$) (Scheme 11) which is easily observed and monitored by UV–Vis spectroscopy (λ_{max} (ε) = 900 nm (2 x 10^4 $M^{-1}\cdot cm^{-1}$).[130] By adding DMA, if the reaction proceeds through a coupled "O"/e^- transfer, it may be possible for DMA to be the source of the electron and $TMB^{\bullet+}$ should be observed.

Scheme 11. Three-electron Oxidation Mechanism of *N,N*-dimethylaniline (DMA) to form the *N,N,N',N'*-tetramethylbenzidine Radical Cation ($TMB^{\bullet+}$).

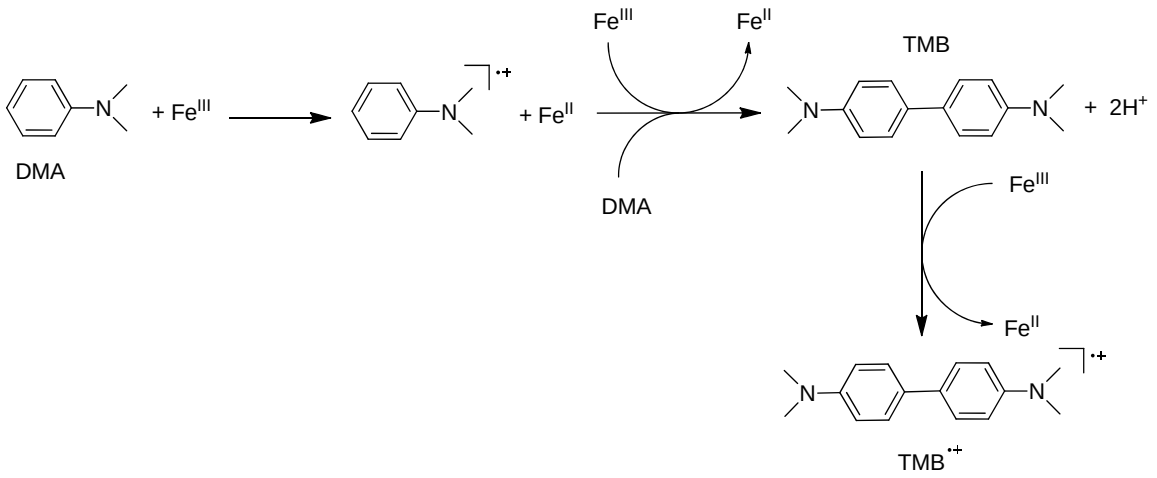

However, when this reaction was carried out in the presence of DMA and monitored by UV–Vis spectroscopy, there was minimal $TMB^{\bullet+}$ formed (<1%), based on the absorbance at 900 nm (1.5×10^1 $M^{-1} \cdot cm^{-1}$). This would signify that in a competitive environment, trimethylamine is the preferred reducing agent over DMA, even though this is contradictory to what the respective redox potentials indicate. This result indicates the reaction will proceed through a net $O^{\bullet-}$ ion transfer from trimethylamine *N*-oxide (either by a concerted or "O"/e^- coupled step) to the nitrosyl ligand of **1**–NO to form NO_2^- (as the N-bound nitro ligand), followed by a linkage isomerization of the nitro ligand, resulting in the formation of the nitrito complex $[Fe^{II}(tmc)(ONO)]^+$ (Scheme 12).

Scheme 12. Reaction of **1**–NO with Trimethylamine *N*-oxide

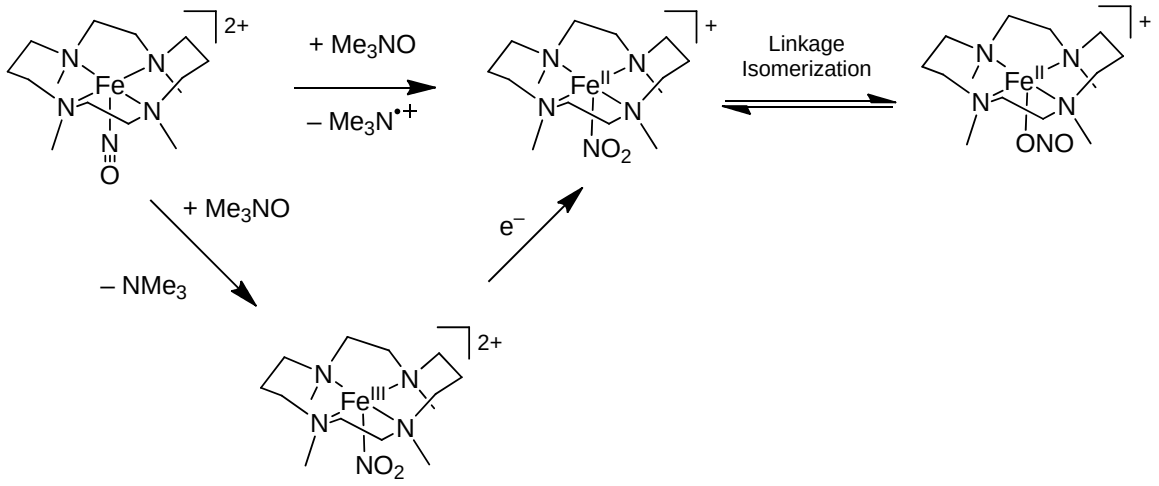

5.4 Conclusion

The reaction of a nitrosyl complex, **1**–NO, with trimethylamine *N*-oxide is very fast and produces NO_2^-, which has been identified using ESI mass spectrometry in the form of a nitritoiron(II) complex, **1**–ONO. Quantification using ESI MS and isotopically labeled $^{15}NO_2^-$ showed that 1 equiv of NO_2^- was produced with respect to Fe. The final product was also verified using single-crystal X-ray diffraction. This reaction proceeds through an intermediate which has been observed at low temperatures using UV–Visible spectroscopy and is proposed to be due to a linkage isomerization. While multiple mechanistic scenarios for the reaction were considered, results are consistent with net $O^{\bullet-}$ ion transfer from trimethylamine *N*-oxide to **1**–NO to form Fe^{II} and NO_2^-, followed by a linkage isomerization to form the final product (Scheme 12). The reaction described here serves as a synthetic example of oxidation of nitrosyl complexes by an oxygen atom donor.

CHAPTER 6

REACTION OF AN OXOIRON(IV) COMPLEX OF [BIS(2-PYRIDYL)METHYL]BIS(2-PYRIDYLMETHYL)AMINE (N4Py) WITH NITROGEN MONOXIDE AND NITRITE: FORMATION OF A NITRATOIRON(II) COMPLEX

6.1 Introduction

In this chapter the reactions of $[FeO(N4Py)]^{2+}$ with sodium nitrite and nitrogen monoxide will be covered. The reaction with sodium nitrite afforded nitrate and an Fe^{II}(N4Py) complex. The reaction was monitored using UV–Vis spectroscopy in which an isosbestic point could be observed. The products were characterized using ESI mass spectrometry and IR spectroscopy. The amount of nitrate formed in this reaction (*ca*. 1 equiv with respect to Fe) was quantified using IR spectroscopy after addition of ^{15}N-enriched $NaNO_3$. The reaction proceeds with no intermediate observed by monitoring with UV–Vis spectroscopy. The observations are consistent with a mechanism involving an oxygen atom transfer from the oxoiron(IV) complex to nitrite to form Fe^{II} and NO_3^-.

The reaction with nitrogen monoxide interestingly afforded the same products, nitrate and an Fe^{II}(N4Py) complex. The reaction was monitored using UV–Vis spectroscopy in which an isosbestic point could be observed only over the first *ca*. 5 min of the reaction, then the progress of the reaction changed. The products were characterized using ESI mass spectrometry and IR spectroscopy. The amount of nitrate formed in this reaction (*ca*. 0.5 equiv with respect to Fe) was quantified using IR spectroscopy after addition of ^{15}N-enriched $NaNO_3$. The 2:1 stoichiometry of $Fe^{IV}O$ to NO is consistent with the formation of nitrate. The results suggest that nitrite is an intermediate in a two step reaction. A possible mechanism could involve a first step oxide(•1–) ion transfer from an oxoiron(IV) complex to NO to form an Fe^{III} complex and

NO_2^-. An oxygen atom transfer from a second equivalent of oxoiron(IV) to the intermediate NO_2^- then occurs to form Fe^{II} and NO_3^-.

The reported reactions serve as synthetic examples of the oxidation of nitrogen monoxide and nitrite *via* oxoiron(IV) complexes. The oxidation of nitrite by the oxoiron(IV) complex is quite unique as it is rare to see nitrite oxidized by oxometal complexes.

6.2 Experimental Section

6.2.1 Materials and Methods

Materials. All reagents and solvents were purchased from commercial sources and were used as received, unless noted otherwise. Acetonitrile, dichloromethane, and diethyl ether were deoxygenated by sparging with N_2 and purified by passage through two packed columns of molecular sieves under an N_2 pressure (MBraun solvent purification system). Nitromethane was refluxed over CaH_2 under an Ar atmosphere, distilled, and passed through a column of basic Al_2O_3.[69] Preparation and handling of air- and moisture-sensitive materials were carried out under an inert gas atmosphere by using standard Schlenk and vacuum line techniques or a glovebox. Nitrogen monoxide was prepared by reaction of concentrated hydrochloric acid with sodium nitrite.[107] The gas mixture produced was passed through a 50-cm column of KOH pellets, a 2-m stainless steel coil cooled to –94 °C (acetone–liquid N_2), and a bubbler charged with a concentrated aqueous NaOH solution for removal of unwanted nitrogen oxides; the gas was dried by passing it through a short column (*ca*. 20 cm) of KOH pellets.[69] (*Caution*: Nitrogen monoxide is a toxic gas.) $Fe(OTf)_2 \cdot 2MeCN$ was synthesized by a modified literature method[70] from anhydrous $FeCl_2$ and trimethylsilyl trifluoromethanesulfonate in acetonitrile and recrystallized from acetonitrile–diethyl ether (TfOH = CF_3SO_3H,

trifluoromethanesulfonic or triflic acid).[71] Isotope-enriched $Na^{15}NO_3$ (98% ^{15}N) and $H_2{}^{18}O$ (98% ^{18}O) were purchased from Cambridge Isotope Laboratories, Andover, MA, USA.

Physical Methods. UV–Visible spectra were recorded on an HP 8453A diode array spectrophotometer (Agilent Technologies) with samples maintained at the desired temperature using a cryostat/heater from Unisoku Scientific Instruments, Japan. IR spectra were recorded on a Bruker Vertex 70 Fourier-transform IR spectrometer using samples prepared by grinding the solid compound with KBr and pressing the mixture into a disk. Mass spectral data were acquired on a quadrupole ion trap ThermoFinnigan LCQ Deca mass spectrometer using an electrospray ionization source.

6.2.2 Synthesis and Reactivity of an Oxoiron(IV) Complex

Synthesis of N,N-bis(2-pyridylmethyl)-N-(bis-2-pyridylmethyl)amine (N4Py). The compound N4Py was synthesized from a modified published procedure.[54,131] A solution of 0.29 g (7.25 mmol) of sodium hydroxide in 1.5 mL water was cooled to 0 °C in an ice bath. To the cooled solution, 1.185 g (7.23 mmol) of solid 2-(chloromethyl)pyridine hydrochloride was slowly added in portions over 10 min while stirring. The cooled solution was then added dropwise to 0.72 g (3.62 mmol) of bis(2-pyridylmethyl)amine at 0 °C followed by an additional 1.5 mL solution of 0.29 g (7.25 mmol) of sodium hydroxide in water, cooled to 0 °C. This solution was left to stir for 42 h at 25 °C at which time 3 mL of concentrated perchloric acid was rapidly added to precipitate a yellow solid, which was separated by filtration. The yellow solid was then recrystallized from hot water. This perchlorate salt was then neutralized with 5 M sodium hydroxide and extracted with dichloromethane, 5 x 15 mL. The organic layers were combined, washed with a saturated aqueous NaCl solution (3 x 15 mL), and then dried over $MgSO_4$. Evaporation of the dichloromethane yielded the free amine, N4Py (0.25 g,

19% yield). Successful formation of N4Py·$HClO_4$ was confirmed by ^{1}H NMR. ^{1}H NMR (300 MHz, $CDCl_3$, δ): 8.65 (d, 4H, Py), 8.09 (m, 4H, Py), 7.60 (m, 8H, Py), 5.80 (s, 1H, CH), 4.35 (s, 4H, CH_2).

Synthesis of [Fe^{II}(N4Py)(NCMe)](OTf)$_2$ (3–NCMe). The complex **3**–NCMe was synthesized from a modified published procedure.[54,131] A solution of 0.16 g (0.34 mmol) of $Fe(OTf)_2 \cdot 2\ CH_3CN$ in 2.5 mL acetonitrile was added dropwise to a solution of 0.125 g (0.34 mmol) of N4Py in 2.5 mL acetonitrile while stirring under an inert atmosphere at 25 °C for 14 h. The solution became deep red in color within 5 min of stirring. The acetonitrile was then removed under reduced pressure and the intense orange residue was then redissolved in acetonitrle and recrystallized from vapor diffusion of diethyl ether into the solution at –30 °C. Yield: 0.15 g (58%). ^{1}H NMR (300 MHz, CD_3CN, δ): 9.03 (d, 2H, Py), 8.89 (d, 2H, Py), 7.90 (m, 4H, Py), 7.69 (m, 2H, Py), 7.36 (m, 4H, Py), 7.06 (m, 2H, Py), 6.32 (s, 1H, CH), 4.33 (q, 4H, CH_2), 2.13 (s, 3H, CH_3). ESI(+)MS (MeCN) *m/z* calcd for $C_{25}H_{24}FeN_6$ ([Fe^{II}(N4Py)($NCCH_3$)]$^{2+}$, {**3**–NCMe}$^{2+}$), 232.12; found, 232.1 ({**3**–NCMe }$^{2+}$), 368.2 ({N4Py + H}$^+$), 390.3 ({N4Py + Na}$^+$). UV–Vis (MeCN) λ_{max}, nm (ε): 455 (4000).

Generation of [Fe^{IV}O(N4Py)]$^{2+}$ (4). The preparation of **4** was adapted from a previously published procedure by increasing the reaction time.[56,65] A 1 mM solution of **3**-NCMe (0.002 mmol) in 2 mL in acetonitrile was treated with 8.8 x 10^{-4} g (0.004 mmol) iodosylbenzne at 25 °C and left to stir for 40 min. Removal of the unreacted solids *via* filtration afforded a blue-green solution. The blue-green solution was then subjected to ESI mass spectrometry and measured with UV–Vis spectroscopy. ESI(+)MS (MeCN) *m/z* calcd for $C_{23}H_{21}FeN_5O$ ([Fe^{IV}O(N4Py)]$^{2+}$, {**4**}$^{2+}$), 219.61; found, 219.5 ({**4**}$^{2+}$), 368.2 ({N4Py + H}$^+$), 390.3 ({N4Py + Na}$^+$). UV–Vis (MeCN) λ_{max}, nm (ε): 695 (400).

6.2.3 Reactivity of $[Fe^{IV}O(N4Py)]^{2+}$ Toward NO_2^- and Product Charaterization

Reaction of 4 with NO_2^-. A 1 mM solution of **4** (0.002 mmol) in 2 mL of acetonitrile was prepared as described above at 25 °C and placed in a 1-cm UV–Vis cuvette. The solution was purged for *ca*. 10 min with Ar to remove O_2. While being monitored by UV–Visible spectroscopy, the solution was treated with 0.002 mol of $NaNO_2$ in 0.050 mL of acetonitrile/methanol (9:1). After complete disappearance of the characteristic bands of **4** and formation of the characteristic bands of **3**–NCMe (*ca*. 5 min), the intense orange product solution was subjected to ESI mass spectrometry and prepared for IR spectroscopy. The full formation of the characteristic bands of **3**–NCMe was determined by measuring a UV–Vis spectrum of the product solution that was diluted to 10% of the original concentration. ESI(+)MS (MeCN) *m/z* calcd for $C_{23}H_{21}FeN_6O_3$ ($\{$**3**–$ONO_2\}^+$), 485.23. Found, 485.2 ($\{$**3**–$ONO_2\}^+$), 368.3 ($\{$N4Py + $H\}^+$), 390.1 ($\{$N4Py + $Na^+\}^+$). IR (KBr, cm^{-1}): 1385 (ν_{NO}). UV–Vis of product solution diluted to 10% original concentration of reaction (MeCN) λ_{max}, nm (ε): 455 (4000).

Quantification of NO_3^- Formed in the Reaction of 4 with NO_2^-. The reaction of **4** with $NaNO_2$ at 25 °C was carried out as described above. After full formation of **3** as monitored by UV–Vis spectroscopy, a solution of $Na^{15}NO_3$ (0.002 mmol, 98% ^{15}N) in 0.015 mL of methanol was added as a standard to the product solution at 25 °C (1 equiv of $Na^{15}NO_3$ with respect to Fe). Following an equilibration time of 1 h, the solvent was removed under reduced pressure to leave behind a solid yellow-orange residue. A pellet consisting of the solid residue and KBr was prepared for and subjected to IR spectroscopy. The intensity of the transmittance of the signals due to free NO_3^- (1385 cm^{-1}) produced by the reaction and $^{15}NO_3^-$ (1352 cm^{-1}) added were compared. In three trials, the ratio of NO_3^- produced in the reaction to $^{15}NO_3^-$ added (and thus to Fe) ranged from 0.51:1 – 0.60:1 [average, 0.54:1]. The validity of this method was tested on a

series of authentic samples consisting of equimolar amounts of **3**–NCMe and $Na^{15}NO_3$ and varying amounts of $Na^{n.a.}NO_3$ (0.5–2.0 equiv). The ratio of NO_3^- to ^{15}N-enriched NO_3^-determined from the observed intensity ratio was within 5%.

6.2.4 Reactivity of $[Fe^{IV}O(N4Py)]^{2+}$ Toward NO and Product Charaterization

Reaction of 4 with NO. A 1 mM solution of **4** (0.002 mmol) in 2 mL of acetonitrile was prepared as described above at 25 °C and placed in a 1-cm UV–Vis cuvette. The solution was purged for *ca*. 10 min with Ar to remove O_2. A total of 0.025 mL of NO(g) (0.001 mmol) was then added *via* gas-tight syringe to the solution and the reaction was monitored by UV–Visible spectroscopy. After complete disappearance of the characteristic bands of **4** (*ca*. 5 min) and formation of the characteristic bands of **3**–NCMe (*ca*. 60 min), the reaction solution was purged for *ca*. 10 min with Ar to remove excess NO. The full formation of the characteristic bands of **3**–NCMe was determined by measuring a UV–Vis spectrum of the product solution that was diluted to 10% of the original concentration. The intense orange product solution was then subjected to ESI mass spectrometry and prepared for IR spectroscopy (*vide infra*). ESI(+)MS (MeCN) *m/z* calcd for $C_{23}H_{21}FeN_6O_3$ ($\{$**3**–$ONO_2\}^+$), 485.23. Found, 485.2 ($\{$**3**–$ONO_2\}^+$), 368.3 ($\{N4Py + H\}^+$), 390.1 ($\{N4Py + Na\}^+$). IR (KBr, cm^{-1}): 1385 (ν_{NO}) UV–Vis of product solution diluted to 10% original concentration of reaction (MeCN) λ_{max}, nm (ε): 455 (4000

Quantification of NO_3^- Formed in the Reaction of 4 with NO. The reaction of **4** with NO at 25 °C was carried out as described above. After removal of excess NO, a solution of $Na^{15}NO_3$ (0.002 mmol, 98% ^{15}N) in 0.015 mL of methanol was added as a standard to the product solution at 25 °C (1 equiv of $Na^{15}NO_3$ with respect to Fe). Following an equilibration time of 1 h, the solvent was removed under reduced pressure

to leave behind a solid yellow-orange residue. A pellet consisting of the solid residue and KBr was prepared for and subjected to IR spectroscopy. The intensity of the absorbance of the signals due to free NO_3^- (1385 cm^{-1}) produced by the reaction and $^{15}NO_3^-$ (1352 cm^{-1}) added were compared. In three trials, the ratio of NO_3^- produced in the reaction to $^{15}NO_3^-$ added (and thus to Fe) ranged from 0.93:1 – 1.09:1 [average, 1.02:1].

6.2.5 Isotope Labeling Studies

The generation of **4** was carried out as described above, but in nitromethane (the study was also carried out in acetonitrile; however incorporation of ^{18}O into **4** was poor). For the formation of ^{18}O-enriched $[Fe^{IV}(^{18}O)(N4Py)]^{2+}$, [$^{18}O$]-**4**, a solution of **4** in nitromethane was treated with 0.004 mL (100 equiv) of $H_2{}^{18}O$ (98% ^{18}O) for 60 min at 25 °C.[132] The reaction of [^{18}O]-**4** with NO or NO_2^- was carried out as described above for **4**. To determine the extent of ^{18}O incorporation, the isotope distribution patterns observed by ESI mass spectrometry for {**4**–OTf}$^+$ and {**3**–ONO_2}$^+$, respectively, were simulated using the patterns calculated for the ^{16}O and ^{18}O isotopologues. For **4**–OTf, ^{18}O incorporation was in the range of 28–65% (based on the peaks at *m/z* = 588.0 and 590.0 for {[^{16}O]-**4**–OTf}$^+$ and {[^{18}O]-**4**–OTf}$^+$, respectively). For **3**–ONO_2 produced in the reaction of NO_2^- with [^{18}O]-**4**, ^{18}O incorporation was in the range of 59–71% (based on the peaks at *m/z* = 485.0, 487.0 and 489.0 for {**3**–$^{16}ON^{16}O_2$}$^+$, {**3**–$^{18}ON^{16}O_2$}$^+$ and {**3**–$^{16}ON^{18}O_2$}$^+$, respectively). The retention of ^{18}O in **3**–ONO_2 from **4** was 129–171% (average of three trials, 148%). For **3**–ONO_2 produced in the reaction of NO with [^{18}O]-**4**, ^{18}O incorporation was in the range of 28–54% (based on the peaks at *m/z* = 485.0, 487.0 and 489.0 for {**3**–$^{16}ON^{16}O_2$}$^+$, {**3**–$^{18}ON^{16}O_2$}$^+$ and {**3**–$^{16}ON^{18}O_2$}$^+$, respectively). The retention of ^{18}O in **3**–ONO_2 from **4** was 46–198% (average of three trials, 114%). In acetonitrile, the ^{18}O incorporation into **4**–OTf was in the range of 9–15% (based on the peaks at *m/z* = 588.0 and 590.0 for {[^{16}O]-**4**–OTf}$^+$ and {[^{18}O]-**4**–OTf}$^+$, respectively).

For **3**–ONO_2 produced in the reaction of NO_2^- with [^{18}O]-**4**, ^{18}O incorporation was in the range of 48–60% (based on the peaks at *m/z* = 485.0, 487.0 and 489.0 for {**3**–$^{16}ON^{16}O_2$}$^+$, {**3**–$^{18}ON^{16}O_2$}$^+$ and {**3**–$^{16}ON^{18}O_2$}$^+$, respectively). The retention of ^{18}O in **3**–ONO_2 from **4** was 313–416% (average of three trials, 374%). For **3**–ONO_2 produced in the reaction of NO with [^{18}O]-**4**, ^{18}O incorporation was in the range of 61–64% (based on the peaks at *m/z* = 485.0, 487.0 and 489.0 for {**3**–$^{16}ON^{16}O_2$}$^+$, {**3**–$^{18}ON^{16}O_2$}$^+$ and {**3**–$^{16}ON^{18}O_2$}$^+$, respectively). The retention of ^{18}O in **3**–ONO_2 from **4** was 441–688% (average of three trials, 524%).

6.3 Results and Discussion

6.3.1 Oxidation of Nitrite

The oxidation of nitrite by **4** was examined at 25 °C, and the reaction was monitored by UV–Visible spectroscopy to observe the disappearance of the indicative band of **4** (λ = 695 nm), and the formation of a new band at 455 nm demonstrating the direct reaction of **4** with nitrite (Figure 25). The resulting spectrum, including the band at 455 nm (ε = 4000 $M^{-1}\cdot cm^{-1}$) is consistent with the spectrum of the precursor Fe^{II} complex **3**–NCMe.[54] The complete decay of **4** and full formation of the resulting product spectrum was confirmed by dilution of the product solution to 10% of the original concentration of **4** (1 mM to 0.1 mM). This spectrum is shown in Figure 26. The complete decay of **4** and full formation of the resulting product spectrum required 1 equiv NO (with respect to Fe), implying a 1:1 stoichiometry for the reaction. The decay of **4** exhibited a half-life of *ca*. 50 s.

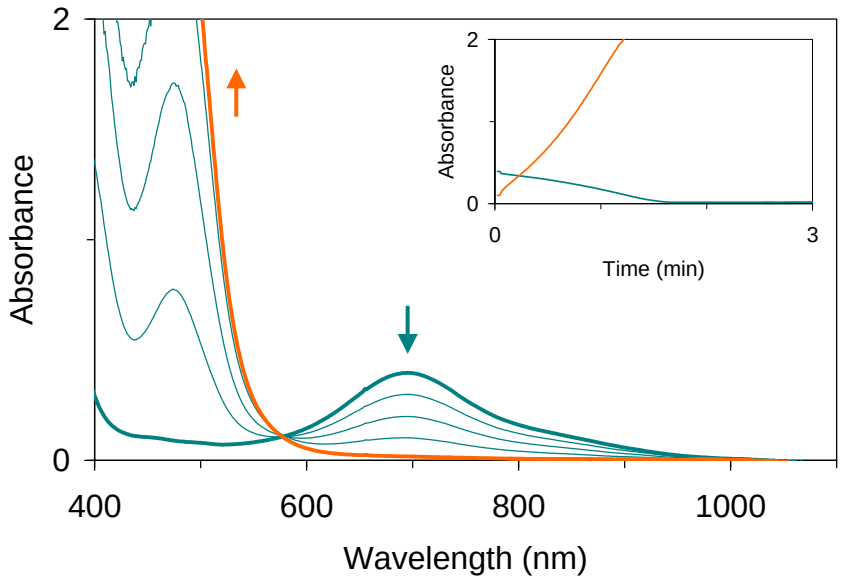

Figure 25. Reaction of 1 mM **4** (—, teal) with 1 equiv $NaNO_2$ in acetonitrile at 25 °C (reaction solution after *ca*. 2 min, —, orange), as monitored by electronic absorption spectroscopy (path length, 1 cm). Inset: Time course of the reaction [λ = 695 (—, teal) and 455 nm (—, orange)].

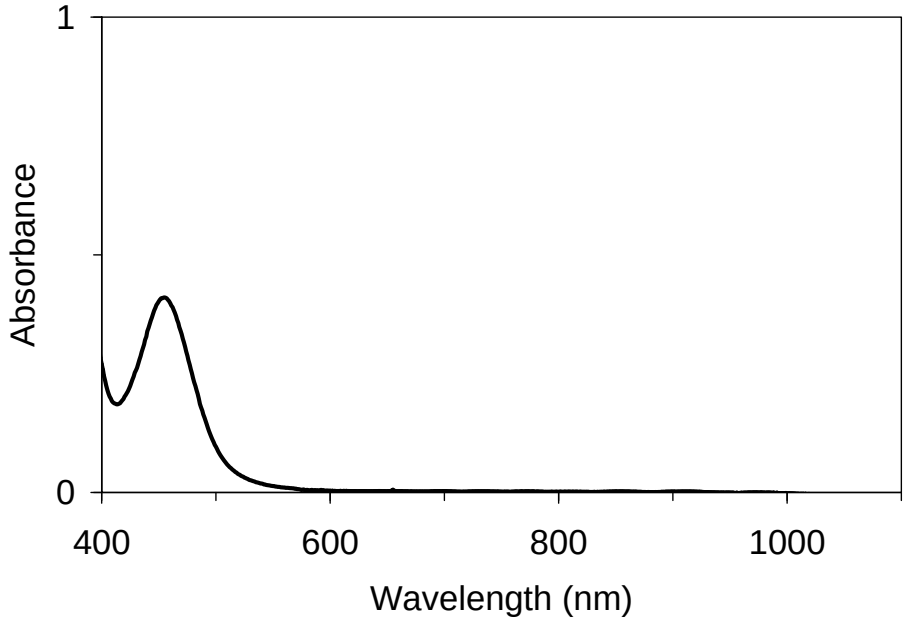

Figure 26. UV–Vis spectrum of the product solution from the reaction of 1 mM **4** with 1 equiv $NaNO_2$ in acetonitrile at 25 °C, diluted to 10% of the original concentration. (path length, 1 cm).

Analysis of the product solution by ESI mass spectrometry revealed a peak at *m*/*z* = 485, the mass and isotope distribution pattern consistent with $[Fe^{II}(N4Py)(ONO_2)]^+$ (**3**–ONO_2) and a peak at *m*/*z* = 211.5, consistent with $[Fe^{II}(N4Py)(NCMe)]^{2+}$ (**3**–NCMe). This feature was also observed in an authentic sample produced from equimolar amounts of $[Fe^{II}(N4Py)(NCMe)]^{2+}$ and $NaNO_3$. Analysis of the product solution by IR spectroscopy confirmed the presence of nitrate as a product, revealing a band at 1385 cm^{-1} (Figure 27) that was not present in the IR spectrum of **3**–NCMe.

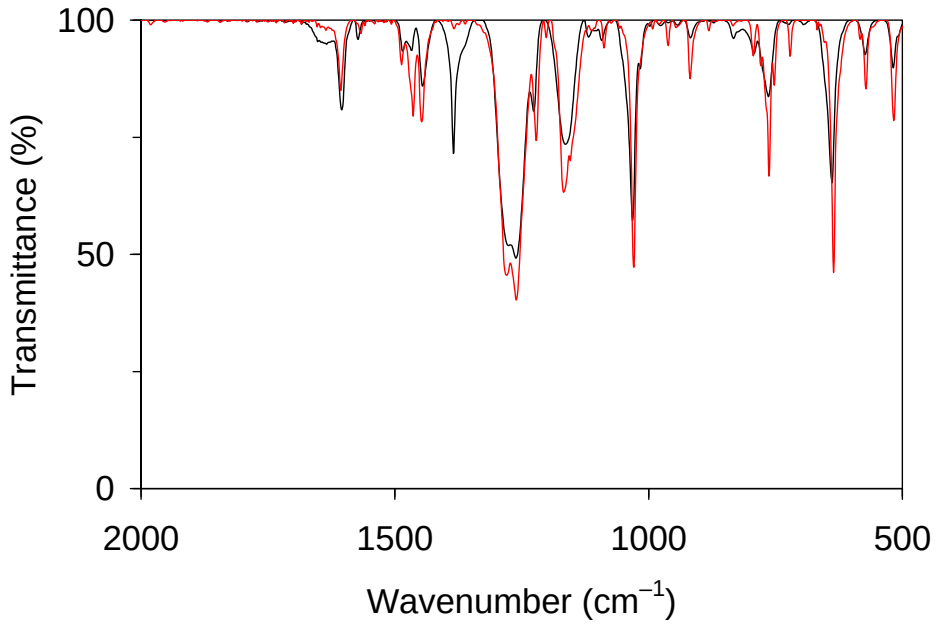

Figure 27. Solid-state IR (KBr) spectra of the products from the reaction of **4** with 1 equiv $NaNO_2$ in acetonitrile at 25 °C (black, —) and **3**–NCMe (red, —).

This band is indicative of unbound nitrate, and previous work has shown that nitrate bound to a metal center can be exchanged with bromide upon preparation of a KBr pellet for IR spectroscopy.[133-134] Upon comparison with the IR spectrum of **3**–NCMe, no other new signals were present in the product spectrum other than that due to unbound nitrate, indicating that all nitrate observed in the IR spectrum, and thus produced by the reaction, was in the unbound state. The nitrate produced by the reaction was quantified by

addition of 1 equiv $Na^{15}NO_3$ to the product solution prior to preparation of a pellet for IR spectroscopic analysis and utilizing the band arising from unbound ^{15}N-nitrate (Figure 28). Because the ratio of Fe^{II}(N4Py) : $^{15}NO_3^-$ was known, the yield of nitrate from the reaction of **4** with nitrite could be calculated from the intensity ratio of the bands associated with unbound nitrate (1385 cm^{-1}) and ^{15}N-nitrate (1352 cm^{-1}). The results from three trials indicate that a range of 0.93 to 1.09 (avg. 1.02) equiv of NO_3^- (with respect to Fe) was produced (Table 17). Taken together, the observations reveal that the reaction of **4** with NO_2^- caused reduction of the Fe^{IV} center to Fe^{II} and produced 1 equiv NO_3^-.

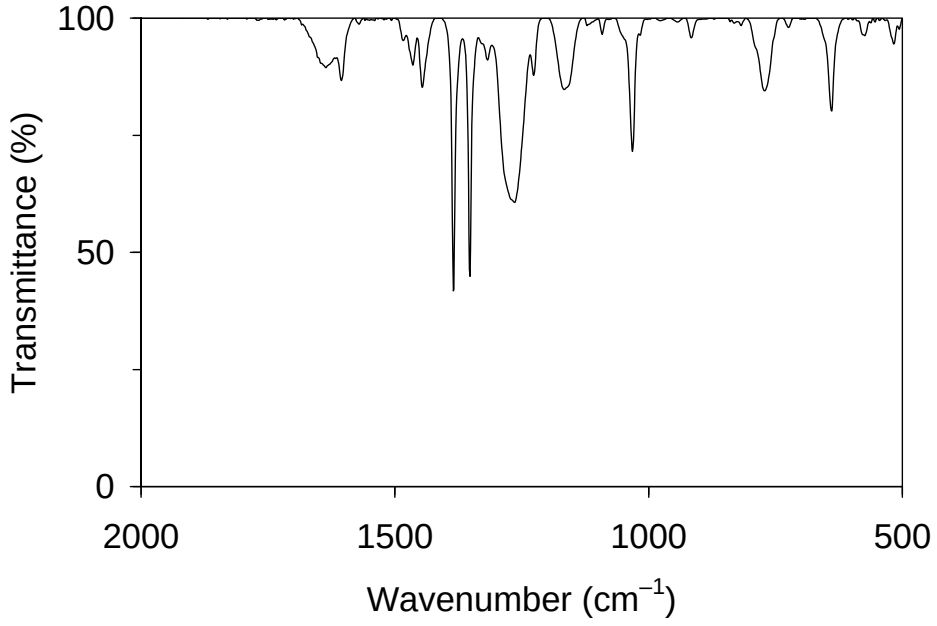

Figure 28. Solid-state IR (KBr) spectrum of the products from the reaction of **4** with 1 equiv $NaNO_2$ with the addition of 1 equiv $^{15}NO_3^-$ with respect to Fe.

Table 17. IR data for quantification of NO_3^- from the reaction of **4** with NO_2^- in acetonitrile at 25 °C[a]

Trial	Observed Transmittance at 1385 cm^{-1} : 1352 cm^{-1} [b]	Equiv of NO_3^- produced (with respect to Fe)
1	48.25 : 44.43	1.09
2	64.14 : 68.85	0.93
3	56.49 : 53.85	1.05
Avg.		1.02

[a] Described in Section 6.2.3
[b] 1385 cm^{-1} and 1352 cm^{-1} corresponds to IR bands of NO_3^- and $^{15}NO_3^-$ respectively.

A plausible mechanism could consist of a 2 e^- oxygen atom transfer from the Fe^{IV}=O moiety to nitrite to form Fe^{II} and NO_3^- (Scheme 13).

Scheme 13. Reaction of **4** with $NaNO_2$.

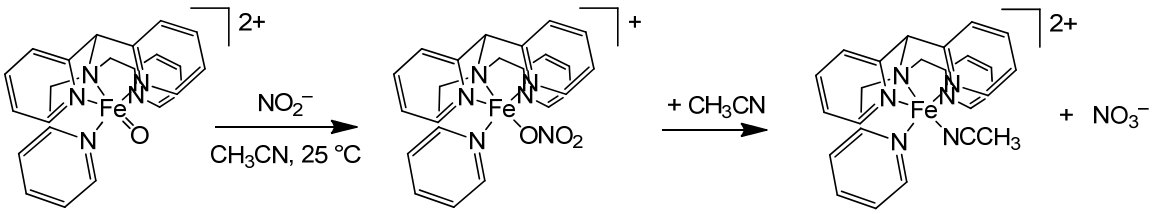

When monitoring the reaction by UV–Visible spectroscopy, the formation of the new band at 455 nm begins to form immediately upon addition of nitrite. This band is indicative of **3**–NCMe, and its formation with concomitant decay of the band at 695 nm due to **4** is consistent with a one-step reaction.

The chemistry of an oxygen atom transfer mechanism from **4** to NO_2^- would result in the formation of **3**–ONO_2 and this product is observed in the ESI mass spectrum. The nitrate then dissociates, and free NO_3^- is observed in the IR spectrum of the products from the reaction of **4** with NO_2^-. The observation of **3**–ONO_2 in the mass spectrum and

free nitrate in the IR spectrum, along with the quantification measurements indicating 1 equiv of nitrate formed (with respect to Fe), as observed in IR spectroscopy, are consistent with the proposed mechanism of an oxygen atom transfer.

6.3.2 Oxidation of Nitrogen Monoxide

The oxidation of NO by **4** was examined at 25 °C, and the reaction was monitored by UV–Visible spectroscopy to observe the disappearance of the indicative band of **4** (λ = 695 nm), and the formation of a new band at 455 nm demonstrating the direct reaction of **4** with NO. The new band at 455 nm did not form immediately upon addition of NO, but instead a slight delay (<5 s) occurred between initiating decay of the 695 nm band with addition of NO, and commencement of the formation of the band at 455 nm (Figure 29).

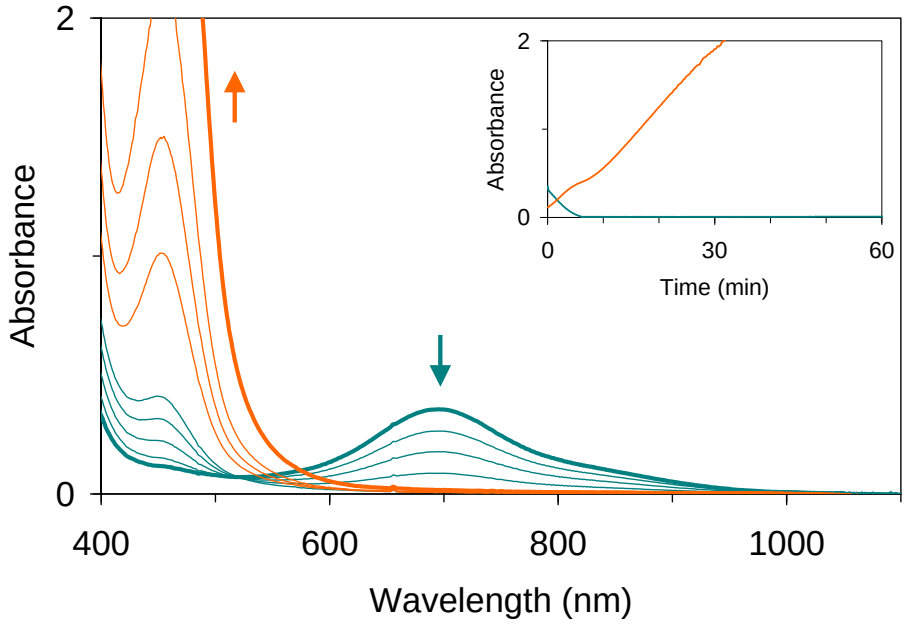

Figure 29. Reaction of 1 mM **4** (—, teal) with 0.025 mL (*ca*. 0.5 equiv) NO in acetonitrile at 25 °C (reaction solution after *ca*. 20 min, —, orange, after *ca*. 50 min, —, orange), as monitored by electronic absorption spectroscopy (path length, 1 cm). Inset: Time course of the reaction [λ = 695 (—, teal) and 455 nm (—, orange)].

The resulting product spectrum, including the band at 455 nm (ε = 4000 $M^{-1}cm^{-1}$) is consistent with the spectrum of the precursor Fe^{II} complex **3**–NCMe.[54] The complete decay of **4** and full formation of the resulting product spectrum was confirmed by dilution of the product solution to 10% of the original concentration of **4** (1 mM to 0.1 mM) and is shown in Figure 30. The complete decay of **4** and full formation of the resulting product spectrum required 0.5 equiv NO (with respect to Fe), implying a 2:1 stoichiometry for the reaction. The decay of **4** exhibited a half-life of *ca*. 3 min. The reaction progresses similarly with 1 equiv of NO, resulting in an identical product spectrum.

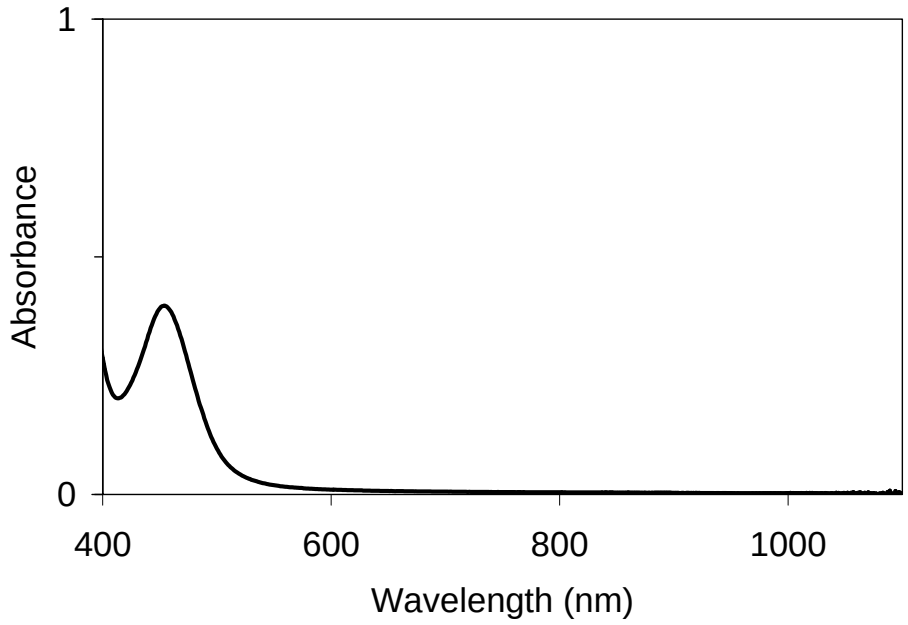

Figure 30. UV–Vis spectrum of the product solution from the reaction of 1 mM **4** with 0.025 mL (*ca*. 0.5 equiv) NO in acetonitrile at 25 °C, diluted to 10% of the original concentration. (path length, 1 cm).

Analysis of the product solution by ESI mass spectrometry revealed a peak at *m*/*z* = 485, which as previously stated displayed a mass and isotope distribution pattern consistent with $[Fe^{II}(N4Py)(ONO_2)]^+$ (**3**–ONO_2). Analysis of the product solution by IR spectroscopy confirmed the presence of nitrate as a product, revealing a band at

1385 cm^{-1}, indicative of unbound nitrate (Figure 31). This band was not present in the spectrum of **3**–NCMe. It should be noted that upon checking in the appropriate IR regions (see Chapter 3), there was no band indicative of unbound nitrite.

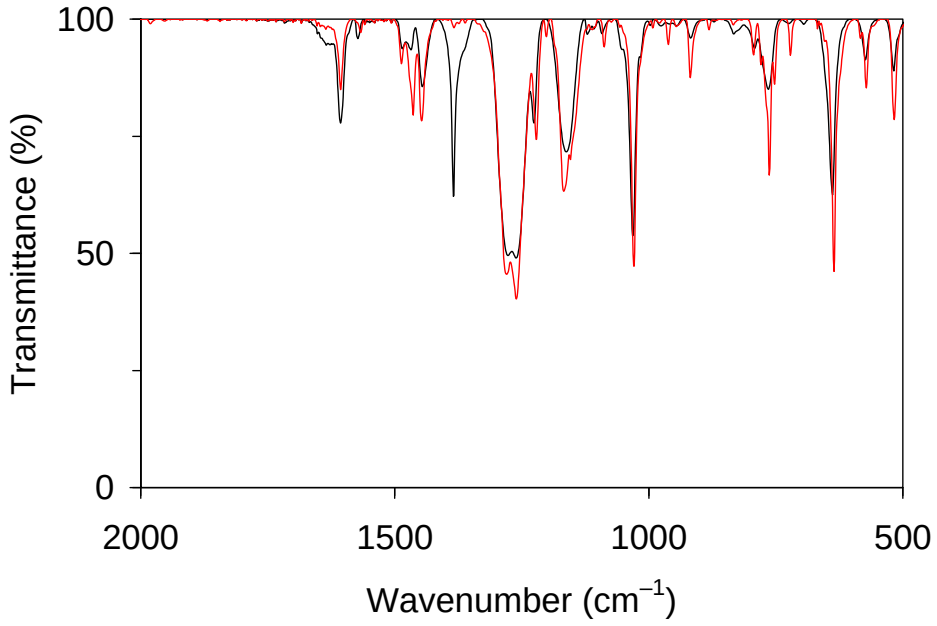

Figure 31. Solid-state IR (KBr) spectra of the products from the reaction of **4** with NO (black, —) and **3**–NCMe (red, —).

Upon comparison with the IR spectrum of **3**–NCMe, no other new signals were present in the product spectrum other than that indicating unbound nitrate, indicating that all nitrate observed in the IR spectrum, and thus produced by the reaction, was in the unbound state. The nitrate produced by the reaction was quantified in the same way as the nitrite reaction with **4** (see Section 6.2.2), by addition of 1 equiv $Na^{15}NO_3$ to the product solution prior to preparation of a pellet for IR spectroscopic analysis and utilizing the band arising from unbound ^{15}N-nitrate (Figure 32). The results from three trials indicate that a range of 0.51 to 0.60 (avg. 0.54) equiv of NO_3^- (with respect to Fe) was produced (Table 18). Taken together, the observations reveal that the reaction of **4** with NO caused

reduction of the Fe^{IV} center to Fe^{II} and produced 0.5 equiv NO_3^- [with no observed formation of NO_2^- (ν_s = 1335 cm^{-1}, ν_{as} = 1250 cm^{-1})].

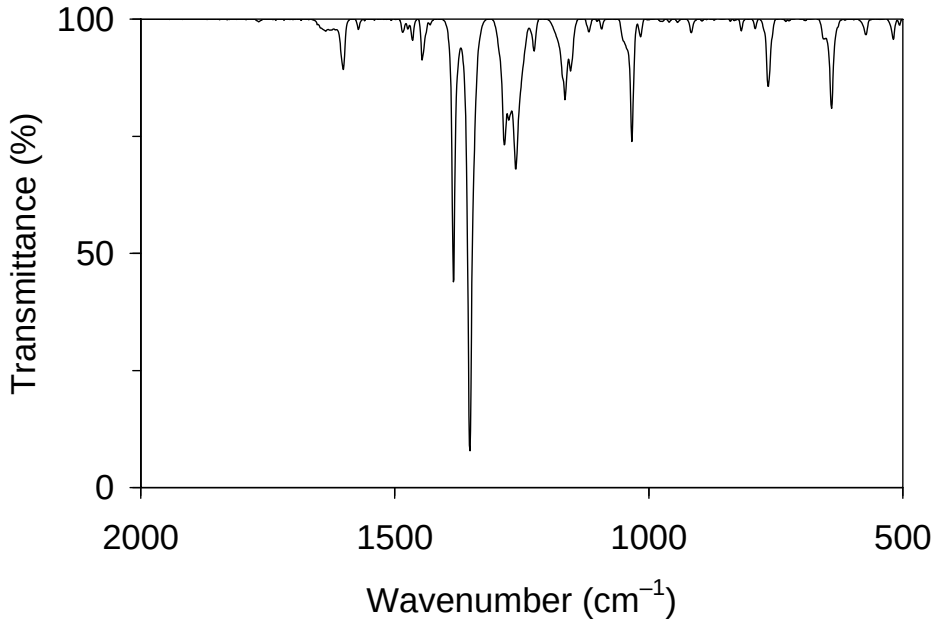

Figure 32. Solid-state IR (KBr) spectrum of the products from the reaction of **4** with NO with the addition of 1 equiv $^{15}NO_3^-$ with respect to Fe.

Table 18. IR data for quantification of NO_3^- from the reaction of **4** with NO in acetonitrile at 25 °C[a]

Trial	Observed absorbance at 1385 cm^{-1} : 1352 cm^{-1} [b]	Equiv of NO_3^- produced (with respect to Fe)
1	0.69 : 1.31	0.52
2	0.13 : 0.26	0.51
3	0.55 : 0.92	0.60
Avg.		0.54

[a] Described in Section 6.2.3
[b] 1385 cm^{-1} and 1352 cm^{-1} corresponds to IR bands of NO_3^- and $^{15}NO_3^-$ respectively.

With the 2:1 stoichiometry for the reaction of **4** with NO established, a plausible mechanism would consist of an initial oxide ion transfer from the Fe^{IV}=O moiety to NO to form Fe^{III} and NO_2^- as intermediate products. This initial step would be followed by continuing oxidation of the NO_2^- intermediate to NO_3^- with a second equivalent of Fe^{IV}=O *via* an oxygen atom transfer (Scheme 14).

Scheme 14. Reaction of **4** with 0.5 equiv NO

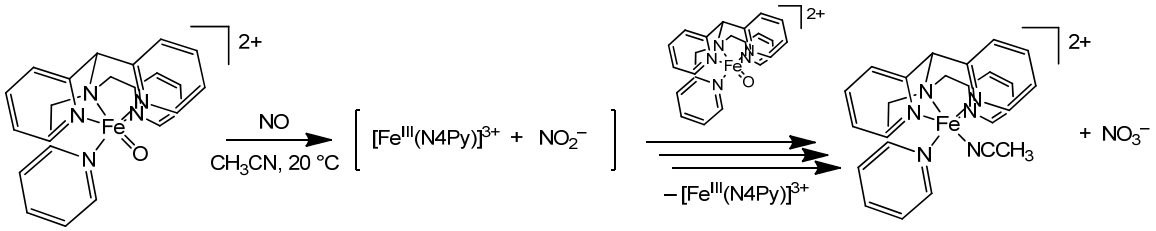

The initial delay between addition of NO to a solution of **4**, and the formation of the band at 455 nm indicative of an Fe^{II} complex could be explained by the initial step required to form NO_2^- and Fe^{III}. Thus, this first step would not be able to be an oxygen atom transfer, since Fe^{II} (and accordingly, the band at 455 nm) would form concurrently with the decay of **4**. Thus, the first step is likely an $O^{\bullet-}$ ion transfer to form $[Fe^{III}(N4Py)(ONO)]^{2+}$ (eq 9). The nitrite could then dissociate and be replaced by acetonitrile to form $[Fe^{III}(N4Py)(NCMe)]^{3+}$ (eq 10). A second equivalent of Fe^{IV}=O would then attack the intermediate NO_2^- to form $[Fe^{II}(N4Py)(ONO_2)]^+$ by oxygen atom transfer (eq 11). Lastly, nitrate would dissociate to yield free nitrate, and the solvento complex $[Fe^{II}(N4Py)(NCMe)]^{2+}$ (eq 12). This chemistry has already been demonstrated to be possible (Section 6.3.2).

$$[Fe^{IV}O(N4Py)]^{2+} + NO \rightarrow \{[Fe^{III}(N4Py)(ONO)]^{2+}\} \quad (9)$$

$$\{[Fe^{III}(N4Py)(ONO)]^{2+}\} \rightarrow \{[Fe^{III}(N4Py)(NCMe)]^{3+} + NO_2^- \quad (10)$$

$$[Fe^{IV}O(N4Py)]^{2+} + NO_2^- \rightarrow [Fe^{II}(N4Py)(ONO_2)]^+ \quad (11)$$

$$\{[Fe^{II}(N4Py)(ONO_2)]^+\} \rightarrow \{[Fe^{II}(N4Py)(NCMe)]^{2+} + NO_2^- \quad (12)$$

The Fe^{III} intermediate resulting from eq 10 then must decay to form Fe^{II}. It is known that Fe^{III}(N4Py) complexes can form metastable mono- and dinuclear complexes,[55] but probing for these products did not reveal their presence, as they have indicative UV–Vis bands and ESI mass spectrometry signals {$[Fe^{III}OOH(N4Py)]^{2+}$, m/z = 228, $\lambda(\varepsilon)$ = 530 nm (1100 $M^{-1}\cdot cm^{-1}$); $[Fe^{III}{}_2O(N4Py)]^{4+}$, $\lambda(\varepsilon)$ = 316 nm (41000 $M^{-1}\cdot cm^{-1}$)}[54-55]. Mutli-step oxidations of NO by oxometal complexes have been shown before,[106,135] and it is possible to have two steps with two different mechanisms, just as what is being observed in the case of this reaction. Taking all these observations together, including the delayed formation of Fe^{II} as observed in UV–Vis spectroscopy, the 2:1 ratio of Fe^{IV}=O : NO as confirmed by quantification of product in IR spectrum, and the products observed as Fe^{II} and nitrate, this reaction is consistent with a two-step mechanism – first an $O^{\bullet-}$ ion transfer from Fe^{IV}=O to form NO_2^-, followed secondly by an oxygen atom transfer from a second equivalent of Fe^{IV}=O to NO_2^- to form NO_3^-.

6.3.3 Isotope Labeling Study

Further insights into the mechanism by which NO_3^- is formed were sought from an ^{18}O-labeling study. This study was carried out in nitromethane and the reaction proceeds similarly as monitored by UV–Vis spectroscopy and similar products are observed in the ESI mass spectrum. When the reactions involving NO_2^- and NO were carried out with ^{18}O-enriched **4**, peaks at m/z = 485, 487 and 489 were observed,

indivative of 3–ONO_2, 3–$^{18}ONO_2$ and 3–$ON^{18}O_2$, respectively. The results are presented in Tables 19 and 20. These results indicate *ca*. 150% and *ca*. 110% of the ^{18}O was retained into **3**–ONO_2 for the reaction involving NO_2^- and NO, respectively.

These results demonstrated that the oxoiron(IV) unit is capable of transferring its oxygen to NO or NO_2^- to afford NO_3^-. The high/over 100% ^{18}O incorporation into **3**–ONO_2 from ^{18}O-enriched **4** in cases of each reaction (NO and NO_2^-) indicates that isotope scrambling had occurred involving the excess $H_2{}^{18}O$ in solution.

Table 19. ESI(+)MS data for ^{18}O labeling study for the reaction of **4** with NO_2^- in nitromethane at 25 °C.[a]

Trial	Percent Incorporation of ^{18}O			Percent Retention of ^{18}O
	[^{18}O]-**4**–OTf	**3**–$^{18}ONO_2$	**3**–$ON^{18}O_2$	
1	45.9	38.7	20.6	129
2	47.0	39.1	28.6	144
3	41.8	38.4	32.8	171
Avg.	44.9	38.7	27.3	148

[a] Described in Section 6.2.5

Table 20. ESI(+)MS data for ^{18}O labeling study for the reaction of **4** with NO in nitromethane at 25 °C.[a]

Trial	Percent Incorporation of ^{18}O			Percent Retention of ^{18}O
	[^{18}O]-**4**–OTf	**3**–$^{18}ONO_2$	**3**–$ON^{18}O_2$	
1	27.4	33.0	21.2	198
2	64.8	21.7	7.8	46
3	28.1	27.9	0	99
Avg.	40.1	27.5	9.7	114

[a] Described in Section 6.2.5

A possible mechanism accounting for increase of labeled O atoms involves linkage isomerization of the nitrato ligand and reversible N–O bond cleavage. This process generates unlabeled **4** (which can be re-labeled by excess $H_2{}^{18}O$) and $N^{18}O^{16}O^-$. The re-labeled [^{18}O]-**4** can then further react with $N^{18}O^{16}O^-$ to form the doubly-labeled $^{16}ON^{18}O_2^-$ (eqs 13–15). A similar mechanism has previously been described for a nitratooxoruthenium(IV) complex, and was mentioned in Chapter 4.[127] It should also be noted that another explanation for the observation of the doubly-labeled $ON^{18}O_2^-$ product in the NO reaction could be due to the fact that NO reacts with two equivalents of Fe^{IV}=O (eqs 9–12), which could account for two ^{18}O atoms in the product. This however, does not account for the overall increase of ^{18}O incorporation in the nitrate product, which remains a result of probable isotope scrambling due to $H_2{}^{18}O$.

$$L_nFe^{II}–{}^{18}ONO_2 \rightleftharpoons L_nFe^{II}–ONO^{18}O \rightleftharpoons L_nFe^{IV}=O + NO^{18}O^- \quad (13)$$

$$L_nFe^{IV}=O + H_2{}^{18}O \rightleftharpoons L_nFe^{IV}={}^{18}O + H_2O \quad (14)$$

$$L_nFe^{IV}={}^{18}O + N^{18}OO^- \rightleftharpoons L_nFe^{II}–ON^{18}O_2 \rightleftharpoons L_nFe^{II} + ON^{18}O_2^- \quad (15)$$

This isotope labeling study was also carried out in acetonitrile in the exact same manner, but the ^{18}O incorporation into **4** was insufficient when compared to the study carried out in nitromethane. The data has been included in Tables 21 and 22. The same *m*/*z* peaks and same trends of results were observed, with the ^{18}O transfer into the nitrate products being of higher percentage than what was initially available in the [^{18}O]-**4** starting material. Thus, the reaction is considered to progress in the same manner in acetonitrile as in nitromethane.

Table 21. ESI(+)MS data for ^{18}O labeling study for the reaction of **4** with NO_2^- in acetonitrile at 25 °C.[a]

Trial	Percent Incorporation of ^{18}O			Percent Retention of ^{18}O
	[^{18}O]-**4**–OTf	**3**–$^{18}ONO_2$	**3**–$ON^{18}O_2$	
1	15.3	19.7	40.4	393
2	14.5	20.6	39.8	417
3	15.3	23.0	25.0	314
Avg.	15.0	21.1	35.0	374

[a] Described in Section 6.2.5

Table 22. ESI(+)MS data for ^{18}O labeling study for the reaction of **4** with NO in acetonitrile at 25 °C.[a]

Trial	Percent Incorporation of ^{18}O			Percent Retention of ^{18}O
	[^{18}O]-**4**–OTf	**3**–$^{18}ONO_2$	**3**–$ON^{18}O_2$	
1	8.8	43.7	16.8	688
2	13.8	44.7	16.6	444
3	14.5	40.7	23.2	441
Avg.	12.4	43.0	18.8	524

[a] Described in Section 6.2.5

6.4 Conclusion

The reaction of the oxoiron(IV) complex **4** with nitrite is quick and produces NO_3^- (identified in the form of the nitratoiron(II) complex **3**–ONO_2 by ESI MS and in the form of free nitrate by IR spectroscopy) and the Fe^{II} solvento complex **3**–NCMe. Studies afforded results that are consistent with an oxygen atom transfer from **4** to nitrite to form Fe^{II} and NO_3^- (Scheme 13). The amount of nitrate produced (*ca*. 1 equiv with respect to Fe) was quantified using IR spectroscopy.

The reaction of the oxoiron(IV) complex **4** with NO is much slower and produces NO_3^- (identified in the form of the nitratoiron(II) complex **3**–ONO_2 by ESI MS and in the form of free nitrate by IR spectroscopy) and the Fe^{II} solvento complex **3**–NCMe. Studies afforded results that are consistent with a two-step mechanism – 1) an $O^{\bullet-}$ ion transfer from **4** to NO to form Fe^{III} and NO_2^-, then 2) an oxygen atom transfer from a second equivalent of **4** to the intermediate nitrite to form Fe^{II} and NO_3^- (Scheme 14). The amount of nitrate produced (*ca*. 0.5 equiv with respect to Fe) was quantified using IR spectroscopy.

In addition to expanding the fundamental chemistry of oxoiron(IV) complexes, the reactions described here serve as an example of the oxidation of nitrogen monoxide and a unique example of the oxidation of nitrite by a transition metal complex.

CHAPTER 7

REACTION OF OXOIRON(IV) COMPLEXES OF 1,4,8,11-TETRAMETHYL-1,4,8,11-TETRAAZACYCLOTETRADECANE WITH ORGANIC SUBSTRATES

7.1 Introduction

In this chapter the reactions of a series of $[Fe^{IV}O(tmc)X]^+$ complexes with triphenylphosphine (PPh_3) and 9,10-dihydroanthracene (DHA) will be covered. The tmc ligand provides a stabilizing environment for the $Fe^{IV}O$ unit, and the axial ligands (X = TfO^-, $CF_3CO_2^-$, and AcO^-) were chosen for there trend in electron donating/withdrawing properties. The generation of each oxoiron(IV) complex will be covered as simple ligand exchange can convert the $[Fe^{IV}O(tmc)(OTf)]^+$ complex to the acetato or trifluoroacetato complex. The reaction with PPh_3 afforded $[Fe^{II}(tmc)X]^+$ and $OPPh_3$. The amount of $OPPh_3$ produced in this reaction (*ca*. 1 equiv with respect to Fe) was determined by ^{31}P nuclear magnetic resonance (NMR) spectroscopy. The reaction was monitored by UV–Visible spectroscopy. The reaction with DHA was monitored by UV–Visible spectroscopy and progressed as previously reported in the literature,[111] indicating formation of Fe^{III} and anthracene.

The oxygen atom transfer reactions to PPh_3 followed a trend in which the more electron withdrawing axial ligands enhanced the reactivity. The hydrogen atom abstraction reactions with DHA followed an opposite trend in which the more electron donating axial ligands enhanced the reactivity. This is consistent with data reported in the literature for other series of axial ligands for $Fe^{IV}O(tmc)$ complexes which have been studied in different solvent systems.[111,136-142]

7.2 Experimental Section

7.2.1 Materials and Methods

Materials. All reagents and solvents were purchased from commercial sources and were used as received, unless noted otherwise. Nitromethane was refluxed over CaH_2 under an Ar atmosphere, distilled, and passed through a column of basic Al_2O_3.[69] Preparation and handling of air- and moisture-sensitive materials were carried out under an inert gas atmosphere by using standard Schlenk and vacuum line techniques or a glovebox. $Fe(OTf)_2 \cdot 2MeCN$ was synthesized by a modified literature method[70] from anhydrous $FeCl_2$ and trimethylsilyl trifluoromethanesulfonate in acetonitrile and recrystallized from acetonitrile–diethyl ether (TfOH = CF_3SO_3H, trifluoromethanesulfonic or triflic acid).[71] The ligand 1,4,8,11-tetramethyl-1,4,8,11-tetraazacyclotetradecane (tmc),[72] and $[Fe^{II}(tmc)(OTf)]OTf$[73] [**1**–OTf(OTf), stored under an N_2 atmosphere], and iodosylbenzene[108] were prepared following published procedures. (*Caution*: Iodosylbenzene is potentially explosive, if dried extensively, and should be handled with care.[109]).

Physical Methods. UV–Visible spectra were recorded on an HP 8453A diode array spectrophotometer (Agilent Technologies) with samples maintained at the desired temperature using a cryostat/heater from Unisoku Scientific Instruments, Japan. NMR spectra were recorded on a Bruker Avance DPX 300 spectrometer at ambient temperature. Mass spectral data were acquired on a quadrupole ion trap ThermoFinnigan LCQ Deca mass spectrometer using an electrospray ionization source.

7.2.2 Generation of Oxoiron(IV) Complexes

Generation of [Fe^{IV}O(tmc)(OTf)]OTf, 2–OTf(OTf), and [Fe^{IV}O(tmc)(X)]OTf, 2–X(OTf). A 1 mM solution of **1**–OTf(OTf) (0.002 mmol) in 2.0 mL of nitromethane was placed in a 1-cm UV–Vis cuvette and precooled to –20 °C. Upon addition of 0.050 mL of a solution of iodosylbenzene (0.002 mmol) in methanol (anhydrous, 99%), **2**–OTf formed within 5 min. ESI(+)MS ($MeNO_2$) *m/z*: M^+ calcd for $C_{15}H_{32}F_3FeN_4O_4S$ ({**2**–OTf}$^+$), 477.14; found, 477.1 (M^+), 461.2 ({M – O}$^+$), 257.3 ({tmc + H}$^+$). UV–Vis ($MeNO_2$) λ_{max}, nm (ε): 825 (230).

Subsequently, a solution of 0.002 mmol of NR_4X in 0.050 mL of nitromethane was added to the solution of **2**–OTf in nitromethane at –20 °C (X = NO_2^-, NO_3^-, AcO^-, $CF_3CO_2^-$). The formation of **2**–X from **2**–OTf was indicated by a change in the UV–Vis spectrum resulting in the new spectrum of **2**–X.

[FeO(tmc)(OAc)]$^+$, 2–OAc. ESI(+)MS ($MeNO_2$) *m/z*: M^+ calcd for $C_{16}H_{35}FeN_4O_3$ ({**2**–OAc}$^+$), 387.21; found, 387.0 (M^+), 371.3 ({M – O}$^+$), 257.3 ({tmc + H}$^+$). UV–Vis ($MeNO_2$) λ_{max}, nm (ε): 825 (120), 995 (100).

[FeO(tmc)(ONO)]$^+$, 2–ONO. ESI(+)MS ($MeNO_2$) *m/z*: M^+ calcd for $C_{14}H_{32}FeN_5O_3$ ({**2**–ONO}$^+$), 374.21; found, 374.0 (M^+), 358.2 ({M – O}$^+$), 257.3 ({tmc + H}$^+$). UV–Vis ($MeNO_2$) λ_{max}, nm (ε): 830 (135), 995 (100).

[FeO(tmc)(ONO$_2$)]$^+$, 2–ONO$_2$. ESI(+)MS ($MeNO_2$) *m/z*: M^+ calcd for $C_{14}H_{32}FeN_5O_4$ ({**2**–ONO$_2$}$^+$), 390.19; found, 390.1 (M^+), 374.3 ({M – O}$^+$), 257.3 ({tmc + H}$^+$). UV–Vis ($MeNO_2$) λ_{max}, nm (ε): 825 (170).

[FeO(tmc)(OC(O)CF$_3$)]$^+$, 2–OC(O)CF$_3$. ESI(+)MS ($MeNO_2$) *m/z*: M^+ calcd for $C_{16}H_{32}FeN_4O_3F_3$ ({**2**–OC(O)CF$_3$}$^+$), 441.29; found, 441.1 (M^+), 425.2 ({M – O}$^+$), 257.3 ({tmc + H}$^+$). UV–Vis ($MeNO_2$) λ_{max}, nm (ε): 830 (190), 995 (145).

7.2.3 Reaction of Oxoiron(IV) Complexes with Organic Substrates

Reaction of 2–X with Triphenylphosphine. A 1 mM solution of **2**–X (0.002 mmol) in 2.0 mL of nitromethane was prepared in a UV–Vis cuvette as described above at –20 °C, cooled to –25 °C, and treated with a solution of 0.020 mmol of triphenylphosphine in 0.35 mL of nitromethane. The product solution was evaporated to dryness, and the residue was dissolved in $CDCl_3$ for ^{31}P NMR spectroscopy. ^{31}P NMR (121.5 MHz, $CDCl_3$, δ): 29.0 ($OPPh_3$), –5.4 (PPh_3).

Subsequently, each reaction was also carried out at 20 °C, in which the solution of **2**–X in the UV–Vis cuvette was rapidly (< 1 min) warmed to 20 °C in a water bath before placement in the spectrophotometer and addition of triphenylphosphine.

In addition, **2**–OAc was also subjected to separate reactions with tri-tert-butyl phosphine and trimethoxyphosphine in a similar manner at –25 °C, monitored by UV–Vis spectroscopy.

Reaction of 2–X with 9,10-dihydroanthracene. A 1 mM solution of **2**–X (0.002 mmol) in 2.0 mL of nitromethane was prepared in a UV–Vis cuvette as described above at –20 °C, cooled to –25 °C, and treated with a solution of 0.020 mmol of 9,10-dihydroanthracene in 0.20 mL of nitromethane Subsequently, each reaction was also carried out at 20 °C, in which the solution of **2**–X in the UV–Vis cuvette was rapidly (< 1 min) warmed to 20 °C in a water bath before placement in the spectrophotometer and addition of 9,10-dihydroanthracene.

7.3 Results and Discussion

7.3.1 Generation and Characterization of Oxoiron(IV) Complexes

Scheme 15. Structures of **1**–X and **2**–X[a]

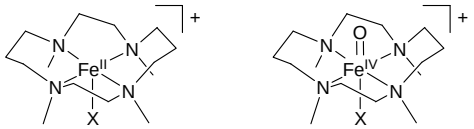

1–X **2**–X

[a] X = TfO^-, AcO^-, $CF_3CO_2^-$.

The complexes $[Fe^{IV}O(tmc)(OTf)]^+$, **2**–OTf, $[Fe^{IV}O(tmc)(OAc)]^+$, **2**–OAc, and $[Fe^{IV}O(tmc)\{OC(O)CF_3\}]^+$, **2**–$OC(O)CF_3$,(Scheme 15) were generated by oxidation of $[Fe^{II}(tmc)(OTf)]^+$, **1**–OTf, and subsequent ligand substitution in a manner similar to that reported for the corresponding trifluoroacetato complex, $[Fe^{IV}O(tmc)\{OC(O)CF_3\}]^+$,[111] where necessary. Reaction of **1**–OTf with iodosylbenzene in the weakly coordinating solvent nitromethane at –20 °C produced $[Fe^{IV}O(tmc)(OTf)]^+$, **2**–OTf, which was converted into **2**–OAc or **2**–$OC(O)CF_3$ by exchange of the triflato ligand with acetate or trifluoracetate. Each complex, **2**–OTf, **2**–OAc and **2**–$OC(O)CF_3$ exhibit absorption bands in the near-IR region characteristic of $[Fe^{IV}O(tmc)(L/X)]^{2+/+}$ complexes[111] [**2**–OTf, λ_{max} = 825 nm (ε = 230 $M^{-1}\cdot cm^{-1}$); **2**–OAc, λ_{max} = 825 (ε = 120 $M^{-1}\cdot cm^{-1}$) and 995 nm (100); **2**–$OC(O)CF_3$, λ_{max} = 830 (ε = 190 $M^{-1}\cdot cm^{-1}$), 995 nm (145)]. As shown by incremental addition of NEt_4AcO, 1 equiv of acetate is required for the conversion of **2**–OTf into **2**–OAc in nitromethane (Chapter 4) and the same holds true for **2**–$OC(O)CF_3$. The complexes also were identified by peaks at *m*/*z* = 477 (**2**–OTf), 387 (**2**–OAc) and 425 (**2**–$OC(O)CF_3$) in the corresponding ESI mass spectra.

7.3.2 Reactivity of Oxoiron(IV) Complexes Toward PPh_3

The oxygen-atom-transfer reactivity of **2**–OAc, **2**–$OC(O)CF_3$, and **2**–OTf was examined by reaction with PPh_3 affording $[Fe^{II}(tmc)(OAc)]^+$ (**1**–OAc), $[Fe^{II}(tmc)\{OC(O)CF_3\}]^+$ (**1**– $OC(O)CF_3$) and $[Fe^{II}(tmc)(OTf)]^+$ (**1**–OTf) respectively, and $OPPh_3$ (eq 1, Chapter 4). The amount of $OPPh_3$ produced was quantified using ^{31}P NMR and in each case *ca*. 1 equiv of $OPPh_3$ was produced with respect to Fe. When a solution of 1 mM **2**–X (X = TfO^-, AcO^-, $CF_3CO_2^-$) was reacted with 10 equiv of PPh_3 at –25 °C, the half life was *ca*. 10, 2.25, and 1 min for **2**–OAc, **2**–$OC(O)CF_3$ and **2**–OTf respectively, as indicated by the disappearance of the near-IR features associated with **2**–X (Figure 14, see chapter 4, Figure 33, Figure 34). No intermediate was detected in this reaction in any of the three cases.

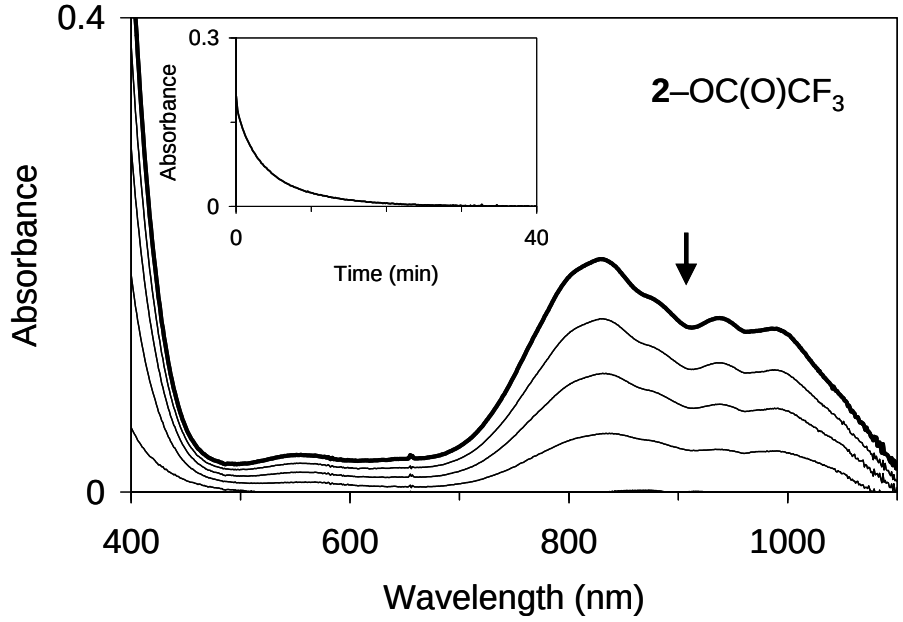

Figure 33. Reaction of 1 mM **2**–$OC(O)CF_3$ with 10 equiv of PPh_3 in nitromethane at –25 °C as monitored by electronic absorption spectroscopy (path length, 1 cm). Inset: Time course of the reaction (λ = 830 nm).

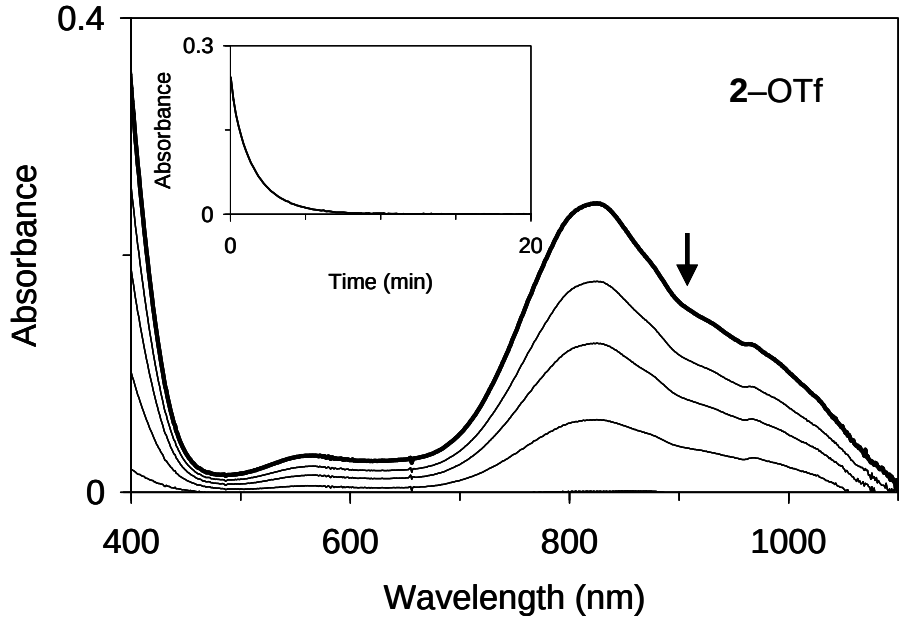

Figure 34. Reaction of 1 mM **2**–OTf with 10 equiv of PPh_3 in nitromethane at –25 °C as monitored by electronic absorption spectroscopy (path length, 1 cm). Inset: Time course of the reaction (λ = 825 nm).

7.3.3 Reactivity of Oxoiron(IV) Complexes Toward 9,10-dihydroanthracene (DHA)

The hydrogen-atom-abstraction reactivity of **2**–OAc, **2**–$OC(O)CF_3$, and **2**–OTf was examined by reaction with DHA. This reaction is known to react in a *ca*. 2:1 stoichiometry of $Fe^{IV}O$: DHA to afford Fe^{III}(tmc) complexes and anthracene[111]. When a solution of 1 mM **2**–X was reacted with 10 equiv of DHA at –25 °C, the half life was *ca*. 5, 10, and 40 min for **2**–OAc, **2**–$OC(O)CF_3$ and **2**–OTf respectively, as indicated by the disappearance of the near-IR features associated with **2**–X (Figure 35, Figure 36, Figure 37). No intermediate was detected in this reaction in any of the three cases, however there is a different progression as monitored in the UV–Vis spectra. Unlike with PPh_3, the reaction with DHA causes an increase in absorbance in the 400–600 nm range, consistent with the formation of and Fe^{III}(tmc) complex.

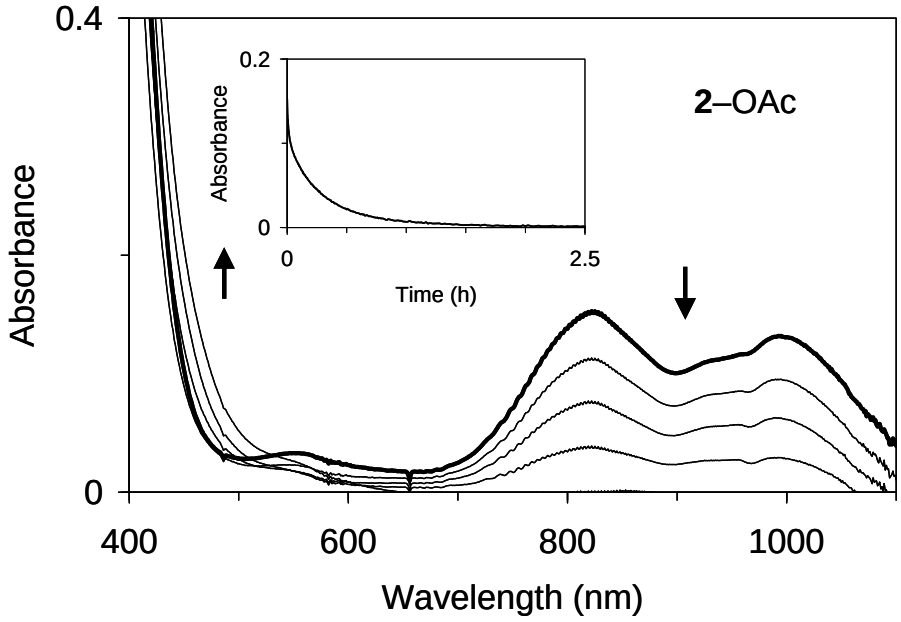

Figure 35. Reaction of 1 mM **2**–OAc with 10 equiv of DHA in nitromethane at –25 °C as monitored by electronic absorption spectroscopy (path length, 1 cm). Inset: Time course of the reaction (λ = 825 nm).

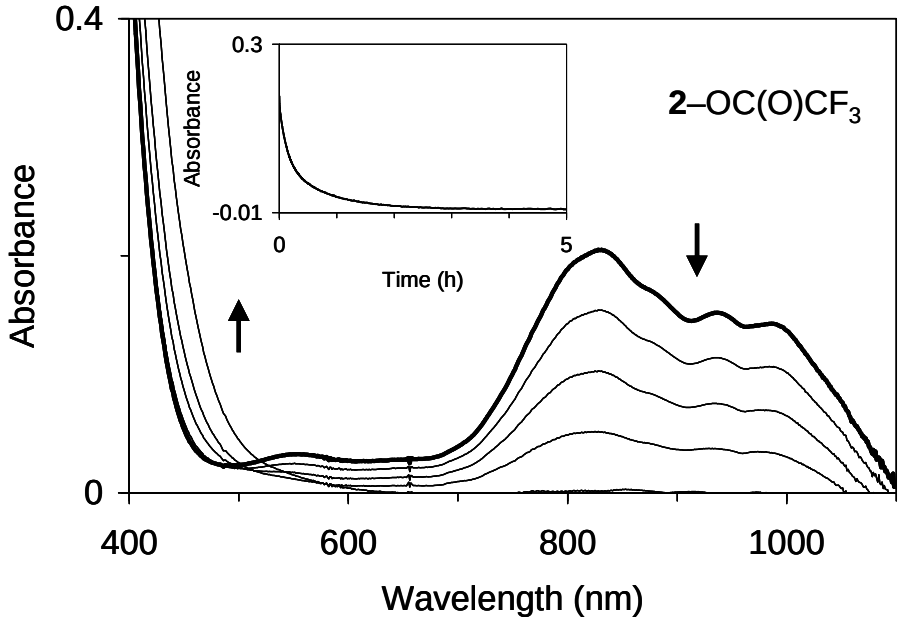

Figure 36. Reaction of 1 mM **2**–$OC(O)CF_3$ with 10 equiv of DHA in nitromethane at –25 °C as monitored by electronic absorption spectroscopy (path length, 1 cm). Inset: Time course of the reaction (λ = 830 nm).

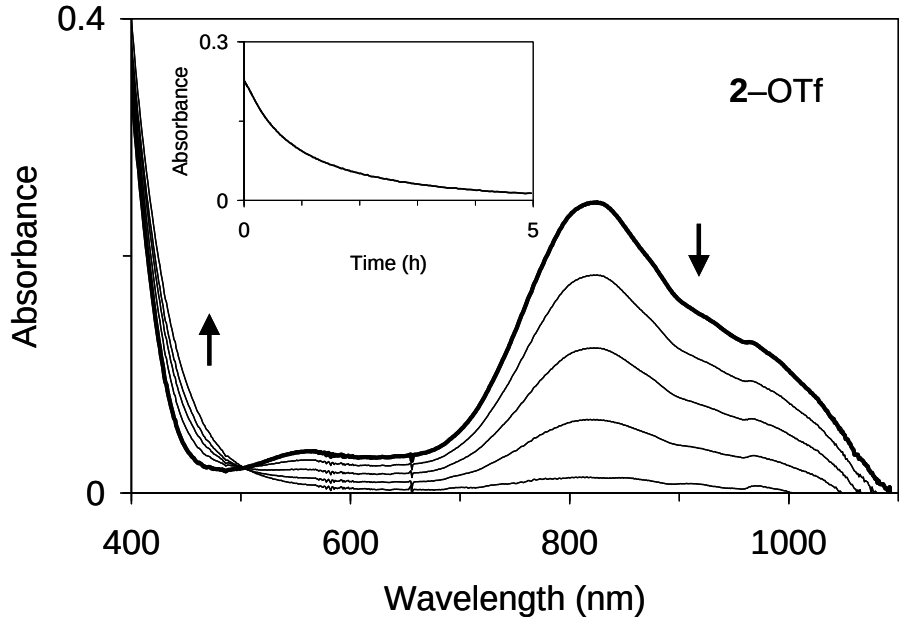

Figure 37. Reaction of 1 mM **2**–OTF with 10 equiv of DHA in nitromethane at –25 °C as monitored by electronic absorption spectroscopy (path length, 1 cm). Inset: Time course of the reaction (λ = 825 nm).

A trend becomes apparent when examining the two different types of reactivity. In the case of the oxygen atom transfer, the reactivity increases with more electron withdrawing axial ligands ($TfO^- > CF_3CO_2^- > AcO^-$), suggesting that as an oxygen atom transfer reagent, the oxoiron(IV) unit acts as an electrophile. The opposite is true with the hydrogen atom abstraction reactions as the more electron withdrawing axial ligands ($AcO^- < CF_3CO_2^- < TfO^-$) accelerate the reactivity toward DHA (Table 23).

This is counterintuitive since the more electron-rich $Fe^{IV}O$ center should not be more reactive in the electrophilic activation of the C–H bond in the reaction in DHA. However, it has been previously reported[136-142] to be due to the fact that the increased electron donation to the $Fe^{IV}O$ unit reduces the reduction potential of the $Fe^{IV}O$ unit thus enhancing its hydrogen atom abstraction reactivity.

Table 23. Decay data from reactions of $[Fe^{IV}O(tmc)(X)]^+$ with organic substrates in nitromethane at –25 °C.[a]

X	Substrate	$t_{1/2}$ (s)	Complete Decay (s)
TfO^-	PPh_3	60	800
$CF_3CO_2^-$	PPh_3	130	2000
AcO^-	PPh_3	600	10800
TfO^-	DHA	2700	18000
$CF_3CO_2^-$	DHA	630	12000
AcO^-	DHA	450	7200

[a] Described in Section 7.2.3

When considered together, the reactivity of this series of oxoiron(IV) complexes as oxygen atom transfer reagents and hydrogen atom abstraction reagents is consistent with known trends in the literature.[136-142] Previous work had involved work $Fe^{IV}O(tmc)$ complexes with a different series of ligands (i.e., $NCCH_3$, N_3^-, $CF_3CO_2^-$) and reactions were carried out at room temperature in acetontrile.

7.4 Conclusion

By introducing a series of axial ligands to the oxoiron(IV) center supported by the tmc ligand, we have been able to investigate the effects the different axial ligands have on oxygen atom transfer and hydrogen atom abstraction reactivity with PPh_3 and DHA, respectively. Consistent with known axial ligand effects, this series of ligands causes enhancement of oxygen atom transfer reactivity when the axial ligand becomes more electron withdrawing and accelerates hydrogen atom abstraction as the axial ligand becomes more electron donating. This study offers a synthetic example of reactivity trends of nonheme oxoiron(IV) complexes, many of which are proposed intermediates in enzymatic processes.

CHAPTER 8

SUMMARY AND CONCLUSION

The synthesis and characterization of iron(II) complexes of the nonheme tetraamine ligand 1,4,8,11-tetramethyl-1,4,8,11-tetraazacyclotetradecane (tmc) has been achieved. Investigation of the reduction/oxidation potentials of these complexes was discussed in context of the accessibility of the iron(III) oxidation state, and what it might mean for any intermediates observed in the course of the reactions between oxoiron(IV) complexes and NO. Discussion of the single crystal X-ray structures included looking at the unique bidentate binding modes of the nitritoiron(II) and nitratoiron(II) complexes. Spectroscopic characterization of the iron(II) complexes were shown to be consistent with results of the single crystal X-ray crystallography.

The reactivity of the high valent oxoiron(IV) complex of tmc toward NO was carried out and discussed. This reaction resulted in the reduction of Fe^{IV} to Fe^{II} and the production of nitrite, observed as the nitritoiron(II) complex of tmc using ESI MS. Monitoring of the reaction by UV–Vis spectroscopy and ESI MS revealed an Fe^{III} intermediate that is able to be observed for approximately 15 minutes after initiation of the reaction. Quantification of the nitrite product revealed 1 equiv of nitrite formed with respect to iron. This study concluded that the oxo ligand is transferred to NO to form the nitrite product by an oxide(•1–) ion transfer mechanism.

The oxidation of the nitrosyl complex $[Fe(tmc)(NO)]^{2+}$ with trimethylamine *N*-oxide was covered. The results of this reaction included the formation of 1 equiv of nitrite, quantified in the same manner as in chapter 4, using ESI MS and isotopically labeled ^{15}N nitrite. Studies indicated the reaction proceeds through an oxide(•1–) ion transfer mechanism, followed by a linkage isomerization to form the O-bound nitritoiron(II) product. Analysis of single crystal X-ray data from the product depicts the

nitrito ligand to be bidentate, identical to the independently synthesized nitritoiron(II) complex of tmc.

The reaction of a different oxoiron(IV) complex, supported by the ligand N4Py, with NO was discussed. This reaction results in a 2:1 stoichiometry between Fe^{IV} and NO, in which nitrate and Fe^{II} are formed as products. Mechanistic studies utilizing UV–Vis and IR spectroscopy and ESI MS revealed a two-step mechanism – an initial oxide(•1–) ion transfer from Fe^{IV} to NO to form nitrite, followed by an oxygen atom transfer from a second equivalent of Fe^{IV} to nitrite to form nitrate. The chemistry of the second step was investigated by reacting $[Fe^{IV}O(N4Py)]^{2+}$ with nitrite to confirm a 1:1 stoichiometry between Fe^{IV} and nitrite, in which mechanistic studies support an oxygen atom transfer to form Fe^{II} and nitrate.

The reactivity of a series of oxoiron(IV) complexes of tmc with organic substrates were described. The complexes $[Fe^{IV}O(tmc)X]^{+}$, where X = TfO^{-}, AcO^{-}, $CF_3CO_2^{-}$, have been reacted with triphenylphosphine, and the relative rates of reactions have been compared. In another set of reactions, the oxoiron(IV) complexes were reacted with the organic substrate 9,10-dihydroanthracene, proceeding through a known H atom abstraction mechanism. When comparing the two reactivity modes in regard to this series of oxoiron(IV), the trend in which a electron donating axial ligand, trans to the oxo ligand, results in faster reaction with 9,10-dihydroanthracene emerged, while the reactivity toward triphenylphosphine is enhanced by an electron donating axial ligand.

This project highlights two thorough investigations of the reactivity of an oxometal complex toward nitrogen monoxide. Comparisons of the reactions of NO with $[Fe^{IV}O(tmc)(OAc)]^{+}$ (**2**–OAc), $[Fe^{IV}O(N4Py)]^{2+}$ (**4**), and the dioxorhodium(VI)[135] complex can be made, as each results in a different reactivity pathway. **2**–OAc reacts through an $O^{\bullet-}$ ion transfer from the $Fe^{IV}O$ unit to NO to form NO_2^{-} and there is no further oxidation. The reaction of **4** with NO begins in the same way, with a likely initial $O^{\bullet-}$ ion transfer from $Fe^{IV}O$ to NO to likely form NO_2^{-}, however the NO_2^{-} is further

oxidized *via* an O atom transfer to form NO_3^-. On the other hand, the dioxoruthenium(VI) complex reacts with NO through an initial O atom transfer to form NO_2 and an oxoruthenium(IV) complex which further reacts with NO to form NO_2^- by way of an $O^{\bullet-}$ ion transfer. In the context of these studies, it was also found that **4** can oxidize NO_2^- to form NO_3^-, likely through an O atom transfer. This is an interesting result as it is not common for oxometal complexes of relatively low valency to be able to oxidize NO_2^-, as shown in the case of **2**–OAc. However, the dioxoruthenium(VI) complex has also been shown to oxidize NO_2^- to form NO_3^- through an O atom transfer.[127] These thorough studies provide a greater understanding in the area of NO oxidation by oxometal complexes, and there results are summarized in Scheme 16.

Scheme 16. Summarized Results of the Oxidation of NO_2^- and NO by Oxometal Complexes.

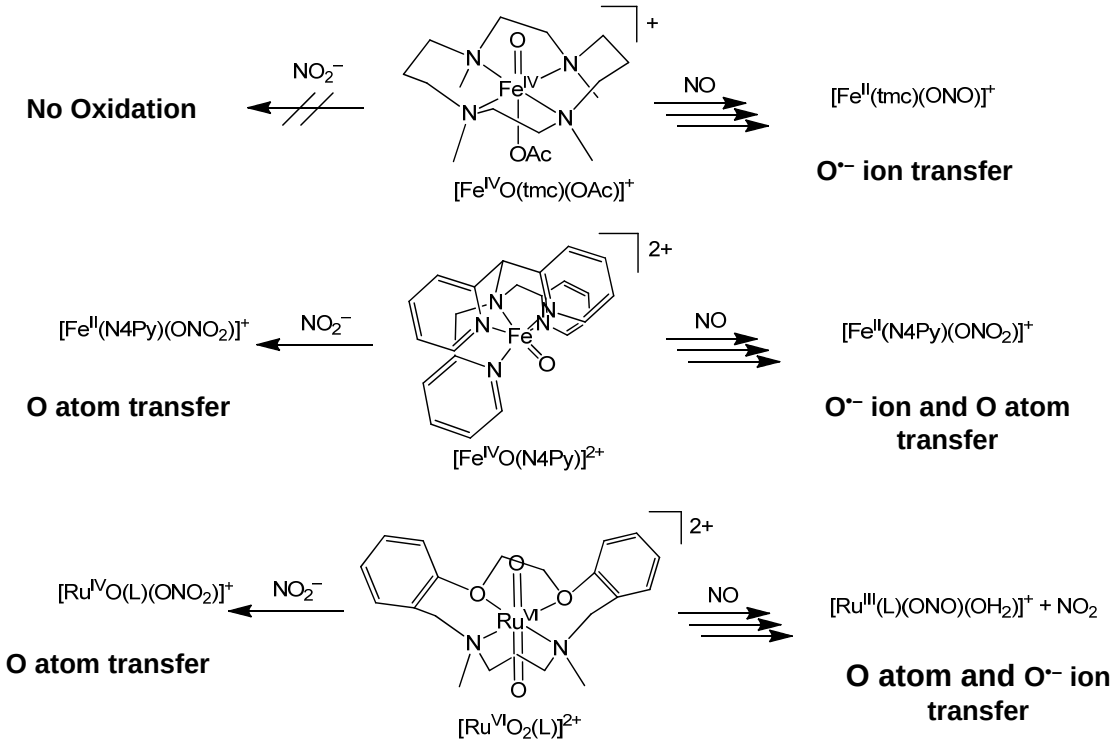

There are a number of directions in which this project could continue for further investigation. To continue an analgous study using the N4Py ligand, the corresponding iron-nitrosyl complex should be generated, and its oxidation by an O atom donor (such as trimethylamine *N*-oxide) should be investigated. The effect that the supporting ligand has on this chemistry would be interesting to determine. Additionally, other supporting ligands of the $Fe^{IV}O$ moiety could be used to generate oxoiron(IV) complexes, and their reactivity towards NO could be studied. There has already been quite a difference observed between the reaction of **2**–OAc and **4** with NO, so it would be useful to continue a series of investigations to see what other effects the supporting ligand might have on this chemistry. Lastly, reactivity of oxoiron(IV) complexes toward other small inorganic molecules (such as nitrogen dioxide) could be studied, and this could continue to broaden the scope of this project and provide thorough and mechanistic information about the chemistry of oxoiron(IV) complexes.

REFERENCES

1. Cullotta, E.; Koshland, D. E. *Science* **1992**, *258*, 1862.

2. Bult, H.; Boeckxstaens, G. E.; Pelckmans, P.A.; Jordaens, F. H.; Van Maercke, Y. M.; Herman, A. G. *Nature* **1990**, *345*, 346.

3. Heck, D. E.; Laskin, D. L.; Gardner, C. R. *J. Biol. Chem.* **1992**, *267*, 21277.

4. Herold, S.; Rehmann, F.-J. K. *J. Biol. Inorg. Chem.* **2001**, *6*, 543.

5. Herold, S.; Rehmann, F.-J. K. *Free Radical Biol. Med.* **2003**, *34*, 531.

6. Gardner, P. R. *J. Inorg. Biochem.* **2005**, *99*, 247.

7. Gardner, P. R.; Gardner, A. M.; Brashear, W. T.; Suzuki, T.; Hvitved, A. N.; Setchell, K. D. R.; Olson, J. S. *J. Inorg. Biochem.* **2006**, *100*, 542.

8. Yukl, E. T.; de Vries, S.; Moënne-Loccoz, P. *J. Am. Chem. Soc.* **2009**, *131*, 7234.

9. Su, J.; Groves, J. T. *J. Am. Chem. Soc.* **2009**, *131*, 12979.

10. Su, J.; Groves, J. T. *Inorg. Chem.* **2010**, *49*, 6317.

11. Herold, S.; Puppo, A. *J. Biol. Inorg. Chem.* **2005**, *10*, 946.

12. Ascenzi, P.; De Marinis, E.; Coletta, M.; Visca, P. *Biochem. Biophys. Res. Commun.* **2008**, *373*, 197.

13. De Marinis, E.; Casella, L.; Ciaccio, C.; Coletta, M.; Visca, P.; Ascenzi, P. *IUBMB Life* **2009**, *61*, 62.

14. Bruckdorfer, K. R.; Dee, G.; Jacobs, M.; Rice-Evans, C. A. *Biochem. Soc. Trans.* **1990**, *18*, 285.

15. Dee, G.; Rice-Evans, C.; Obeyesekera, S.; Meraji, S.; Jacobs, M.; Bruckdorfer, K. R. *FEBS Lett.* **1991**, *294*, 38.

16. Gorbunov, N. V.; Osipov, A. N.; Day, B. W.; Zayas-Rivera, B.; Kagan, V. E.; Elsayed, N. M. *Biochemistry* **1995**, *34*, 6689.

17. Osipov, A. N.; Gorbunov, N. V.; Day, B. W.; Elsayed, N. M.; Kagan, V. E. *Methods Enzymol.* **1996**, *268*, 193.

18. Glover, R. E.; Koshkin, V.; Dunford, H. B.; Mason, R. P. *Nitric Oxide* **1999**, *3*, 439.

19. Abu-Soud, H. M.; Hazen, S. L. *J. Biol. Chem.* **2000**, *275*, 5425.

20. Abu-Soud, H. M.; Hazen, S. L. *J. Biol. Chem.* **2000**, *275*, 37524.

21. Abu-Soud, H. M.; Khassawneh, M. Y.; Sohn, J.-T.; Murray, P.; Haxhiu, M. A.; Hazen, S. L. *Biochemistry* **2001**, *40*, 11866.

22. Brunelli, L.; Yermilov, V.; Beckman, J. S. *Free Radical Biol. Med.* **2001**, *30*, 709.

23. Borisov, V. B.; Forte, E.; Sarti, P.; Brunori, M.; Konstantinov, A. A.; Giuffrè, A. *FEBS Lett.* **2006**, *580*, 4823.

24. Wick, P. K.; Kissner, R.; Koppenol, W. H. *Helv. Chim. Acta* **2000**, *83*, 748.

25. Wick, P. K.; Kissner, R.; Koppenol, W. H. *Helv. Chim. Acta* **2001**, *84*, 3057.

26. Herold, S.; Koppenol, W. H. *Coord. Chem. Rev.* **2005**, *249*, 499.

27. Nemes, A.; Pestovsky, O.; Bakac, A. *J. Am. Chem. Soc.* **2002**, *124*, 421.

28. Pestovsky, O.; Bakac, A. *J. Am. Chem. Soc.* **2002**, *124*, 1698.

29. Maiti, D.; Lee, D.-H.; Narducci Sarjeant, A. A.; Pau, M. Y. M.; Solomon, E. I.; Gaoutchenova, K.; Sundermeyer, J.; Karlin, K. D. *J. Am. Chem. Soc.* **2008**, *130*, 6700.

30. Schopfer, M. P.; Mondal, B.; Lee, D.-H.; Sarjeant, A. A. N.; Karlin, K. D. *J. Am. Chem. Soc.* **2009**, *131*, 11304.

31. Park, G. Y.; Deepalatha, S.; Puiu, S. C.; Lee, D.-H.; Mondal, B.; Narducci Sarjeant, A. A.; del Rio, D.; Pau, M. Y. M.; Solomon, E. I.; Karlin, K. D. *J. Biol. Inorg. Chem.* **2009**, *14*, 1301.

32. De Leo, M.; Ford, P. C. *J. Am. Chem. Soc.* **1999**, *121*, 1980.

33. DeLeo, M. A.; Ford, P. C. *Coord. Chem. Rev.* **2000**, *208*, 47.

34. Sharpe, M. A.; Ollosson, R.; Stewart, V. C.; Clark, J. B. *Biochem. J.* **2002**, *366*, 97.

35. Crestoni, M. E.; Fornarini, S. *Inorg. Chem.* **2005**, *44*, 5379.

36. Crestoni, M. E.; Fornarini, S. *Inorg. Chem.* **2007**, *46*, 9018.

37. Chiavarino, B.; Cipollini, R.; Crestoni, M. E.; Fornarini, S.; Lanucara, F.; Lapi, A. *J. Am. Chem. Soc.* **2008**, *130*, 3208.

38. Lei, J.; Trofimova, N. S.; Ikeda, O. *Chem. Lett.* **2003**, *32*, 610.

39. Lei, J.; Ju, H.; Ikeda, O. *J. Electroanal. Chem.* **2004**, *567*, 331.

40. Trofimova, N. S.; Safronov, A. Y.; Ikeda, O. *Electrochim. Acta* **2005**, *50*, 4637.

41. Suslick, K. S.; Watson, R. A. *Inorg. Chem.* **1991**, *30*, 912.

42. Suslick, K. S.; Bautista, J. F.; Watson, R. A. *J. Am. Chem. Soc.* **1991**, *113*, 6111.

43. Yamaji, M.; Hama, Y.; Miyazaki, Y.; Hoshino, M. *Inorg. Chem.* **1992**, *31*, 932.

44. Crestoni, M. E.; Fornarini, S.; Lanucara, F.; Warren, J. J.; Mayer, J. M. *J. Am. Chem. Soc.* **2010**, *132*, 4336.

45. McCarthy, M. R.; Crevier, T. J.; Bennett, B.; Dehestani, A.; Mayer, J. M. *J. Am. Chem. Soc.* **2000**, *122*, 12391.

46. Walstrom, A.; Pink, M.; Fan, H.; Tomaszewski, J.; Caulton, K. G. *Inorg. Chem.* **2007**, *46*, 7704.

47. Andersen, H. J.; Skibsted, L. H. *J. Agric. Food Chem.* **1992**, *40*, 1741.

48. Tran, N.G.; Kalyvas, H.; Skodje, K. M.; Hayashi, T.; Moënne-Loccoz, P.; Callan, P. E.; Shearer, J.; Kirschenbaum, L. J.; Kim, E. *J. Am. Chem. Soc.* **2011**, *133*, 1184.

49. Skodje, K. M.; Williard, P. G.; Kim, E. *Dalton Trans.* **2012**, *41*, 7849.

50. Park, G. Y.; Deepalatha, S.; Puiu, S. C.; Lee, D.-H.; Mondal, B.; Narducci Sarjeant, A. A.; del Rio, D.; Pau, M. Y. M.; Solomon, E. I.; Karlin, K. D. *J. Biol. Inorg. Chem.* **2009**, *14*, 1301.

51. Nam, W. *Acc. Chem. Res.* **2007**, *40*, 522.

52. Lee, Y.-M.; Kotani, H.; Suenobu, T.; Nam, W.; Fukuzumi, S. *J. Am. Chem. Soc.* **2008**, *130*, 434.

53. Fukuzumi, S.; Kotani, H.; Lee, Y.-M.; Nam, W. *J. Am. Chem. Soc.* **2008**, *130*, 15134.

54. Lubben, M.; Meetsma, A; Wilkinson, E. C.; Feringa, B.; Que Jr., L. *Angew. Chem. Int. Ed.* **1995**, *34*, 1512.

55. Roelfes, G.; Lubben, M.; Chen, K.; Ho, R. Y. N.; Meetsma, A.; Genseberger, S.; Hermant, R. M.; Hage, R.; Mandal, S. K.; Young, Jr., V. G.; Zang, Y.; Kooijman, H.; Spek, A. L.; Que, Jr., L.; Feringa, B. L. *Inorg. Chem.* **1999**, *38*, 1929.

56. Kaiser, J.; Kliner, E. J.; Oh, N. Y.; Rohde, J.-U.; Song, W. J.; Stubna, A.; Kim, J.; Münck, E.; Nam, W.; Que Jr., L. *J. Am. Chem. Soc.* **2004**, *126*, 472.

57. Collins, M. J.; Kallol, R.; Que Jr., L. *Inorg. Chem.* **2006**, *45*, 8009.

58. Kotani, H.; Suenobu, T.; Lee, Y.-M.; Nam, W.; Fukuzumi, S. *J. Am. Chem. Soc.* **2011**, *133*, 3249.

59. Klinker, E. J.; Kaizer, J.; Brennessel, W. W.; Woodrum, N. L.; Cramer, C. J.; Que, Jr., L. *Angew. Chem. Int. Ed.* **2005**, *44*, 3690.

60. Oh, N. Y.; Suh, Y.; Park, M. J.; Seo, Mi S.; Kim, J.; Nam, W. *Angew. Chem. Int. Ed.* **2005**, *44*, 4235.

61. Lee, Y.-M.; Kotani, H.; Suenobu, T.; Nam, W.; Fukuzumi, S. *J. Am. Chem. Soc.* **2008**, *130*, 434.

62. Campanali, A. A.; Kwiecien, T. D.; Hryhorczuk, L.; Kodanko, J. J. *Inorg. Chem.* **2010**, *49*, 4759.

63. Wang, D.; Zhang, M.; Buhlmann, P.; Que Jr., L. *J. Am. Chem. Soc.* **2010**, *132*, 7638.

64. Park, J.; Morimoto, Y.; Lee, Y.-M.; You, Y.; Nam, W.; Fukuzumi, S. *Inorg. Chem.* **2011**, *50*, 11612.

65. Braymer, J. J.; O'Neill, K. P.; Rohde, J.-U.; Lim, M. H.. *Angew. Chem. Int. Ed.* **2012**, *51*, 5376.

66. Nakamoto, K. *Infrared and Raman Spectra of Inorganic and Coordination Compounds, Applications in Coordination, Organometallic, and Bioinorganic Chemistry*; Wiliey: New Jersey, 2009; pp 52-94.

67. Hodges, K. D.; Wollmann, R. G.; Kessel, S. L.; Hendrickson, D. N.; Van Derveer, D. G.; Barefield, E. K. *J. Am. Chem. Soc.* **1979**, *101*, 906.

68. Cho, J.; Jeon, S.; Wilson, S. A.; Liu, L. V.; Kang, E. A.; Braymer, J. J.; Lim, M. H.; Hedman, B.; Hodgson, K. O.; Valentine, J. S.; Solomon, E. I.; Nam, W. *Nature* **2011**, *478*, 502.

69. Armarego, W. L. F.; Chai, C. *Purification of Laboratory Chemicals*, 5th ed.; Butterworth-Heinemann: Oxford, U.K., 2003.

70. Hagen, K. S. *Inorg. Chem.* **2000**, *39*, 5867.

71. Arnold, J.; Hoffman, C. G.; Dawson, D. Y.; Hollander, F. J. *Organometallics* **1993**, *12*, 3645.

72. Royal, G.; Dihaoui-Gindrey, V.; Dahaoui, S.; Tabard, A.; Guilard, R.; Pullumbi, P.; Lecomte, C. *Eur. J. Org. Chem.* **1998**, 1971.

73. Rohde, J.-U.; In, J.-H.; Lim, M. H.; Brennessel, W. W.; Bukowski, M. R.; Stubna, A.; Münck, E.; Nam, W.; Que, L., Jr. *Science* **2003**, *299*, 1037.

74. Connelly, N. G.; Geiger, W. E. *Chem. Rev.* **1996**, *96*, 877.

75. Chang, D.; Malinski, T.; Ulman, A.; Kadish, K. M. *Inorg. Chem.* **1984**, *23*, 817.

76. *CRC Handbook of Chemistry and Physics*, 89th ed.; Lide, D. R., Ed.; CRC Press/Taylor & Francis: Boca Raton, FL, 2008.

77. Addison, A. W.; Rao, T. N. *J. Chem. Soc., Dalton Trans.* **1984**, *7*, 1349.

78. Bosnich, B.; Poon, C. K.; Tobe, M. L. *Inorg. Chem.* **1965**, *4*, 1102.

79. Fiedler, A. T.; Halfen, H. L.; Halfen, J. A.; Brunold, T. C. *J. Am. Chem. Soc.* **2005**, *127*, 1675.

80. McDonald, A. R.; Bukowski, M. R.; Farquhar, E. R.; Jackson, T. A.; Koehntop, K. D.; Seo, M. S.; De Hont, R. F.; Stubna, A.; Halfen, J. A.; Münck, E.; Nam, W.; Que, L. Jr. *J. Am. Chem. Soc.* **2010**, *132*, 17118.

81. Sastri, C. V.; Park, M. J.; Ohta, T.; Jackson, T. A.; Stubna, A.; Seo, M. S.; Lee, J.; Kim, J.; Kitagawa, T.; Münck, E.; Que, Jr., L.; Nam, W.; *J. Am. Chem. Soc.* **2005**, *127*, 12494.

82. Fukuzumi, S.; Morimoto, Y.; Kotani, H.; Naumov, P.; Lee, Y.-M.; Nam, W. *Nature Chem.* **2010**, *2*, 756.

83. Arulsamy, N.; Bohle, D. S.; Hansert, B.; Powell, A. K.; Thomson, A. J.; Wocaldo, S. *Inorg. Chem.* **1997**, *37*, 746.

84. Tsai, F.-T.; Kuo, T.-S.; Liaw, W.-F. *J. Am. Chem. Soc.* **2009**, *131*, 3426.

85. Tsai, F.-T.; Chen, P.-L.; Liaw, W.-F. *J. Am. Chem. Soc.* **2010**, *132*, 5290.

86. Weber, B.; Kapplinger, I.; Gorls, H.; Jager, E.-G. *Eur. J. Inorg. Chem.* **2005**, 2794.

87. Hauser, C.; Glaser, T.; Bill, E.; Weyhermuller, T.; Wieghardt, K. *J. Am. Chem. Soc.* **2000**, *122*, 4352.

88. Yatsunyk, L.A.; Walker, F.A. *J. Porphyrins Phthalocyanines*, **2005**, *9*, 214.

89. Nasri, H.; Ellison, M. K.; Shaevitz, B.; Gupta, G. P.; Scheidt, W. R. *Inorg. Chem.* **2006**, *45*, 5284.

90. Ellison, M. K.; Shang, M.; Kim, J.; Scheidt, W. R. *Acta Crystallogr., Sect. C: Cryst. Struct. Commun.* **1996**, *52*, 3040.

91. Schopfer, M. P.; Mondal, B.; Lee, D.-H.; Sarjeant, A. A. N.; Karlin, K. D. *J. Am. Chem. Soc.* **2009**, *131*, 11304.

92. Resce, J. L.; Fanning, J. C.; Day, C. S.; Uhm, S.-J.; Croisy, A. F.; Keefer, L. K. *Acta Crystallogr., Sect. C: Cryst. Struct. Commun.* **1987**, *43*, 2100.

93. Siemer, C. J.; Meece, F. A.; Armstrong, W. H.; Eichhorn, D. M. *Polyhedron* **2001**, *20*, 2637.

94. Merkel, M.; Schnieders, D.; Baldeau, S. M.; Krebs, B. *Eur. J. Inorg. Chem.* **2004**, 783.

95. Patra, A. K.; Rose, M. J.; Olmstead, M. M.; Mascharak, P. K. *J. Am. Chem. Soc.* **2004**, *126*, 4780.

96. Visvaganesan, K.; Mayilmurugan, R.; Suresh, E.; Palaniandavar, M. *Inorg. Chem.* **2007**, *46*, 10294.

97. Phillippi, M. A.; Baenziger, N. C.; Goff, H. M. *Inorg. Chem.* **1981**, *20*, 3904.

98. Wyllie, G. R. A.; Munro, O. Q.; Schulz, C. E.; Scheidt, W. R. *Polyhedron* **2007**, *26*, 4664.

99. Munro, O. Q.; Scheidt, W. R. *Inorg. Chem.* **1998**, *37*, 2308.

100. Wang, X.; Pennington, W. T.; Ankers, D. L.; Fanning, J. C. *Polyhedron* **1992**, *11*, 2253.

101. Strautmann, J. B. H.; George, S. D.; Bothe, E.; Bill, E.; Weyhermuller, T.; Stammler, A.; Bogge, H.; Glaser, T. *Inorg. Chem.* **2008**, *47*, 6804.

102. Fanning, J. C.; Wang, X.; Koziol, A. E.; Palenik, G. J. *Inorg. Chim. Acta*, **1995**, *232*, 199.

103. Xu, Z.; Thompson, L. K.; Miller, D. O.; Clase, H. J.; Howard, J. A. K.; Goeta, A. E. *Inorg. Chem.* **1998**, *37*, 3620.

104. Raptopoulou, C. P.; Sanakis, Y. ; Boudalis, A. K. *Eur. J. Inorg. Chem.* **2008**, 5632.

105. Slep, L. D.; Calvo, R.; Nascimento, O. R.; Baggio, R.; Garland, M. T.; Pena, O.; Perec, M. *Inorg. Chim. Acta* **2007**, *360*, 2911.

106. Owen, T. M.; Rohde, J.-U. *Inorg. Chem.* **2011**, *50*, 5283.

107. Holleman, A. F.; Wiberg, E.; Wiberg, N. *Inorganic Chemistry*, 101st ed.; Walter de Gruyter: Berlin, Germany, 2001.

108. Saltzman, H.; Sharefkin, J. G. In *Organic Syntheses*; Wiley & Sons: New York, NY, 1973; Collect. Vol. V, pp 658–659.

109. McQuaid, K. M.; Pettus, T. R. R. *Synlett* **2004**, 2403.

110. Young, C. L. *IUPAC Solubility Data Ser.* **1981**, *8*, 336.

111. Rohde, J.-U.; Que, L., Jr. *Angew. Chem., Int. Ed.* **2005**, *44*, 2255.

112. Hodges, K. D.; Wollmann, R. G.; Barefield, E. K.; Hendrickson, D. N. *Inorg. Chem.* **1977**, *16*, 2746.

113. Wolak, M.; Stochel, G.; Hamza, M.; van Eldik, R. *Inorg. Chem.* **2000**, *39*, 2018.

114. Fernandez, B. O.; Lorkovic, I. M.; Ford, P. C. *Inorg. Chem.* **2003**, *42*, 2.

115. Fernandez, B. O.; Lorkovic, I. M.; Ford, P. C. *Inorg. Chem.* **2004**, *43*, 5393.

116. Awad, H. H.; Stanbury, D. M. *Int. J. Chem. Kinet.* **1993**, *25*, 375.

117. Ford, P. C.; Wink, D. A.; Stanbury, D. M. *FEBS Lett.* **1993**, *326*, 1.

118. Franz, K. J.; Lippard, S. J. *J. Am. Chem. Soc.* **1998**, *120*, 9034.

119. Franz, K. J.; Lippard, S. J. *J. Am. Chem. Soc.* **1999**, *121*, 10504.

120. Ford, P. C.; Lorkovic, I. M. *Chem. Rev.* **2002**, *102*, 993.

121. Gwost, D.; Caulton, K. G. *J. Chem. Soc., Chem. Commun.* **1973**, 64.

122. Gwost, D.; Caulton, K. G. *Inorg. Chem.* **1973**, *12*, 2095.

123. Wayland, B. B.; Olson, L. W. *J. Chem. Soc., Chem. Commun.* **1973**, 897.

124. Wayland, B. B.; Olson, L. W. *J. Am. Chem. Soc.* **1974**, *96*, 6037.

125. Tran, D.; Skelton, B. W.; White, A. H.; Laverman, L. E.; Ford, P. C. *Inorg. Chem.* **1998**, *37*, 2505.

126. Ford, P. C.; Fernandez, B. O.; Lim, M. D. *Chem. Rev.* **2005**, *105*, 2439.

127. Man, W.-L.; Lam, W. W. Y.; Wong, W.-Y.; Lau, T.-C. *J. Am. Chem. Soc.* **2006**, *128*, 14669.

128. Lee, K. Y.; Kuchynka, D. J.; Kochi, J. K. *Inorg. Chem.* **1990**, *29*, 4196.

129. Wasmus, S.; Tryk, D. A.; Vielstich, W. *J. Electroanal. Chem.* **1994**, *377*, 205.

130. Park, J.; Morimoto, Y.; Lee, Y.-M.; You, Y.; Nam, W.; Fukuzumi, S. *Inorg. Chem.* **2011**, *50*, 11612.

131. Roelfes, G.; Lubben, M.; Leppard, S. W.; Schudde, E. P.; Hermant, R. M.; Hage, R.; Wilkinson, E. C.; Que Jr., L.; Feringa, B. L. *J. Mol. Catal., A* **1997**, *117*, 223.

132. Seo, M. S.; In, J.-H.; Kim, S. O.; Oh, N. Y.; Hong, J.; Kim, J.; Que Jr., L..; Nam, W. *Angew. Chem. Int. Ed.* **2004**, *43*, 2417.

133. Williamson, M. M.; Hill, C. L. *Inorg. Chem.* **1986**, *25*, 4648.

134. Gulyan, G. M.; Kurtikyan, T. S.; Ford, P. C. *Inorg. Chem.* **2008**, *47*, 787.

135. Man, W.-L.; Lam, W. W. Y.; Ng, S.-M.; Tsang, W. Y. K.; Lau, T.-C. *Chem. Eur. J.* **2012**

136. Fukuzumi, S.; Kotani, H.; Suenobu, T.; Hong, S.; Lee, Y.-M.; Nam, W. *Chem. Eur. J.* **2010**, *16*, 354.

137. Bukowski, M. R.; Koehntop, K. D.; Stubna, A.; Bominaar, E. L.; Halfen, J. A.; Münck, E.; Nam, W.; Que Jr., L. *Science* **2005**, *310*, 1000.

138. Sastri, C. V.; Lee, J.; Oh, K.; Lee, Y. J.; Lee, J.; Jackson, T. A.; Ray, K.; Hirao, H.; Shin, W.; Halfen, J. A.; Kim, J.; Que, Jr., L.; Shaik, S.; Nam, W. *Proc. Natl. Acad. Sci. USA* **2007**, *104*, 19181.

139. Zhou, Y.; Shan, X.; Mas-Ballesté, R.; Bukowski, M. R.; Stubna, A.; Chakrabarti, M.; Slominski, L.; Halfen, J. A.; Münck, E.; Que, Jr., L. *Angew. Chem. Int. Ed.* **2008**, *47*, 1896.

140. Hirao, H.; Que, Jr., L.; Nam, W.; Shaik, S. *Chem. Eur. J.* **2008**, *14*, 1740.

141. Dhuri, S. N.; Seo, M. S.; Lee, Y.-M.; Hirao, H.; Wang, Y.; Nam, W.; Shaik, S. *Angew.* Chem. Int. Ed. 2008, 47, 3356.

142. Jackson, T. A.; Rohde, J.-U.; Seo, M. S.; Sastri, C. V.; DeHont, R.; Stubna, A.; Ohta, T.; Kitagawa, T.; Münck, E.; Nam, W.; Que Jr., L. *J. Am. Chem. Soc.* **2008**, *130*, 12394.